Madagascar Demantoid
Andesine and Zircon from China
Vietnamese Aquamarine
Coloration of Saltwater Pearls

JEWELS OF THE TRADE

Sooner or later, the world's most extraordinary gems will cross paths with

RAHUL KADAKIA.

Here, Christie's Senior VP, Head of Jewelry Americas, shares priceless insight into the jewelry business and the value of an expert education.

A master eye for gems ... born or made? Coming from four generations of jewelers undoubtedly piqued my interest in this great business. But one needs to constantly train their eye by looking at gems – the more you learn, the better you will be at identifying and pricing gems, as well as being an effective salesperson and well-rounded businessman.

Something most people don't know about you. GIA is what brought me to Christie's. After studying in Santa Monica, I attended a GIA Career Fair where I had my first interview with the company.

Ok. Definitely a story there? I started work when I was 17 and five years into it, I thought I knew pretty much everything there was to know ... until I enrolled at GIA. The Institute's meticulous training and high standards exposed me to a whole new world of expertise.

Ultimate sales edge ... emotion or expertise? Jewelry is an emotional shopping experience, but expertise plays a decisive role. It's wonderful to show people a brilliant diamond, but it means more when you can follow up with a skillful explanation of the 4Cs exemplified in that particular gem.

Lean economy. Less jewelry? At the nexus of the downturn in late 2008, we sold the Wittelsbach Blue Diamond for $24 million, a world record price back then for any gem ever sold at auction. When you have great gems and jewels, the money makes itself available.

Any advice to the up and coming? Don't lose the passion that brought you to this business, and above all, keep learning every day.

GIA gratefully acknowledges those who, for 80 years, have used our resources to further world expertise in gems. Invest in your success at **WWW.GIA.EDU**

GIA®

Editorial

pg. 5

pg. 17

pg. 60

GEMS & GEMOLOGY

SUBSCRIPTIONS

DATABASE COVERAGE

MANUSCRIPT SUBMISSIONS

COPYRIGHT AND REPRINT PERMISSIONS

ABOUT THE COVER

In 2009, a deposit near the village of Antetezambato, in northern Madagascar, emerged as an important source of demantoid. In this issue, Dr. Federico Pezzotta and coauthors characterize the material and present new data. The Bulgari necklace in white gold features Madagascar demantoid (107.47 carats total weight), round brilliant-cut diamonds (16.94 carats), and pavé diamonds (8.76 carats). The loose demantoid (7.17 ct) and the crystal specimen (4 cm across) are courtesy of F. Pezzotta. Photo by Robert Weldon.

The
Dr. Edward J. Gübelin
Most Valuable Article
AWARD

The votes are in, and we're pleased to announce the winners of the 2010 Dr. Edward J. Gübelin Most Valuable Article Award, as voted by hundreds of *G&G* readers. We extend our thanks to all the subscribers who participated.

The article that took first place was "Gemstone Enhancement and Its Detection in the 2000s" (Fall 2010), which looked back at an eventful decade of new treatment processes and advances in identifying them. Placing second was "Synthetic Gem Materials in the 2000s: A Decade in Review" (Winter 2010), a retrospective of important developments in the synthetic gem industry. Third place went to "The Wittelsbach-Graff and Hope Diamonds: Not Cut from the Same Rough" (Summer 2010), which examined the two famous diamonds to see if they shared a common ancestry.

Congratulations also to
Julie H. Bennett
of Friendswood, Texas, whose ballot was drawn from the many entries to win a two-year print and online subscription to *G&G*, plus a flash drive containing the 2001–2010 back issues of the journal.

Most Valuable Article

First Place

GEMSTONE ENHANCEMENT AND ITS DETECTION IN THE 2000S

Shane F. McClure, Robert E. Kane, and Nicholas Sturman

Shane McClure is director of identification services at the GIA Laboratory in Carlsbad. With more than 30 years of experience in the field, he is well known for his many articles and lectures on gem identification. An accomplished gem photographer, he is also co-editor of the journal's Lab Notes section. **Robert Kane** is president and CEO of Fine Gems International in Helena, Montana, and has been a member of the *G&G* Editorial Review Board since 1981. A former director of the Gübelin Gem Lab, Mr. Kane has written numerous articles and spoken frequently on diamonds, gemstones, and gem identification. **Nicholas Sturman** is supervisor of pearl identification at the GIA Laboratory in Bangkok. After obtaining his F.G.A. diploma, he worked as a gemologist at the Gem Testing Laboratory of Great Britain in London. He then spent 16 years studying pearls and working as an advisor for the government-run Gem & Pearl Testing Laboratory in Bahrain before joining GIA in 2008.

Shane F. McClure

Robert E. Kane

Nicholas Sturman

DEMANTOID AND TOPAZOLITE FROM ANTETEZAMBATO, NORTHERN MADAGASCAR: REVIEW AND NEW DATA

Federico Pezzotta, Ilaria Adamo, and Valeria Diella

An important deposit of andradite, containing demantoid and topazolite varieties, has been mined near the village of Antetezambato in northern Madagascar since early 2009. Most of the activity took place from April through November 2009, and yielded a large quantity of rough material in a wide range of colors. The deposit has a skarn origin, related to contact metamorphism between Cenozoic magmatic intrusions and Mesozoic calcareous sediments. The garnets' internal features consist mainly of fluid inclusions, fractures, wollastonite needles (or their remnant channels), and diopside aggregates. The chemical composition is close to pure andradite, with negligible Cr and V contents; thus, iron is likely the main chromophore. LA-ICP-MS analysis showed a relatively high content of light rare-earth elements.

Since early 2009, the village of Antetezambato in northern Madagascar has become known for producing fine andradite gem rough and crystal specimens. The deposit has yielded a range of andradite colors, including yellow-green to bluish green demantoid (figure 1), greenish/brownish yellow to brown topazolite, and rare dark brownish red to red material. Several articles describing the locality and its andradite production have been published. Following the preliminary gemological data reported by Mocquet et al. (2009a), further details were provided by Danet (2009), Mocquet et al. (2009b), Rondeau et al. (2009a), and the authors listed below. Pezzotta (2010a) provided historical, geological, and mineralogical information, including the andradite's paragenesis and crystal morphology; some mineralogical information also appeared in Praszkier and Gajowniczek (2010) and Pezzotta (2010b). Local newspaper articles (e.g., Razafindramiadana, 2009) and various websites documented the rush of miners, brokers, and dealers to the site, as well as the many social and security problems that have plagued the area.

The notable features of gem andradite from this locality can be summarized as:

- A skarn origin (Pezzotta, 2010a).

- A wide range of color varieties, mostly demantoid but also topazolite, as documented by several authors, particularly Rondeau et al. (2009b) and Pezzotta (2010a,b); a review of andradite color variety names appears in Pezzotta (2010a).

- Growth zoning, anomalous extinction (strain), and the absence of horsetail inclusions (Rondeau et al., 2009b).

- An almost pure andradite composition, as documented on one sample by Bocchio et al. (2010) and on two samples by Adamo et al. (2011).

- The relative absence of chromium, as documented by Rondeau et al. (2009b); nevertheless, Schmetzer and Karampelas (2009) reported that

Figure 1. Since early 2009, substantial quantities of attractive demantoid have emerged from the Antetezambato area of northern Madagascar. The stones shown here range from 1.86 to 3.99 ct. Courtesy of Fine Gemstones Madagascar; photo by Matteo Chinellato.

minor amounts of chromium were responsible, at least in part, for the green color.

- The significant presence of rare-earth elements (REEs), as pointed out on one sample by Bocchio et al. (2010).

This article provides an update on the mining activity and production and distribution of demantoid from the Antetezambato deposit. A complete gemological characterization, including quantitative chemical data, is also presented. This study confirms previously published data, establishes the characteristic features of gem andradite from this locality, and offers new information concerning inclusions, trace-element profiles, and UV-Vis-NIR spectra. In addition, a genetic model for the andradite's formation is presented.

LOCATION

The andradite deposit is located in the Antsiranana region of northern Madagascar, ~2.5 km west of the village of Antetezambato (figure 2). The mining area covers ~20 hectares and is centered at 13°30.460'S, 48°32.652'E; most of the mining takes place within a mangrove swamp that is subject to daily tidal flooding (figure 3). Detailed information about the locality and its geomorphology, including tidal effects, was presented by Pezzotta (2010a).

HISTORY

Lacroix (1922) reported finding pale green andradite crystals in the cavities of a nepheline syenite of Mount Bezavona, an intrusive massif of Cretaceous age located south of the Nosy Be archipelago on the Ampasindava peninsula. Beyond this one entry, there is no other mention in the literature of green andradite from Madagascar. Gem-quality green grossular (tsavorite) has been found at Gogogogo in the Toliara region (Mercier et al., 1997), and at Itrafo in the Antananarivo region.

A detailed description of the Antetezambato deposit's discovery and mining activity up to early 2010 appears in Pezzotta (2010a), and a brief review is given here. Between 2006 and 2008, a few local people from Antetezambato (at the time a small village of ~20 huts) recovered a small quantity of stones from a tidal estuary that were initially thought to be zircon or sapphire. As word spread that they had found demantoid, thousands of people rushed to the site in 2009 (e.g., figures 4 and 5).

Unfortunately, the situation deteriorated quickly. Armed robberies became more frequent as organized crime from the Ilakaka and Ambondromifehy sapphire trade spread to the Ambanja and Antetezambato areas. Since October 2009, authorities have brought the situation somewhat under control, though the area is still considered very dangerous.

Production has also diminished significantly since October 2009—largely because of the difficulty and danger of continued mining as deeper pits are required to reach productive zones—and most of the workers have left the area. In April 2010, a few groups of miners began working with better-organized systems, but the infiltration of seawater into the pits and tunnels during high tide greatly limited output. At the beginning of the rainy season in November 2010, only a few dozen miners were still working, and Antetezambato had shrunk to a population of about 200.

In December 2010, all the claims covering the demantoid deposit were legally acquired by a joint venture of Italian, German, and Malagasy mining operators, with the aim of investigating the down-dip extension of the demantoid occurrence and eval-

Figure 2. The Antetezambato garnet deposit is located just southeast of the Nosy Be archipelago in the Antsiranana region of northern Madagascar.

uating the economic potential of organized mining in the future.

PRODUCTION AND DISTRIBUTION

No official production figures exist for the Antetezambato deposit, and any estimates are approximate due to the lack of any organization and regulation. Based on the experience of the lead author and information gathered from several gem and mineral dealers in Madagascar, however, it is certain that most of the production (probably more than 90% of the total to date) was mined between April and November 2009. Only a very small percentage was mined subsequently, and virtually none since November 2010.

Numerous mineral specimens also have been produced (e.g., figure 6), and by far the finest one observed by the lead author consisted of several lustrous eye-clean crystals up to 2.8 cm across on matrix, each characterized by a green core with a thin brown-yellow overgrowth.

During the peak of the mining activity in 2009, ~20 kg of gem material were produced weekly, as well as a much larger quantity of low-quality rough. Thus, the total production of gem rough (e.g., figure 7) can be estimated to be on the order of hundreds of kilograms. However, high-quality pieces weighing 1+

g with good clarity and green color have always been scarce, and the total production is probably no more than a few kilograms. Eye-clean rough material of good color weighing 2.5+ g is exceptionally rare. High-quality cut gemstones weighing 4+ ct are very scarce, and those larger than 6 ct (e.g., figure 8) are exceptional. Most of the cut andradite consists of demantoid, while some topazolite and a small amount of red-brown material also has been faceted (e.g., figure 9).

The outlook for future production is uncertain. Small-scale and hand mining have become very difficult and unproductive, mostly because of the daily tidal flooding. Nevertheless, large reserves of demantoid are inferred at deeper levels of the deposit, as most of the garnet-rich veins dip steeply and occur over an area of several hectares. Since the present tunnels reach a depth of no more than 5–20 m, it is reasonable to speculate that only a small percentage of the total deposit has been mined. Still, a large and well-organized mining operation will be necessary to

NEED TO KNOW

- Commercial quantities of gem-quality andradite have been produced at Antetezambato in northern Madagascar, mainly in 2009.
- The production consists primarily of yellow-green to bluish green demantoid and greenish/brownish yellow to brown topazolite.
- The skarn origin is reflected by inclusions of wollastonite and diopside (but no "horsetails"), as well as relatively high concentrations of light rare-earth elements.
- The demantoid contains very low Cr and V; the green color appears related to intrinsic Fe^{3+}.

overcome the flooding problems and achieve significant production.

The vast majority of the gem demantoid production from Antetezambato has been traded out of Madagascar by Thai dealers. The first significant quantity of rough and cut stones reached the Bangkok market in September-October 2009, followed by a notable amount (including sets of calibrated stones) at the February 2010 Tucson gem shows. In the early stages of production, prices for top-quality material were very high, but they have since stabilized. Larger good-quality cut stones continue to command high prices.

Figure 3. The garnet mining area is located in a mangrove swamp, seen here during low tide in November 2009 (left, photo by F. Pezzotta) and at high tide in September 2009 (right, photo by Marco Lorenzoni).

GEOLOGY AND GARNET FORMATION

Northwestern Madagascar is characterized by significant magmatism of Upper Mesozoic to Cenozoic age, affecting both the Pan-African crystalline basement and the Permo-Mesozoic sedimentary sequence of the Mahajunga Basin. The plutonic and volcanic complexes are distributed from the Nosy Be archipelago and the Ampasindava peninsula to the southeast toward Antongil Bay, forming an elongate area presumed to be related to a rift zone (de Wit, 2003). The Antetezambato garnet deposit occurs on the northwestern side of this magmatic area and rep-

resents the first important gem deposit in Madagascar formed by contact metamorphism within the Permian-Mesozoic sedimentary cover.

The Antetezambato area (again, see figure 2) is composed of sediments of the Isalo Formation (mostly sandstone) and intrusive rocks of the Ambato alkaline-granite massif (Melluso et al., 2007). The garnet deposit consists of a tilted block of layered sediments (dipping 45–60° south) that is intruded by a network of lamprophyric dikes (figure 10). The lamprophyric rocks (not reported in the geologic map of Besairie, 1962) bound the garnet deposit on the north and west

Figure 4. In this September 2009 photo, two Malagasy women hand-pick andradite crystals from material they have washed using metal sieves. Photo by Marco Lorenzoni.

Figure 5. Thousands of miners have dug numerous pits in search of demantoid at the Antetezambato deposit. Because of the tidal influx, they must carefully reinforce their diggings and pump seawater out of the pits before mining can resume each day. Photo by F. Pezzotta, November 2009.

Figure 6. The Antetezambato deposit is the source of fine garnet specimens, such as these demantoid (left and center) and topazolite crystals (right). The largest crystals measure 1.2 cm (left) and 2.2 cm (center); the specimen on the right is 4.2 cm tall. Courtesy of Daniel Trinchillo; photos by James Elliott.

sides. The sediments, originally composed of fine- to medium-grained fossiliferous sandstones interlayered with silica-rich limestones, are metasomatically altered along structural discontinuities such as layer boundaries, fractures, and contacts with the lamprophyric intrusions. The alteration is related to pneumatolytic and hydrothermal fluid circulations generated by the intrusions, resulting in a network of veins consisting of very fine-grained, garnet-rich skarn rock that is white to pale green. Locally, even fossil shells and corals in the sediments have been replaced by the fine-grained skarn minerals. Cavities in the skarn veins contain the garnet crystals.

The relative absence of titanium in the sedimentary rocks resulted in the crystallization of the andradite as green to brown demantoid and topazolite varieties (sometimes as color-zoned crystals; see figure 11), rather than the more common titanium-rich andradite (melanite), which is black.

MATERIALS AND METHODS

We examined 24 representative samples (20 demantoid and 4 topazolite; tables 1 and 2), consisting of 11 faceted gems (0.67–4.22 ct; figure 12) and 13 pieces of partially polished rough (~0.1–8.5 g). Two samples of matrix rock were prepared as polished thin sections.

The faceted samples were examined by standard gemological methods at the Italian Gemological Institute in Milan to determine their optical properties, hydrostatic SG, UV fluorescence, and microscopic features. Raman analysis of inclusions in the 7.17 ct sample pictured in figure 8 were performed at the GIA Laboratory in Carlsbad.

Quantitative chemical analysis was performed on all of the rough samples at the Earth Sciences

Figure 7. This parcel of gem-quality demantoid was shown by a Malagasy dealer in Antetezambato in May 2010. Photo by F. Pezzotta.

Figure 8. This faceted demantoid (7.17 ct) is representative of the finest material from Antetezambato. Photo by Matteo Chinellato.
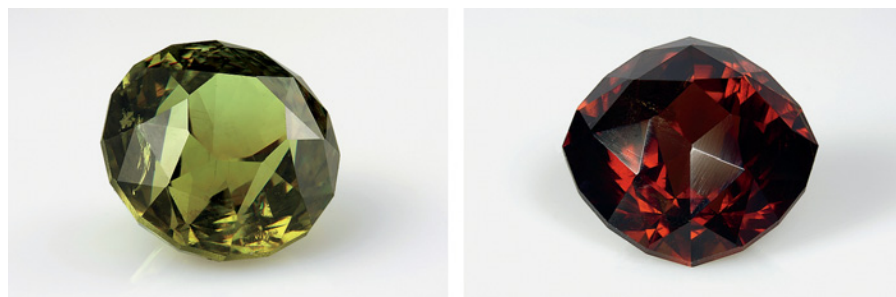
Figure 9. This topazolite (left, 1.38 ct) and rare brownish red andradite (right, 1.86 ct) were faceted from material recovered at Antetezambato. Courtesy of Vadim Fedder; photos by Matteo Chinellato.

Department of the University of Milan. We used a JEOL JXA-8200 electron microprobe in wavelength-dispersive mode, with an accelerating voltage of 15 kV, a beam current of 15 nA, count times of 60 seconds on peaks and 30 seconds on background, and a beam diameter of ~1 μm. The following elements were analyzed: Na, Mg, Al, Si, K, Ca, Ti, V, Cr, Mn, and Fe. We corrected the raw data for matrix effects using a conventional ϕρZ routine in the JEOL software package. The two polished thin sections were examined with a petrographic microscope and analyzed by microprobe as well as by a scanning electron microscope (JEOL JSM 5610 LV) equipped with an energy-dispersive spectrometer.

The trace-element composition of the same 13 rough samples was determined by laser ablation–inductively coupled plasma–mass spectrometry (LA-ICP-MS) at the CNR Geosciences and Georesources Institute of Pavia, Italy. The instrument consisted of a Quantel Brilliant 266 nm Nd:YAG laser coupled to a PerkinElmer DRCe quadrupole ICP-MS. Spot size was 50 μm. NIST-SRM612 glass was used as the external calibration standard, while ^{43}Ca was the internal standard. In each analytical run, USGS reference sample BCR2 was analyzed together with unknowns for quality control; precision and accuracy were better than 5% and 10%, respectively. Data reduction was carried out using the Glitter software package (van Achterbergh et al., 2001) to analyze the following elements: Li, Be, B, Na, Mg, Al, Sc, Ti, V, Cr, Mn, Co, Ni, Cu, Zn, Rb, Sr, Y, Zr, Nb, Cs, Ba, Hf, Ta, Th, U, Pb, and the rare-earth elements from La to Lu.

Ultraviolet/visible/near-infrared (UV-Vis-NIR) spectroscopic measurements over the 250–900 nm range were performed at the Materials Science Department of the University of Milan-Bicocca with a PerkinElmer Lambda 950 spectrophotometer, equipped with an integrating sphere and operating with a spectral resolution of 0.05 and 0.30 nm/minute for the UV-Vis and NIR intervals, respectively, at a 1 nm/minute scan rate. Spectra were collected on two of the rough samples (nos. 1 and 13).

Spectroscopic measurements of all the rough

Figure 10. The Antetezambato deposit is located within a mangrove swamp (1), and the geology is characterized by a weathered horizon with dispersed broken crystals of andradite (2), which is underlain by sandstone and limestone (3) that are locally metasomatized and contain andradite-bearing skarn veins (4). The veins developed along fractures in the sedimentary rocks and along contacts with lamprophyre intrusions (5).

Properties	A	B	D	E	I	M	L	H	C	G	F
Color (in daylight)	Bluish green	Green	Green	Green	Green	Green	Yellowish green	Yellow-green	Greenish brown	Yellowish brown	Brown
Weight (ct)	1.37	1.15	3.04	1.99	4.22	2.82	1.88	2.30	0.67	3.17	1.23
Specific gravity	3.81	3.86	3.83	3.88	3.81	3.79	3.82	3.83	3.90	3.84	3.86
Internal features[a]	Fractures (some partially healed), wollastonite and diopside inclusions, straight and angular growth structures, growth channels	Two-phase inclusions, wollastonite inclusions	Two-phase inclusions, fractures (some partially healed)	Diopside inclusions, straight and angular growth structures, growth channels	Fractures (some partially healed), wollastonite and diopside inclusions	Fractures, diopside inclusions	Two-phase inclusions, fractures (some partially healed), diopside and pyrite inclusions	Fractures	Two-phase inclusions, diopside inclusions	Fractures	Wollastonite inclusions, growth channels, color zoning

[a] Liquid inclusions were observed in all samples.

---

samples over the mid-infrared range (4000–400 cm⁻¹) were performed with a Nicolet Nexus Fourier-transform infrared (FTIR) spectrometer, equipped with a Spectra-Tech diffuse reflectance (DRIFT) accessory, at a resolution of 4 cm⁻¹ and 200 scans per sample.

RESULTS

Color and Morphology. The demantoid ranged from yellow-green to bluish green, with low to moderate saturation (see tables 1–2 and figure 12). The topazolite samples were greenish brown, yellowish brown, and brown. Five of the samples (rough nos. 9 and 10, and faceted samples G, H, and L) showed a signifi-

Figure 11. This andradite crystal (1.8 cm in diameter) from Antetezambato shows a green core and a yellowish brown rim. Courtesy of Riccardo Caprilli; photo by Roberto Appiani.

cant color shift from yellowish green in daylight to pinkish yellow in incandescent light. Moreover, an unusual bluish green hue was noted in two samples (12 and A) only in daylight and not under incandescent light (in which they appeared green).

The most common forms exhibited by the crystals investigated here consisted of various combinations of the dodecahedron {110} and trapezohedron {110}, the former more typical in demantoid and the latter in topazolite. Several more-complex forms were reported by Pezzotta (2010a).

Gemological Properties. The standard gemological properties of the faceted samples are provided in table 1. All the stones were transparent, singly refractive with moderate anomalous double refraction, and had an RI value of >1.81 and SGs of 3.79–3.90. They were inert to long- and short-wave UV radiation.

With magnification, we observed liquid inclusions in all the stones, mostly consisting of liquid veils, with some two-phase inclusions (figure 13A). Fractures were common, and some of them were partially healed into "fingerprints." In addition, some samples contained white acicular crystalline inclusions, often in aggregates, that SEM-EDS identified as wollastonite (figure 14); most of these were strongly corroded or completely leached, leaving empty channels. Also present were birefringent aggregates of white crystals identified by Raman spectroscopy in one sample as diopside (figure 13B). In another sample, an opaque crystalline inclusion with a brassy yellow color, metallic luster, and cubic morphology with striated faces was visually identified as pyrite. We also observed some growth channels (figure 13C) distinct from those left behind by leached wollastonite, as well as distinct straight and

angular growth structures (figure 13D) and color zoning. Most samples showed moderate to strong anomalous double refraction between crossed polarizers (again, see figure 13D).

Chemical Composition. The chemical compositions of the 13 rough samples are reported in tables 2 and 3. Electron microprobe analyses showed that the garnets consisted of nearly pure andradite (≥98 mol.%). Ti, Al, Mn, Na, and K were present in very low amounts (<0.2 wt.%), while Cr and V were below the detection limit (0.01 wt.%) in all samples. The main trace elements measured by LA-ICP-MS were Mg (307–1423 ppm), Al (15–5467 ppm), and Mn (9–92 ppm). Sc, Ti, V, and Cr contents were consistently very low, with a maximum of only 7.5 ppm for Ti (table 3). Rare-earth element concentrations ranged from 0.037 to 100.8 ppm.

Figure 12. These 11 andradites from Antetezambato (0.67–4.22 ct) are among those studied for this report. Photo by Roberto Appiani.

Microprobe analyses of granular garnet in the skarn host rock showed compositions intermediate between andradite (Adr) and grossular (Grs), ranging from $Adr_{63}Grs_{37}$ to $Adr_{29}Grs_{71}$.

Spectroscopy. *UV-Vis-NIR.* The absorption spectra of representative green and brown samples are shown in

TABLE 2. Average chemical composition obtained by electron microprobe analyses of 13 rough andradite samples from Antetezambato, Madagascar.[a]

Chemical composition	12	1	2	3	4	5	6	7	8	9	10	11	13
Color (in daylight)	Bluish green	Green	Green	Green	Green	Green	Green	Green	Yellowish green	Yellowish green	Yellowish green	Yellowish green	Brown
Weight (g)	0.11	1.51	0.12	0.32	0.58	2.00	0.19	8.49	1.70	0.43	0.38	0.10	0.14
No. points analyzed	10	10	15	15	15	15	10	15	5	8	5	12	15
Oxides (wt.%)													
SiO_2	35.47	34.90	34.90	34.23	34.63	36.09	34.00	34.39	35.94	35.60	35.70	35.05	35.52
TiO_2	0.01	nd	nd	0.01	nd	nd	nd	0.01	0.01	nd	nd	0.01	nd
Al_2O_3	0.01	0.01	0.01	0.02	0.03	nd	nd	nd	0.03	nd	nd	0.18	0.02
Fe_2O_3[b]	31.93	31.54	31.43	31.34	31.50	31.51	31.42	31.18	31.54	31.59	31.46	31.61	31.23
MnO	0.01	0.01	0.01	0.01	0.01	0.01	nd	0.01	0.01	0.01	0.01	0.01	0.01
MgO	0.07	0.08	0.08	0.08	0.06	0.08	0.13	0.10	0.30	0.11	0.12	0.09	0.06
CaO	33.24	32.95	33.20	32.84	32.95	32.67	32.90	33.02	33.38	33.00	32.99	33.28	32.84
Na_2O	nd	0.05	nd	nd	nd	nd	nd	nd	nd	nd	nd	nd	nd
K_2O	nd	0.02	nd	nd	nd	nd	nd	nd	nd	nd	nd	nd	nd
Total	100.74	99.56	99.63	98.53	99.18	100.36	98.45	98.74	101.26	100.31	100.28	100.23	99.68
Ions per 12 oxygens													
Si	2.979	2.964	2.962	2.940	2.954	3.013	2.922	2.945	2.995	3.001	3.009	2.956	3.005
Ti	0.001	nd	nd	0.001	nd	nd	nd	0.001	0.001	nd	nd	0.001	nd
Al	0.001	0.001	0.001	0.002	0.003	nd	nd	0.003	0.008	nd	nd	0.018	0.002
Fe^{3+}	2.018	2.016	2.007	2.025	2.022	1.990	2.032	2.009	1.978	1.998	1.981	2.006	1.988
Mn	0.001	0.001	0.001	0.001	0.001	0.001	nd	0.001	0.001	0.001	0.001	0.001	0.001
Mg	0.009	0.010	0.010	0.010	0.008	0.011	0.017	0.013	0.037	0.014	0.015	0.011	0.008
Ca	2.991	2.998	3.019	3.022	3.012	2.970	3.029	3.029	2.981	2.981	2.979	3.007	2.977
Na	nd	0.008	nd	nd	nd	nd	nd	nd	nd	nd	nd	nd	nd
K	nd	0.002	nd	nd	nd	nd	nd	nd	nd	nd	nd	nd	nd
Mol.% end members													
Andradite	99.70	99.60	99.40	99.60	99.70	99.50	99.50	99.50	98.30	99.50	99.20	99.60	99.60
Others	0.03	0.04	0.06	0.04	0.03	0.05	0.05	0.05	1.40	0.05	0.08	0.04	0.04

[a] *Standards: natural wollastonite (Si, Ca), anorthite (Al), fayalite (Fe), olivine (Mg), rhodonite (Mn), omphacite (Na), ilmenite (Ti), K-feldspar (K), and pure Cr and V for those elements. Abbreviation: nd = not detected (<0.01 wt.%). Chromium and vanadium were below detection limit in all analyses.*
[b] *Total iron is calculated as Fe_2O_3.*
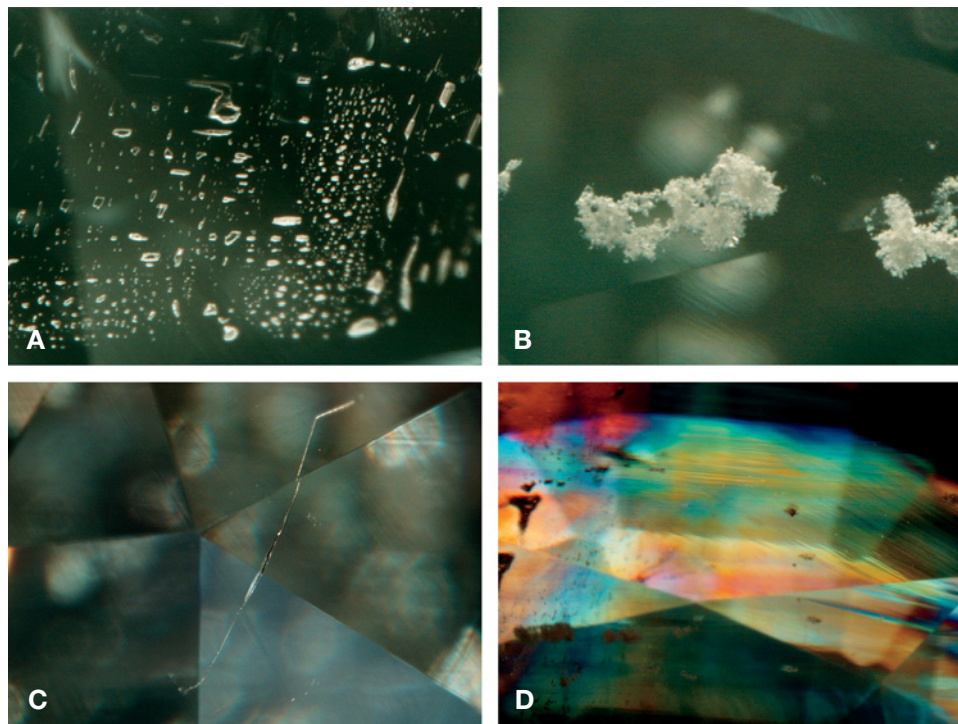
Figure 13. Typical internal features in andradite from Antetezambato are fluid inclusions (A, magnified 55×), crystalline aggregates of diopside (B, 50×), etch channels (C, 35×), and growth structures and strain (D, 15×; crossed polarizers). Photomicrographs by Nathan Renfro.

figure 15. The spectra displayed similar features: total absorption below 390 nm; an intense peak at about 440 nm; a broad band at ~600 nm consisting of two distinct components located at 575 and 610 nm, clearly visible in the spectrum of the green sample (figure 15, inset); and a band at ~850–860 nm. In addition, the brown sample showed continuously increasing absorption in the visible to ultraviolet range.

Mid-Infrared. The mid-IR spectra of all samples showed areas of total absorption in the 2250–400 cm^{-1} range, intrinsic to garnet, along with absorption bands between 3650 and 3500 cm^{-1} (e.g., figure 16). In particular, we observed three distinct peaks at 3610, 3581, and 3560 cm^{-1}.

DISCUSSION

The gemological properties reported here for demantoid and topazolite from Antetezambato are typical of andradite (e.g., O'Donoghue, 2006). They also agree with the results obtained by Rondeau et al. (2009b) and Schmetzer and Karampelas (2009) on samples from this locality. As pointed out by Rondeau et al. (2009a), these garnets show strain exhibited as anomalous double refraction with undulating extinction and "tatami" patterns. Strain is typical in andradite (e.g., Meagher, 1980).

The inclusion features in andradite from Antetezambato differ significantly from those observed in serpentinite-hosted andradites, such as demantoid

from Russia and Italy (Phillips and Talantsev, 1996; Adamo et al., 2009). We did not find any "horsetail" inclusions, which are common in demantoid from serpentinites. The inclusions in the Madagascar demantoid are similar to those found in specimens from Namibia (Gübelin and Koivula, 2005), which also are hosted by skarns.

Gem varieties of andradite typically have a near-end-member composition (Adamo et al., 2009;

Figure 14. This backscattered electron image shows wollastonite crystal inclusions up to 0.4 mm long (medium gray) in andradite. Micrograph by Michele Zilioli.
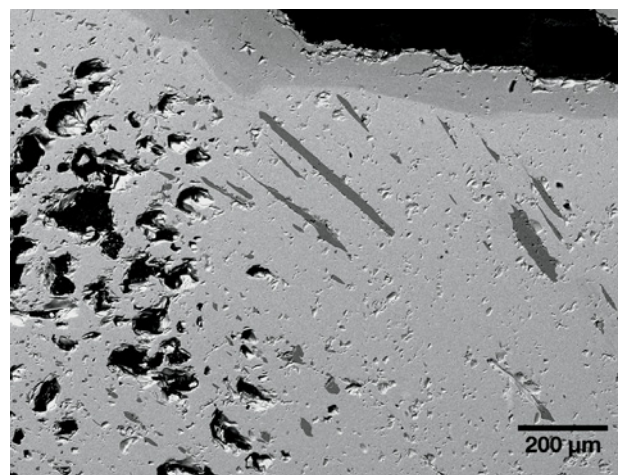
Bocchio et al., 2010), and this was the case for our samples from Antetezambato. Only the garnet microcrystals constituting the skarn host rocks showed chemical zoning, in the grossular-andradite solid solution range. The color zoning exhibited by some andradite crystals reflects inhomogeneities in the distribution of the trace elements, similar to what was described by Meagher (1980).

LA-ICP-MS analyses revealed very low levels of most trace elements, especially chromophore elements. Except for iron (Fe^{3+}), which is intrinsic to andradite, no chromophores were present in significant amounts, and there were no consistent variations in color according to composition. Although traces of chromium were reported in samples from Antetezambato by Schmetzer and Karampelas (2009), we found only extremely low quantities (up to ~3 ppm), consistent with Rondeau et al. (2009b). S. Karampelas and T. Hainschwang (pers. comm., 2011) reported that even photoluminescence spectra (after long acquisitions) showed no evidence of Cr

emission lines. It seems likely that the EDXRF spectroscopy (a bulk analysis technique) performed by Schmetzer and Karampelas (2009) indicated the presence of Cr-bearing inclusions, probably sub-microscopic. In fact, one of the first demantoid samples collected at the locality contained tiny inclusions rich in Cr, as revealed by microprobe analysis (G. Parodi, pers. comm., 2009).

Although Lind et al. (1998) measured small amounts of Cr (0.02–0.13 wt.% Cr_2O_3) in demantoid from Namibia, the results of Bocchio et al. (2010) and our own analyses of Namibian samples found no significant Cr. This is in agreement with the genetic similarity between these deposits (cf., Cairncross and Bahmann, 2006).

The REE distribution of andradite from Antetezambato shows a general enrichment in light rare-earth elements and a depletion of heavy REE (see plot in *G&G* Data Depository at gia.edu/gandg), which is typical of andradite (see Bocchio et al., 2010, and references therein). Moreover, this andra-

TABLE 3. Trace-element composition obtained by LA-ICP-MS analyses of 13 rough andradite samples from Antetezambato, Madagascar.[a]

Element (ppm)	12	1	2	3	4	5	6	7	8	9	10	11	13
Color	Bluish green	Green	Green	Green	Green	Green	Green	Green	Yellowish green	Yellowish green	Yellowish green	Yellowish green	Brown
Mg	418.4	395.9	358.9	449.5	336.0	503.3	408.7	720.3	1423	677.5	720.0	601.5	306.8
Al	26.37	15.14	16.84	58.58	99.02	24.47	42.81	32.10	5467	302.8	180.7	24.97	37.82
Sc	0.58	1.50	1.20	0.89	0.73	0.55	0.97	0.70	1.14	1.13	1.04	0.52	0.55
Ti	2.05	0.17	0.61	3.09	0.95	1.70	1.30	0.24	7.50	5.30	1.23	0.82	0.40
V	0.06	nd	0.03	0.04	0.04	0.02	0.02	nd	3.09	0.36	0.03	0.04	nd
Cr	1.15	0.59	0.59	0.99	0.98	0.00	0.63	0.50	2.20	2.35	2.74	0.50	1.35
Mn	53.98	85.91	37.63	18.09	34.98	9.01	37.12	13.73	29.88	33.45	26.07	91.53	56.45
La	1.24	0.019	0.118	0.515	1.11	0.171	0.386	0.592	0.194	2.60	8.34	0.669	2.74
Ce	12.04	0.009	0.324	3.41	2.66	1.73	1.63	4.26	0.389	7.54	54.21	1.02	22.18
Pr	1.03	0.002	0.026	0.388	0.208	0.203	0.165	0.715	0.036	0.670	8.685	0.056	3.54
Nd	1.25	0.008	0.039	1.04	0.431	0.361	0.375	2.18	0.123	2.16	26.81	0.162	9.93
Sm	0.037	0.002	0.009	0.057	0.019	0.017	0.021	0.036	0.010	0.151	0.729	0.000	0.321
Eu	0.199	0.006	0.006	0.075	0.102	0.053	0.048	0.124	0.085	0.377	1.85	0.013	1.40
Gd	0.034	nd	0.007	0.012	0.004	0.007	0.006	0.017	0.007	0.095	0.136	0.020	0.061
Tb	0.002	nd	nd	0.003	0.002	0.001	0.001	0.002	0.001	0.004	0.007	0.001	0.008
Dy	0.013	0.001	0.002	nd	0.003	0.002	0.002	nd	0.002	0.034	0.004	0.009	0.023
Ho	0.003	0.001	0.001	nd	0.001	0.001	0.001	0.001	0.001	0.010	0.002	nd	0.002
Er	nd	0.003	0.003	0.003	0.002	0.002	0.003	0.002	nd	0.036	0.002	0.003	0.002
Tm	nd	nd	0.001	0.001	nd	0.002	0.001	0.001	nd	0.005	nd	0.001	nd
Yb	0.003	0.002	0.007	0.002	0.008	0.003	0.004	0.003	0.006	0.022	0.002	0.002	0.008
Lu	0.001	0.001	nd	nd	0.001	0.001	0.001	0.001	0.001	0.004	0.001	0.001	0.001
Σ REE	15.85	0.037	0.542	5.51	4.54	2.55	2.64	7.93	0.853	13.70	100.8	1.96	40.21
Σ LREE (La+Ce+Pr+Nd)	15.56	0.030	0.507	5.35	4.40	2.46	2.55	7.75	0.742	12.97	98.04	1.91	38.39
Σ HREE (Er+Tm+Yb+Lu)	0.004	0.005	0.010	0.007	0.010	0.008	0.009	0.007	0.007	0.066	0.005	0.007	0.011

[a] Other elements (Li, Be, B, Na, Co, Ni, Cu, Zn, Rb, Sr, Y, Zr, Nb, Cs, Ba, Hf, Ta, Th, U, and Pb) were <1 ppm (by weight) in all samples.
Abbreviations: nd = not detected, REE = rare-earth elements, LREE = light rare-earth elements, HREE = heavy rare-earth elements.
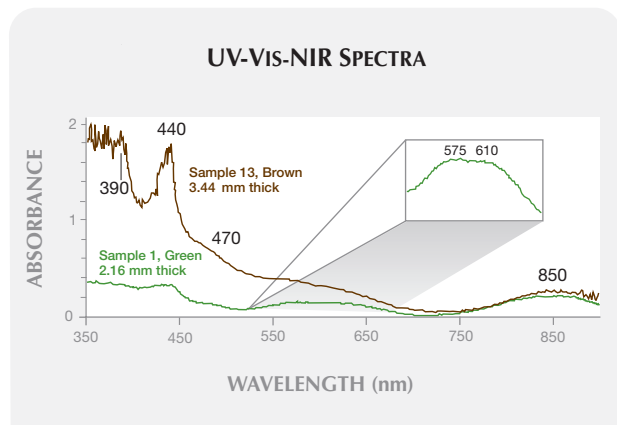
Figure 15. UV-Vis-NIR spectra of two representative andradite samples from Antetezambato show features related to Fe³⁺, which is likely the main chromophore.

dite has a relatively high total REE content, similar to that of Namibian demantoid and generally higher than that of andradite from serpentinites (Bocchio et al., 2010). This relatively high REE content could be caused by the mobility and enrichment of these elements in skarn rocks. The alkaline intrusive rocks associated with the Antetezambato andradite could also be a source of hydrothermally transported REEs (Pezzotta, 2010a).

The UV-Vis-NIR spectra of the green and brown samples showed spectral features related to octahedral Fe^{3+} (Manning, 1972; Moore and White, 1972; Amthauer, 1976; Lind et al., 1998). The gradual increase in absorption from the visible to UV wavelengths, evident in the brown sample's spectrum, is the main cause of its coloration. This absorption feature is usually attributed to an Fe^{2+}-Ti^{4+} intervalence charge transfer (Fritsch and Rossman, 1993; Rondeau et al., 2009b), but this interpretation is not consistent with the very low Ti content (up to ~7 ppm) in our samples. Because our LA-ICP-MS data did not show significant chromophores except iron, it appears likely that Fe^{2+}-Fe^{3+} interactions or tetrahedral Fe^{3+} (Moore and White, 1972) contribute to this continuous absorption. However, further research is needed to assess the cause of the brown coloration.

The color-shift behavior shown by some samples is similar to that seen in demantoid from Quebec, Canada (Amabili et al., 2009). The rare-earth elements cerium and neodymium, though detected only in trace amounts in our specimens, could be involved in the color shift, as documented in color-

change glass (Quinn and Muhlmeister, 2005) and in minerals such as apatite. Further investigation, including systematic trace-element analyses and a detailed study of UV-Vis-NIR spectra, would be necessary to fully characterize this phenomenon.

The mid-IR absorption features at 3610, 3581, and 3560 cm⁻¹ are related to structurally bonded OH^- (Amthauer and Rossman, 1998). Our spectra are very similar to those of andradite from skarn reported by Amthauer and Rossman (1998).

Stephenson and Kouznetsov (2009) reported that Russian demantoid can be heat-treated at temperatures of 640–720°C in a graphite-powder reducing atmosphere to enhance their color. Indeed, this treatment is able to minimize, if not totally eliminate, the yellow color component, giving rise to pure green gems. Despite the rumors in the Madagascar market that Thai treaters can improve the demantoids' color, heating experiments performed recently by G. Pocobelli in collaboration with the lead author did not show any significant changes in color. The experiments were done in oxidizing and reducing atmospheres, at temperatures up to 800°C; further investigations are in progress.

CONCLUSION

A relatively new deposit of demantoid and topazolite at Antetezambato in northern Madagascar has produced attractive gem material (e.g., figure 17), mainly in 2009. This study, performed on representative rough and cut samples selected from a large quantity of material produced since the discovery of the

Figure 16. Peaks at 3610, 3581, and 3560 cm⁻¹ in the mid-IR spectrum (reflectance mode) of Antetezambato andradite are related to hydroxides.
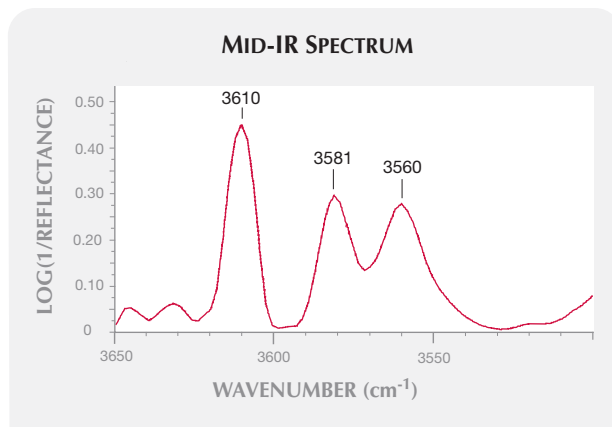
deposit, has confirmed previously published data and significantly added to knowledge of the most typical mineral inclusions (wollastonite and diopside) and the trace-element composition. The relatively high REE content, with a light-REE enrichment, is of particular interest as it characterizes andradite from skarn-type deposits. The skarn origin and some of the gemological features of the Antetezambato demantoid are similar to material from Namibia, but significantly different from those shown by demantoid from serpentinite-related deposits.

The trace-element data show no evidence of systematic compositional variations associated with the wide variety of colors. Moreover, the very low contents of Cr and V, combined with the UV-Vis-NIR spectroscopic results, suggest that the demantoid's green color is related to the constituent Fe^{3+}.

Studies of the Antetezambato mining area by author FP have provided a good understanding of the geologic processes involved in garnet formation. Modeling of the deposit suggests that there is significant potential for further production at depth, although the daily tidal flooding will seriously limit additional mining activities.

Figure 17. Madagascar's Antetezambato deposit became an important source of demantoid and topazolite in 2009. Additional production of fine stones such as these (0.90–1.71 ct) will depend on overcoming the logistical problems associated with daily tidal flooding. Photo by Robert Weldon.

ABOUT THE AUTHORS

Dr. Pezzotta (fpezzotta@yahoo.com) is the mineralogy curator of the Natural History Museum of Milan, Italy. Dr. Adamo is a postdoctoral fellow in the Earth Sciences Department at the University of Milan. Dr. Diella is a senior researcher at the Institute for the Study of the Dynamics of Environmental Processes, National Research Council (CNR), Milan.

REFERENCES

van Achterbergh E., Ryan C.G., Jackson S.E., Griffin W. (2001) Data reduction software for LA-ICP-MS. In P. Sylvester, Ed., *Laser Ablation-ICP-MS in the Earth Sciences: Principles and Applications*, Mineralogical Association of Canada Short Course Handbook, Vol. 29, Mineralogical Association of Canada, Quebec, pp. 239–243.

Adamo I., Bocchio R., Diella V., Pavese A., Vignola P., Prosperi L., Palanza V. (2009) Demantoid from Val Malenco, Italy: Review and update. *G&G*, Vol. 45, No. 4, pp. 280–287.

Adamo I., Gatta G.D., Rotiroti N., Diella V., Pavese A. (2011) Green andradite stones: Gemmological and mineralogical characterisation. *European Journal of Mineralogy*, Vol. 23, pp. 91–100.

Amabili M., Spertini F., Auguste M.B., Bonin G. (2009) Famous mineral localities: The Lac d'Amiante mine, Black Lake, Thetford mines, Quebec. *Mineralogical Record*, Vol. 40, No. 4, pp. 297–304.

Amthauer G. (1976) Crystal chemistry and colour of chromium-bearing garnets. *Neues Jahrbuch für Mineralogie, Abhand-*

lungen, Vol. 126, No. 2, pp. 158–186.

Amthauer G., Rossman G.R. (1998) The hydrous component in andradite garnet. *American Mineralogist*, Vol. 83, No. 7/8, pp. 835–840.

Besairie H. (1962) *Nosy-Be–Ambato*. Geologic map R33–S33, scale 1:100,000, Service Géologique, Antananarivo, Madagascar.

Bocchio R., Adamo I., Diella V. (2010) The profile of trace elements, including the REE, in gem-quality green andradite from classic localities. *Canadian Mineralogist*, Vol. 48, pp. 1205–1216.

Cairncross B., Bahmann U. (2006) The Erongo Mountains, Namibia. *Mineralogical Record*, Vol. 37, No. 5, pp. 361–470.

Danet F. (2009) Gem News International: New discovery of demantoid from Ambanja, Madagascar. *G&G*, Vol. 45, No. 3, pp. 218–219.

Fritsch E., Rossman G.R. (1993) The causes of color in garnets. *Mineralogical Record*, Vol. 24, No. 1, p. 63.

Gübelin E.J., Koivula J.I. (2005) *Photoatlas of Inclusions in Gemstones*, Vol. 2. Opinio Publishers, Basel, Switzerland.

Lacroix A. (1922) *Minéralogie de Madagascar*, Vol. 1. Augustin Challamel Éditeur, Paris, 624 pp.

Lind Th., Henn U., Bank H. (1998) New occurrence of demantoid from Namibia. *Australian Gemmologist*, Vol. 20, No. 2, pp. 75–79.

Manning P.G. (1972) Optical absorption spectra of Fe^{3+} in octahedral and tetrahedral sites in natural garnets. *Canadian Mineralogist*, Vol. 11, No. 4, pp. 826–839.

Meagher E.P. (1980) *Silicate Garnets*. *Reviews in Mineralogy*, Vol. 5, Mineralogical Society of America, Washington, DC, pp. 25–66.

Melluso L., Morra V., Brotzu P., Franciosi L., Grifa C., Lustrino M., Morbidelli P., Riziky H., Vincent M. (2007) The Cenozoic alkaline magmatism in central-northern Madagascar: A brief overview. *Periodico di Mineralogia*, Vol. 76, No. 3, pp. 169–180.

Mercier A., Moine B., Delorme J., Rakotondrazafy M.A.F. (1997) A note on a new occurrence of vanadian grossular garnet from Madagascar. *Journal of Gemmology*, Vol. 25, No. 6, pp. 391–393.

Mocquet B., Lulzac Y., Rondeau B. (2009a) Nouveau gisement de andradite démantoïde à Madagascar. www.gemnantes.fr/recherche/autre/demantoide_mada.php, May 30.

Mocquet B., Lulzac Y., Rondeau B., Fritsch E., Le Quéré J., Mohamady B., Crenn G., Lamiraud C., Scalie S. (2009b) Ambanja, premier gisement d'andradite démantoïde gemme à Madagascar. *Revue de Gemmologie a.f.g.*, No. 169, pp. 4–8.

Moore R.K., White W.B. (1972) Electronic spectra of transition metal ions in silicate garnets. *Canadian Mineralogist*, Vol. 11, No. 4, pp. 791–811.

O'Donoghue M., Ed. (2006) *Gems*, 6th ed. Butterworth-Heinemann, Oxford, UK.

Pezzotta F. (2010a) Andradite from Antetezambato, north Madagascar. *Mineralogical Record*, Vol. 41, No. 3, pp. 209–229.

Pezzotta F. (2010b) Demantoid und Topazolith aus Antetezambato, Nordmadagaskar. *Lapis*, Vol. 35, No. 10, pp. 31–39.

Phillips W.R., Talantsev A.S. (1996) Russian demantoid, czar of the garnet family. *G&G*, Vol. 32, No. 2, pp. 100–111.

Praszkier T., Gajowniczek J. (2010) Demantoide aus Antetezambato auf Madagascar. *Mineralien Welt*, Vol. 21, pp. 32–41.

Quinn E.P., Muhlmeister S. (2005) Gem News International: "Color-change" glass update. *G&G*, Vol. 41, No. 4, pp. 364–365.

Razafindramiadana L. (2009) Un gisement de démantoïde à Ambanja. *Express de Madagascar*, Antananarivo, No. 4327, June 6.

Rondeau B., Fritsch E., Mocquet B., Lulzac Y. (2009a) Ambanja (Madagascar)—A new source of gem demantoid garnet. *InColor*, No. 11, pp. 22–24.

Rondeau B., Mocquet B., Lulzac Y., Fritsch E. (2009b) Les nouveaux grenats démantoïdes d'Ambanja, Province d'Antsiranana, Madagascar. *Le Règne Minéral*, Vol. 90, pp. 41–46.

Schmetzer K., Karampelas S. (2009) Demantoid from a new source. *Gems & Jewellery*, Vol. 18, No. 4, pp. 10–12.

Stephenson J., Kouznetsov N. (2009) Major deposits of demantoid around the world. *InColor*, No. 11, pp. 16–20.

de Wit M.J. (2003) Madagascar: Heads it's a continent, tails it's an island. *Annual Review of Earth and Planetary Sciences*, Vol. 31, pp. 213–248.

THANK YOU DONORS

If you are interested in making a donation and receiving tax benefits information, please contact:

TERRI OTTAWAY
(800) 421-7250, ext. 4157.
From outside the U.S.,
call (760) 603-4157,
fax (760) 603-4056, or
e-mail terri.ottaway@gia.edu.

CIRCLE OF HONOR*

$100,000 and higher, cumulative

The Aaron Group

Dr. Suman Agrawal

Almaza Jewelers
(Ziad H. Noshie)

American Pearl Company

Amsterdam Sauer

Robert and Marlene Anderson

Aurafin Oro America

Banks International Gemology Inc.
(Daniel & Bo Banks)

The Bell Group/Rio Grande

Allan Caplan

Chatham Created Gems, Inc. (Thomas H. Chatham)

PierLuigi Dalla Rovere

The De Beers Group

Debbie and Mark Ebert

Fabricjewelry

Dallas R. Hales

Dr. H. Tracy Hall

Dr. Gary R. and Barbara E. Hansen

James Y. Hung, M.D.

Inta Gems Inc.

J.O. Crystal Company, Inc. (Judith Osmer)

JewelAmerica Inc.
(Zvi & Rachel Wertheimer)

Kazanjian Bros Inc.

KCB Natural Pearls
(K.C. Bell)

William F. & Jeanne H. Larson

Stephen Lentz

Sophie Leu

Honoring Betty H. Llewellyn

Marshall and Janella Martin

Roz & Gene Meieran

Nancy B. & Company

Kurt Nassau, Ph.D.

John & Laura Ramsey

R. Ed Romack

Art Sexauer

Shades of the Earth
(Laura & Wayne Thompson)

Ambaji Shinde

S.H. Silver Company
(Stephen & Eileen Silver)

Dr. Geoffrey A. Smith

D. Swarovski & Co.

Touraine Family Trust

United States Pearl Co.
(James & Venetia Peach)

Robert H. Vanderkay

Vicenza Fair

2010 DONORS*

$50,000 to $99,999
Steve and Betty Neely

$10,000 to $49,999
Cos Altobelli

Jerry Bearman

Dudley Blauwet

Christopher L. Johnston

$5,000 to $9,999
Scott Davies

Alice S. Keller

J. Blue Sheppard

$2,500 to $4,999
Julie and Carter Crow

Syed Iftikhar Hussain

Joseph Tenhagen

$1,000 to $2,499
Anil B. Dholakia Inc.

Nalini Pattni

Nathan Renfro

Joseph Rott

David B. Waller

$500 to $999
Aucoin Hart Jewelers

Jaroslav Hyrsl

Jack Lowell

Michele Macrí

Rosemary Pillin

Provockative Gems

Under $500
Antwerp Diamond Bank

Karen Avakyan

Jean-Claude Boulliard

Sandi Breland

Marco Cheung

Christie's Dubai

Hamed Ettehadi

James Ferrell

Galatea

James K. Hill

Shah Jahan

Kathryn Kimmel

Hyang-Sook Lee

Christina Iu

David Maloof

Hugo Marancenbaum

Barbara Moore

Renee Newman

Jeffrey E. Patterson, Ph.D.

Fazalur Qazi

Roberts Yogo Co.

Rachel Treitelman Rosin

Lee Hyan Sook

Yuko Tanaka

Saravanan Thanharaj

Li Tong

Hong Tuto

Peter Weavers

Paul W. Wickstrom

* All are cumulative donations

THE CHINESE RED FELDSPAR CONTROVERSY: CHRONOLOGY OF RESEARCH THROUGH JULY 2009

George R. Rossman

Red copper-containing plagioclase feldspar from Oregon has been available for over a century. In the early 2000s, new localities for copper-bearing feldspar were reported from the Democratic Republic of the Congo and from Tibet or an unspecified locality in China. The new material has been the subject of widespread concerns about its geographic origin and natural color. In fact, extensive studies of its composition, spectroscopy, physical appearance, and isotopic properties suggest that much of the red andesine on the market is the product of laboratory diffusion of copper into pale yellow andesine from Inner Mongolia. All samples initially subjected to testing as part of this study gave strong evidence or suggestions of treatment. Traces of copper-containing fluxes found on rough stones, and measurements of argon isotopic composition in particular, demonstrate that the tested material was recently heated to high temperatures under conditions where copper diffusion could occur. These results apply to samples that were obtained through July 2009, but do not include samples from expeditions to Tibet in 2010.

This article presents the results of the author's studies at the California Institute of Technology that involve what has come to be known as Chinese red andesine (figure 1), and reviews the key events surrounding this controversy—much of which has transpired outside traditional forums for gemological research—since 2002. It follows a timeline up to mid-2009, after the initial rounds of testing of samples from an expedition to Tibet in 2008 (Abduriyim, 2008, 2009), but before more recent expeditions to purported mines in Tibet. A future article will present the results of testing of samples collected during the 2010 expedition described by Abduriyim and Laurs (2010) and Hughes (2010).

A chronology of the author's research to address the controversy is presented below. The results from studies of a variety of samples obtained from sources listed in the Acknowledgments are briefly summarized, including samples allegedly from the Congo, Tibet, and an unspecified Chinese locality, as well as those from mining districts in Oregon, and pale yellow plagioclase from Mexican localities and Inner Mongolia. Many individuals and organizations were especially generous with their materials and fully willing to cooperate with the investigations. Notably, these sources were not told beforehand about the type of testing that would be conducted on the samples provided. Furthermore, results of the testing were not released until recently, again to avoid the possibility that those tests could be manipulated by donors. Generally, the testing included observation with magnifications up to those of a scanning electron microscope (25,000×), chemical analyses, and spectroscopic and isotopic studies. A list of samples and an overview of the experimental methods is presented in box A, so as not to interrupt the chronology. A partial report of these results has

Figure 1. Red andesine has been the subject of extended controversy regarding its source and the nature of its color. This specimen, represented as Tibetan, weighs 28.51 ct. Courtesy of Jacqueline Li; photo by Robert Weldon.

previously appeared, based on a transcription of a talk presented by the author (Rossman, 2010).

Plagioclase is a feldspar solid-solution series with compositions ranging from albite (Na-rich) to anorthite (Ca-rich), which has been arbitrarily subdivided and named (e.g., *andesine, labradorite*, etc.) according to the anorthite component (see box B on page 28).

PLAGIOCLASE LOCALITIES

Copper-Bearing Plagioclase. An early mention of copper-containing labradorite appears in a report by Anderson (1917), who studied specimens containing inclusions of copper in the Smithsonian's National Museum of Natural History. These showed a red aventurescence or less commonly were translucent with a pale green color. The labradorites were reported to be from Modoc County, California. This area still has not been confirmed as a source of such feldspar, but the author's examination of one of these crystals showed an appearance identical to sunstone from Lake County, Oregon, which is immediately north of Modoc County. (Although the feldspar variety *sunstone* was originally associated with hematite-bearing feldspars from India, Norway, and Tanzania, the copper-containing feldspar from Oregon is now widely known as *Oregon sunstone*.)

Natural copper-containing feldspar occurs in several additional deposits in south-central Oregon, as part of the Steens Mountain volcanic sequence. The composition ranges from labradorite to bytownite (~65–72 mol.% anorthite). It ranges from pale yellow to shades of red to green, and commonly contains thin flakes of native copper. A study of these feldspars by Hofmeister and Rossman (1985) was the first to discuss the origin of color in relationship to

the copper content and copper species. They showed that the pale yellow color is due to Fe^{3+} and the red color is due to copper colloids, and proposed that the green color and strong green to colorless pleochroism is caused by an intervalence interaction between Cu^+ and Cu^0. They also showed that the material's schiller effect was produced by microscopic laths of native copper.

Subsequently (in 1980), another deposit in Oregon was discovered at what is now known as the Ponderosa mine in northwestern Harney County. This labradorite also contains copper platelets and occurs in the same color range (Johnston et al., 1991). Prior to 2002, Oregon was the only reported commercial source of red copper-containing feldspar.

Very rarely, copper impurities have been discovered in small plagioclase crystals from other localities, such as Miyake-Jima, Japan (Petrov, 2010; figure 2, left) and the Pinacate volcanic field in Sonora, Mexico (author's collection; figure 2, center).

Commercial Deposits of Pale Yellow Plagioclase. Gem-quality pale yellow labradorite occurs in large quantities in the Mexican state of Chihuahua, near Casas Grandes, but without copper platelets or the red and green colors (figure 2, right). This material has been available for many years, but has mostly been sold as mineral specimens until fairly recently (e.g., Laurs et al., 2006).

Pale yellow andesine from Inner Mongolia was first described in the Chinese literature in the early 1990s (Li, 1991 and 1992) and later documented in a master's thesis (Cao, 2006). Li (1991) noted that when the Inner Mongolia Geological Survey conducted a general investigation of the region's gem resources, local respondents reported a sedimentary

BOX A: SAMPLES AND EXPERIMENTAL DETAILS

The samples studied by this author for the present article are listed in table A-1. Quantitative elemental microanalyses were conducted with a JEOL 8200 electron microprobe operated at 15 kV and 25 nA in a focused beam mode using Probe for Windows software. Analytical standards were anorthite (Ca$K\alpha$, Al$K\alpha$, Si$K\alpha$), TiO$_2$ (Ti$K\alpha$), fayalite (Fe$K\alpha$), forsterite (MgKa), benitoite (Ba$L\alpha$), and CuO (Cu$K\alpha$). Analyses were processed with the CITZAF correction procedure (Armstrong, 1995).

Secondary electron and backscattered electron images were obtained with a LEO 1550VP field emission scanning electron microscope (FE-SEM). An Oxford INCA X-ray energy-dispersive spectrometer on the SEM was used for elemental analysis. Quantitative analyses were processed with the XPP correction procedure (Pouchou and Pichoir, 1991).

Vis-NIR absorption measurements were carried out using a custom-built diode array spectrometer system. A tungsten-halogen lamp was directed into a highly modified Thermo NicPlan infrared microscope with both silicon and InGaAs diode array detectors for extended wavelength coverage. Polarization was provided by a Glan-Thompson calcite polarizer. In some cases, spectra were also obtained in the UV range using an Ocean Optics HR2000 spectrometer with a deuterium lamp.

Argon isotopic measurements were conducted in the noble gas laboratory at Caltech following procedures similar to those reported by House et al. (2000) and Amidon and Farley (2010) for helium dating. For these measurements, samples were first examined with a binocular microscope for freedom from other phases. Then they were placed in an ultrasonic cleaner for 15 minutes and dried. Next, they were crushed with jaw pliers. The crushed fragments were separated under a microscope to select grains predominantly in the 1–3 mm range. Finely divided particles were excluded from the measurements to minimize surface area upon which atmospheric argon could absorb. Likewise, grains with extensive internal fractures were avoided. The selected grains were washed in purified ethanol to remove adhering particles and allowed to dry at about 50°C.

For the argon extraction, the washed grains were placed in 6 × 3 mm degassed platinum tubes crimped at one end. When filled, they were loosely crimped shut at the other end to retain the feldspar but to allow argon gas to escape. The tubes typically accommodated about 20 mg of sample. The capsules were weighed before and after filling to determine the exact amount of feldspar they contained.

The capsules were placed into wells in a copper planchette in the mass spectrometer line. After a thorough evacuation, the capsules were heated slightly above 1000°C by rastering a Nd-YAG laser across the surface for about 30 minutes. To ensure degassing, the sample was re-extracted by additional rounds of laser rastering. Once the gases were extracted, they were purified by passing them over SAES getters to remove nitrogen and other reactive gases. After expansion into a volume of about 1.5 liters, the argon was cryogenically focused into a magnetic sector mass spectrometer (MAP 215-50), where the argon isotopes were counted. The data were then processed with software to provide the necessary instrumental corrections.

These measurements were intended not to provide a high-accuracy age date, but to clearly indicate if the isotopic ratios of the argon in the samples showed geologic time buildup of radiogenic ^{40}Ar from the decay of naturally occurring ^{40}K. Ratios near those of atmospheric argon would indicate that they had been recently heated to temperatures sufficient to drive out the radiogenic argon.

TABLE A-1. Feldspar samples used in detailed analytical investigations.

Sample number	Claimed locality[a]	Source	Sample type[b]	Methods used[c]
GIA-a	Tibet	GIA	Red rough	Argon
GRR 289	Mexico	Caltech Collection	Pale yellow rough	EMP
GRR 1613	Rogers mine, Oregon	Author's collection	Near-colorless rough	EMP
GRR 1615	Ponderosa mine, Oregon	Chris Johnston	Colored rough	EMP, SEM
GRR 2058	Ponderosa mine, Oregon	Chris Johnston	Near-colorless rough	EMP
GRR 2390	Tibet	Palagems.com	Red rough	Argon
GRR 2428	Tibet	Palagems.com	Red rough	EMP, argon
GRR 2520	Tibet	Ion International	Red faceted	Optical absorption
GRR 2560	Chihuahua, Mexico	B. Barker	Pale yellow rough	SEM
GRR 2570	Chihuahua, Mexico	D. Wallace	Pale yellow rough	EMP, SEM
GRR 2607	"China"	JTV	Pale yellow rough, red rough	EMP
GRR 2611	Dust Devil mine, Oregon	Ion International	Pale red rough	SEM
GRR 2616	Tibet	Ion International	Red faceted	SEM
GRR 2629	Chihuahua, Mexico	B. Barker	Pale yellow rough	EMP, SEM
GRR 2630	"China"	DSN	Red faceted	SEM, argon
GRR 2632	Oregon	Chris Rose	Pale colored rough	SEM
GRR 2633	Oregon	Chris Rose	Red rough	EMP
GRR 2635	"China"	Bangkok dealer	Red rough	SEM, argon
GRR 2639	Chihuahua, Mexico	Andegem	Pale yellow rough	EMP
GRR 2641	"China"	Andegem	Red and green rough	EMP, SEM, argon
GRR 2642	"China"	Andegem	Red and red/green faceted	Argon
GRR 2645	"China"	JTV	Red faceted	SEM
GRR 2646	Inner Mongolia	JTV	Pale yellow rough	SEM, argon
GRR 2649	"China"	DSN	Pale yellow rough	SEM, argon
GRR 2650	"China"	DSN	Red faceted Olympic gems	EMP, SEM
GRR 2651	"China"	Andegem	Pale yellow rough	EMP, argon
GRR 2652	"China"	Andegem	Multicolored rough	Visual examination
GRR 2654	Dust Devil mine, Oregon	Karla Proud	Red rough	EMP
GRR 2655	"China"	Andegem	Pale yellow faceted	Argon
GRR 2659	"China"	Andegem	Green faceted	Argon
GRR 2679	Tibet	JTV	Red rough	EMP, argon
GRR 2886	Tibet	Jacqueline Li	Red rough	EMP, argon
GRR 2887	Tibet	Jacqueline Li	Red faceted	EMP, argon
GRR 2902	Congo	GemFrance	Red faceted	EMP, argon
GRR 2921	Tibet	GAAJ	Red rough	EMP, argon
GRR 2923	Inner Mongolia	GAAJ	Pale yellow rough	EMP, argon
JTV-1	"China"	JTV	Red faceted	Argon
GS 0.44	Tibet	Ion International	Red faceted	EMP
GS 0.45	Tibet	Ion International	Red faceted	EMP
GS 0.46	Tibet	Ion International	Red faceted	EMP
GS 0.47	Tibet	Ion International	Red faceted	EMP
GS 0.50	Tibet	Ion International	Red faceted	EMP
GS 0.55	Tibet	Ion International	Red faceted	EMP
GS oval	Tibet	Ion International	Red faceted	EMP
GS 0.98	Tibet	Ion International	Green faceted	Optical absorption

[a] Only the samples from the Rogers mine were collected by the author. The localities for all others were stated by the donors.
[b] Several of the sample numbers represent batches of multiple crystals or gemstones.
[c] EMP = electron microprobe analysis; argon = argon isotope study; SEM = scanning electron microscopy, including energy-dispersive spectroscopy; many samples were also subjected to optical absorption spectroscopy.

Figure 2. In addition to Oregon, copper-containing feldspar has been reported from Miyake-Jima, Japan (left, 15 mm wide), and the Pinacate volcanic field, Mexico (center, 15 mm wide, with copper platelets). Pale yellow labradorite from Casas Grandes, Mexico (right, 0.55 ct each), is available in large quantities; this material does not contain copper. Photos by Mark Garcia (left) and G. R. Rossman (center and right).

occurrence extending about 20 × 4 km that contained transparent feldspar. Abduriyim (2008) reported that up to 100 tonnes of this andesine have been mined annually. The properties given in this report agree with many subsequent analyses (e.g., Abduriyim and Kobayashi, 2008, and data below).

Several other localities have produced colorless to pale yellow gem-quality plagioclase, but not in commercial quantities.

Figure 3. These 9 × 12 mm (2.78–3.44 ct) andesines supplied by Andegem were reportedly fashioned from material mined "in China." These samples were selected to show the maximum range of color variation, and are therefore photographed table-down. Photo by G. R. Rossman.

CHRONOLOGY OF ANALYSES AND RESULTS: 2002 TO MID-2009

Initial Analytical Work. In 2002, a new locality for red plagioclase feldspar was announced. Gem dealer Dr. Laurent Sikirdji (GemFrance) reported that one of

NEED TO KNOW

- Studies from 2002 to mid-2009 show that red (and green) Cu-bearing andesine-labradorite reportedly from Tibet, "China," and the Democratic Republic of the Congo have overlapping chemical and physical properties.

- Traces of copper-containing fluxes on the surface of rough stones and argon isotopic measurements indicate these feldspars have been heated to high temperatures in the presence of Cu.

- Evidence up to mid-2009 suggests that laboratory diffusion of Cu into pale yellow feldspar from Inner Mongolia (but not Mexico) could account for some or all of the "Asian/Congolese" feldspar in the market.

- This does not eliminate the possibility that andesine deposits in Tibet that were documented in 2010 are genuine.

his suppliers in Bangkok first showed him red andesine in January 2002, and told him it came from an unspecified locality in the Democratic Republic of the Congo (O'Meny, 2002). He sent samples to Dr. Emmanuel Fritsch at the University of Nantes, France, who published the first report about this red andesine (Fritsch, 2002). Krzemnicki (2004) further characterized this material and showed that it had a greater saturation of color and contained more copper
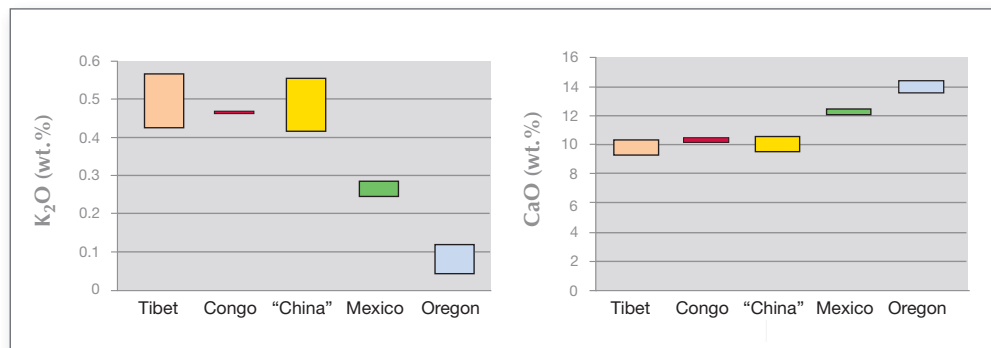
Figure 4. Electron microprobe analyses show no distinction between feldspars allegedly from Tibet and "China," but there are clear differences from those of Mexico and Oregon.

than the Oregon stones, but that its optical absorption spectrum was otherwise similar to the Oregon material. The initial analyses reported by these authors indicated that Dr. Sikirdji's samples had a lower Ca content than feldspar from Oregon, and that their composition fell slightly below and above the nomenclature boundary between andesine and labradorite. (Hereafter, plagioclase of such composition will be referred to as "andesine" for simplicity.)

The exact geographic origin remained undisclosed at the time, and stories soon began to circulate that gem dealers could not confirm the Congo source (Laurs, 2005). Because rough stones and matrix specimens were unavailable, questions arose about the authenticity of the material, or at least the accuracy of its reported locality.

In April and August 2005, this author (and GIA) received a few rounded red pebbles from William Larson of Palagems.com. Their origin was represented to Mr. Larson as Chinese (Tibetan and otherwise). The optical spectra of these samples closely resembled those of Oregon sunstone, indicating that copper was the cause of color. Later that year, Laurs (2005) published a brief report on material represented as Chinese that was obtained at the 2005 JCK show in Las Vegas. This report also contained information from Chinese dealer Jacqueline Li (Do Win Development Co., Ltd.), who offered a modest quantity of red feldspar (including rough material) at the 2006 Tucson show. She claimed it originated from an unspecified Tibetan mine worked by her husband's relatives. As this material entered the market, samples made their way to gem testing laboratories, and some of them were sent to Caltech in May and June 2006 for electron microprobe analysis. Around this time, the author heard concerns that the material might be treated by someone in China who had invented a method to produce red feldspar. Others in the industry had also heard about an unspecified treatment process (Hughes, 2010). The situation was further confused as early as 2006 because vendors were representing the origin of the red (and green)

andesine both as Tibet and China (figure 3), with no clear indication if these represented the same or different localities (Federman, 2006).

The author's detailed electron microprobe analyses of the red and green feldspars received in May-June 2006 indicated that they were members of the plagioclase series and their compositions ranged between An_{47} and An_{50}, which placed them in the andesine compositional range (again, see box B)

Additional electron microprobe analyses of feldspars purportedly from the Congo, Tibet, "China," Mexico, and the two main Oregon districts, conducted from 2006 through 2009 (table 1), showed that the compositions of the Congolese, Tibetan, and "Chinese" samples overlapped and were easily distinguishable from those found in Mexico and Oregon (figure 4). Most of the former group fell in the andesine nomenclature range, though some contained slightly more than 50 mol.% anorthite (An_{50}),

TABLE 1. Electron microprobe analyses of selected feldspars from various claimed localities.

Sample no.	Claimed locality	Composition[a]
GRR 2902	Congo	$An_{50–52}$
GRR 2616	Tibet	An_{44}
GRR 2630	"China"	$An_{43–49}$
GRR 2635	"China"	$An_{44–46}$
GRR 2641	"China"	$An_{43–48}$
GRR 2645	"China"	$An_{45–47}$
GRR 2649	"China"	$An_{44–49}$
GRR 2650	"China"	$An_{42–51}$
GRR 2646	Inner Mongolia	$An_{40–49}$
GRR 2560	Mexico	$An_{52–54}$
GRR 2570	Mexico	An_{53}
GRR 2629	Mexico	$An_{52–57}$
GRR 1615	Oregon	$An_{67–69}$
GRR 2611	Oregon	$An_{61–65}$
GRR 2632	Oregon	$An_{60–73}$

[a] Determined with multiple analyses on samples from each batch. A single number is used when the range of analytical values, expressed as two significant digits, does not exceed the value given.
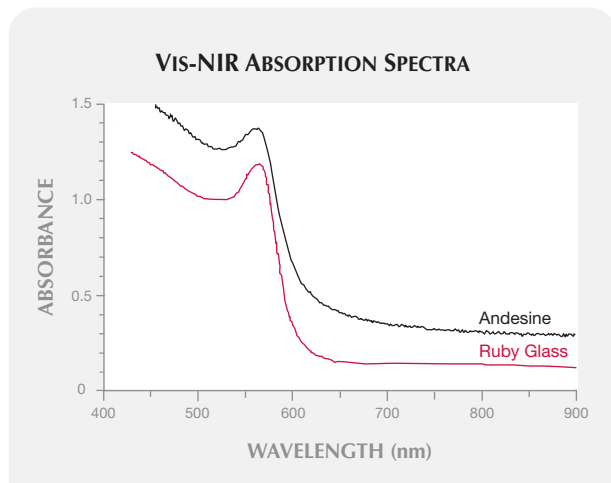
VIS-NIR ABSORPTION SPECTRA

Figure 5. This representative Vis-NIR spectrum of a red andesine reportedly from Tibet (~6 mm thick) is similar to that of a 1-mm-thick copper ruby glass (the latter adapted from figure 2 of Capatina, 2005, p. 284).
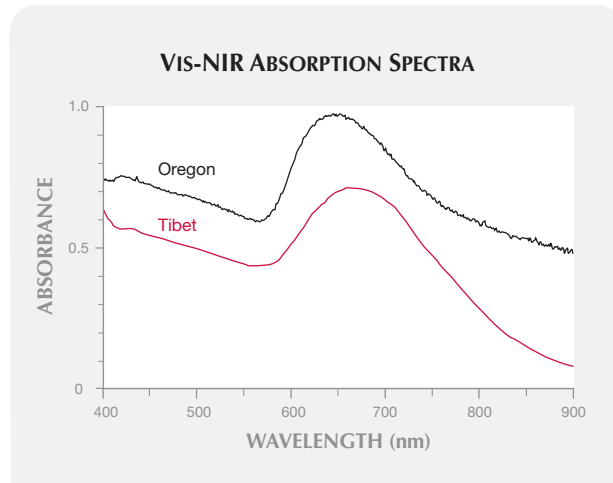

VIS-NIR ABSORPTION SPECTRA

Figure 6. The Vis-NIR spectrum of a faceted green andesine allegedly from Tibet (6 mm thick) shows the greatest absorption in the red portion of the spectrum, similar to a green labradorite from Oregon (2 mm thick).

placing them in the labradorite range. The full microprobe analyses appear in the *G&G* Data Depository (see gia.edu/gandg) and are summarized in figure B-1.

In 2008, we conducted 87 additional chemical analyses with a scanning electron microscope (SEM) using energy-dispersive spectroscopy (EDS). Although SEM-EDS analyses are slightly less accurate than electron microprobe data, they are generally quicker to obtain and less costly, and could still readily distinguish among feldspars alleged to be from the Congo, Tibet/"China," Oregon, and Mexico. These SEM-EDS analyses confirmed the results obtained with the electron microprobe (again, see table 1). Specifically, they showed that the Congolese, Tibetan, and "Chinese" samples fell within the same range of major elements and that they were distinct from the Mexican and Oregon feldspars.

Spectroscopic studies beginning in 2006 and continuing through 2008 demonstrated that the origin of color in the Tibetan/"Chinese" material was the same as in the Oregon sunstone. Dozens of optical spectra were obtained on both red and green andesine samples. The red stones had a dominant absorption band at about 565 nm and rising absorption in the blue region (figure 5). This spectrum bore a strong similarity to that of Oregon sunstone and to decorative red glass known as "copper ruby glass." This glass owes its color to colloids of copper metal (Nakai et al., 1999; Capatina, 2005) and, by analogy, it is reasonable to conclude that red andesine does as well.

The green andesine tested in this study showed strong green to colorless pleochroism, similar to the green Oregon labradorite. The absorption of the green material reached a maximum in the 650 nm region and showed much greater absorption in the red portion of the spectrum (figure 6) than did the

Figure 7. This "burned" red andesine (25 mm across) was said to have been heated to change it from pale yellow to red. Photos by G. R. Rossman (left, interior view) and Mark Garcia (right, surface of sample).
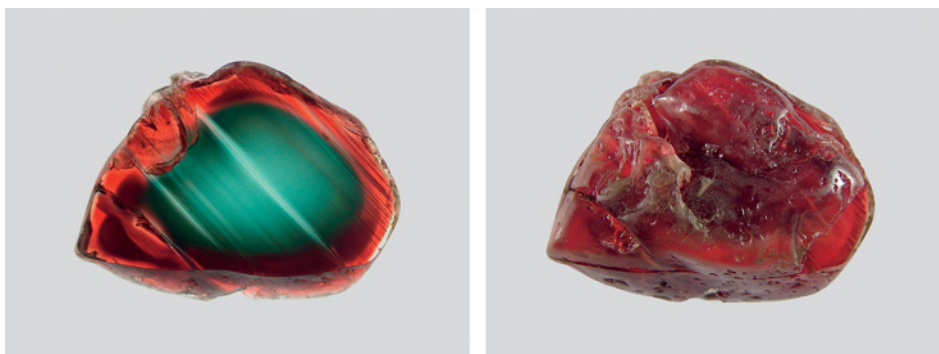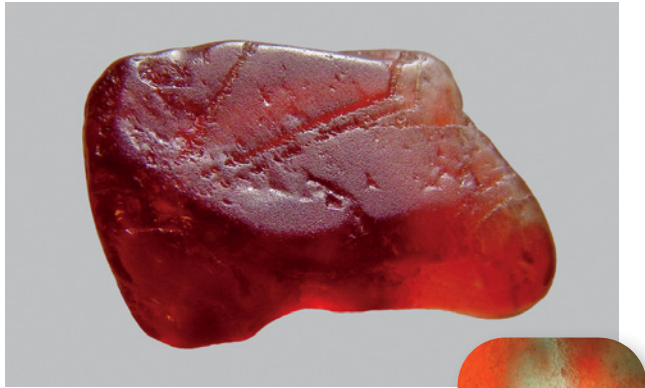
Figure 8. Some rough samples of andesine purportedly from Tibet/"China" showed features that appeared to be etch pits, as in this 17 mm andesine sold to a Bangkok dealer in mid-2003 from a supplier who stated it was mined in China. The pit in the inset is 32 μm wide. Photos by Mark Garcia and G. R. Rossman (inset).

red andesine. There was some variability in the position of the absorption maximum of the green andesine samples, due to the superposition of absorption features from the red regions, and from the Fe^{2+} in the feldspar. The spectrum was generally comparable to that of the green Oregon feldspar reported by Hofmeister and Rossman (1985).

In mid-2006, the author was told by a red andesine customer about a rumor that the Tibetan/"Chinese" material was being treated by a laboratory process in Asia. Although this andesine did have features reminiscent of diffusion, that alone did not prove laboratory treatment, since the Oregon sunstone is also most likely a product of diffusion—*natural* diffusion in the earth.

Red andesine soon became popular with consumers, and in the mid-2000s television networks such as Jewelry Television (JTV) and the Direct Shopping Network (DSN) sold "Chinese" andesine as natural material based on reports issued by various gemological laboratories. In 2007 JTV sent an on-air personality known as "Jewel Hunter Jack" to find the origin of the red feldspar. He ultimately traced the material to an area of Inner Mongolia where significant quantities of pale yellow andesine were being mined, but he saw no red material. He was told that the pale yellow feldspar had to be heated to bring out its "inherent" color, but he was not given the opportunity to actually witness the treatment process. He returned with samples of yellow

and "burned" red andesine (e.g., figure 7).

The pale yellow rough obtained by JTV in Inner Mongolia and rough examples of "burned" feldspar made their way to the author's laboratory by late January 2008 for additional testing. Our analyses of the pale yellow andesine found no copper that could have given rise to the red color with heat treatment alone. Consistent with these analyses, heating experiments of the pale yellow andesine conducted under controlled oxygen fugacity conditions failed to achieve any red color, as did treatment with gamma radiation. By early February 2008, JTV announced that the material originated in Inner Mongolia. Shortly thereafter, concerns about diffusion treatment of andesine became widespread and public (see, e.g., James, 2008a,b; Kratochvil, 2008).

Several of this author's observations on rough stones reportedly from Tibet/"China" also raised questions about their natural origin. Surfaces appeared etched and some showed pits of approximately square pyramidal shape (figure 8). Fragments of feldspar were found attached to the surface but in a different crystallographic orientation from the underlying material, which suggested that separate pieces of feldspar had become fused together (figure 9).

Even more interesting was the presence of a glassy material in cracks and recesses on the surface of some of the rough samples. SEM-EDS analysis of a thin layer of this glass-like material near a fused particle showed a higher concentration of potassium than the feldspar, and a much higher concentration

Figure 9. This 0.3-mm-wide fragment of feldspar was fused to the surface of an andesine sample by a glassy substance. Photo by G. R. Rossman.
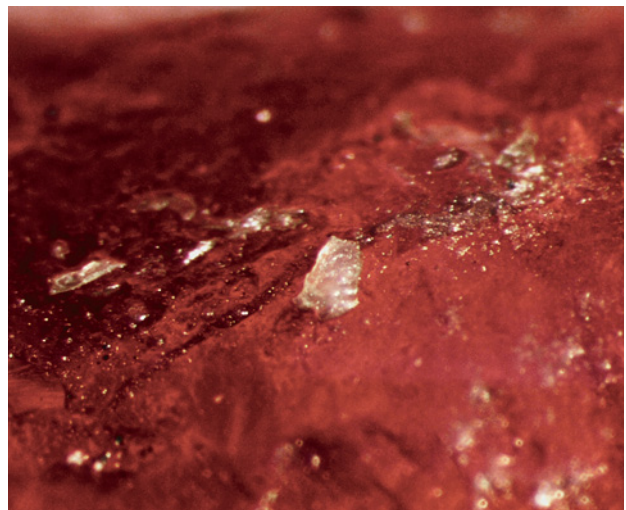
of copper (figure 10). These observations strongly suggested, but did not prove, that the feldspar had been heated in a copper-containing flux to allow the
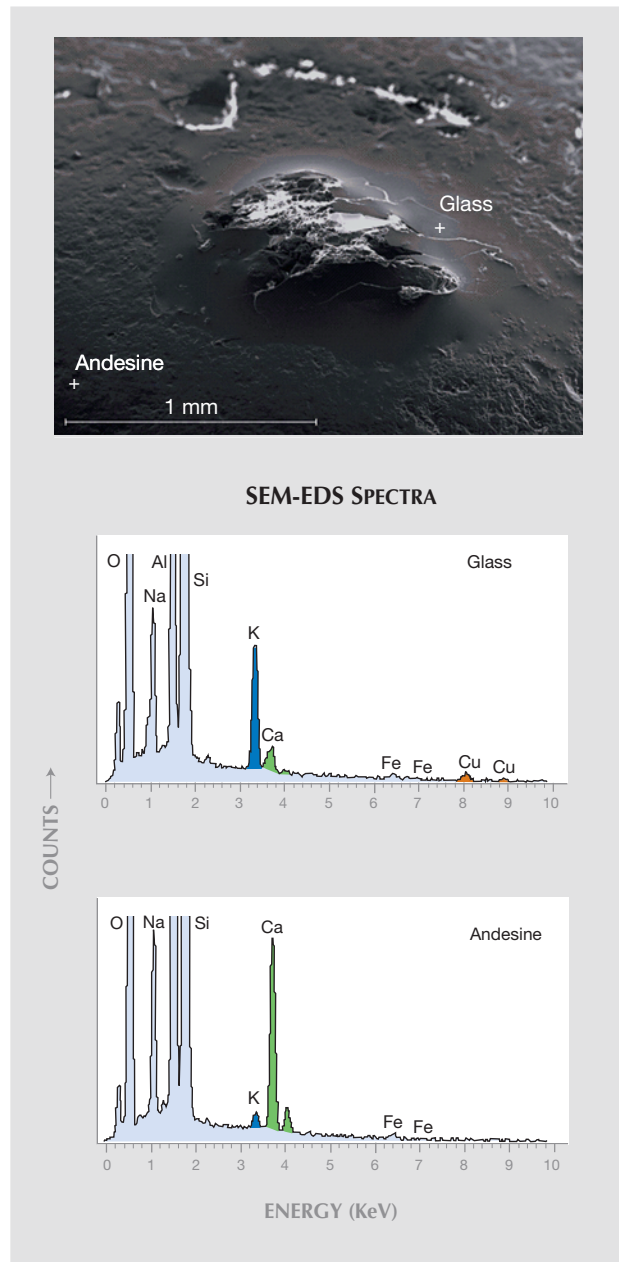

Figure 10. Scanning electron microscopy shows the smooth, glassy region surrounding a fragment fused to the surface of a rough andesine reportedly from Tibet/"China." The SEM-EDS spectra show much greater potassium (K) and copper (Cu) contents in the glassy material than in the andesine, consistent with the possibility that this sample has been in contact with a copper-containing flux. Image by Chi Ma.

diffusion of copper. In ceramics, copper compounds are well-known ingredients in red-colored glazes. And, as noted above, copper is also known to produce a red color when dispersed as colloidal particles.

Diffusion of Copper into Plagioclase. Diffusion experiments conducted in our laboratory in September and October of 2008 found that copper easily enters plagioclase at temperatures above 1200°C, a result independently observed by others (Furuya, 2008; Emmett and Douthit, 2009). Our results also showed that copper diffuses into plagioclase much more readily than cobalt or nickel. These experiments were consistent with the possibility that red andesine was a product of laboratory diffusion, but were not absolute proof that diffusion actually was being used as a treatment process. The fact that something *can* be done is not proof that it *is* being done.

The 2008 GAAJ Expedition. Even so, by 2008 there was substantial evidence that much of the red andesine on the market was treated by a method involving high-temperature diffusion of copper into pale yellow andesine from Inner Mongolia. Yet questions remained about the existence of a natural red andesine mine in Tibet. To address this possibility, an expedition that included representatives of the Gemmological Association of All Japan–Zenhokyo (GAAJ), the Japan Germany Gemmological Laboratory (JGGL), and JTV visited an area near Shigatse, Tibet, that was identified as the Bainang mine. There they were told that gem-quality feldspar had been mined from an alluvial deposit since 2006 (Abduriyim, 2008, 2009). Eighteen samples of rough from this expedition were provided to the author by the GAAJ and JTV representatives.

Further Analytical Work. *Argon Isotopic Analyses.* More stringent proof of high-temperature treatment was offered by argon isotopes. Potassium-40 (^{40}K) is a naturally occurring radioactive isotope in many minerals, including feldspar. Over geologic time, ^{40}K decays to argon-40 (^{40}Ar), a gas with a 1.3 billion year half-life. ^{40}Ar is called *radiogenic* argon because it forms by radioactive decay. It remains within the crystal structure but can escape if heated sufficiently. For example, while mineral crystals are held in a magma chamber, the heat of the magma quickly drives out the Ar gas. Once the volcano erupts, the crystal will ultimately reach a much cooler environment, such as when it sits near the surface of the

earth after eruption. The ^{40}Ar returns over geologic time via decay from ^{40}K, but it is trapped within the crystal because near-surface temperatures are not high enough to remove it. In the case of andesine, traces of potassium were detected in all of the Tibetan/"Chinese," Inner Mongolian, and Congolese feldspars tested. All had a chemical composition of approximately $(Na_{0.51}Ca_{0.47}K_{0.02})[Al_{1.44}Si_{2.55}Fe_{0.01}]O_8$. Radiogenic argon would have built up over time in the ground, but when heated in the laboratory, it would escape.

The argon released from natural, untreated feldspar will have a high ratio of ^{40}Ar to ^{36}Ar (the latter isotope exists naturally in air and can enter feldspars along cracks and cleavages). But if the feldspar was previously heated in a moderate- to high-temperature laboratory process, such as required for copper diffusion, then most of the radiogenic argon would have been released, and the experimental measurement would yield an ^{40}Ar-to-^{36}Ar ratio close to that of air

(about 300). Thus, this measurement would offer a clear indication of whether a specific sample had ever been subjected to heat treatment.

Argon-release experiments were conducted from August 2008 through July 2009 on pale yellow andesine rough from Inner Mongolia that was obtained by Jewel Hunter Jack and from GAAJ (2008 expedition), DSN television, and Andegem. Also tested were a variety of rough and faceted red stones labeled as Tibetan or Chinese that were obtained from the same sources, as well as a Bangkok dealer, GIA, Palagems.com, and Jacqueline Li. An additional green faceted stone from China was obtained from DSN. Again, none of the donors knew beforehand what types of testing would be conducted. To be certain that the heat generated during faceting did not invalidate our argon experiments, a sample of yellow rough was faceted by Andegem and then tested with the other samples.

Our experiments involved laser heating the sample to a temperature of about 1000°C under high vacuum, followed by analysis of the argon in a mass spectrometer (see box A and table 2). Experiments on portions of rough yellow andesine that had been heated for two hours to various temperatures (table 3) showed that the temperature of the laser extraction would not cause all of the sample's argon to be released, but it would clearly indicate if the sample had been heated to a temperature high enough to release *most* of the radiogenic argon. One experiment heated a red andesine to a temperature that completely melted the sample (>1450ºC). Under these conditions, the release of argon was more complete, but the step heating and melting experiments showed that it was difficult to release all of the radiogenic argon on a laboratory time scale, even after the sample was melted.

Despite these caveats, the results (figure 11) show a striking difference between the yellow
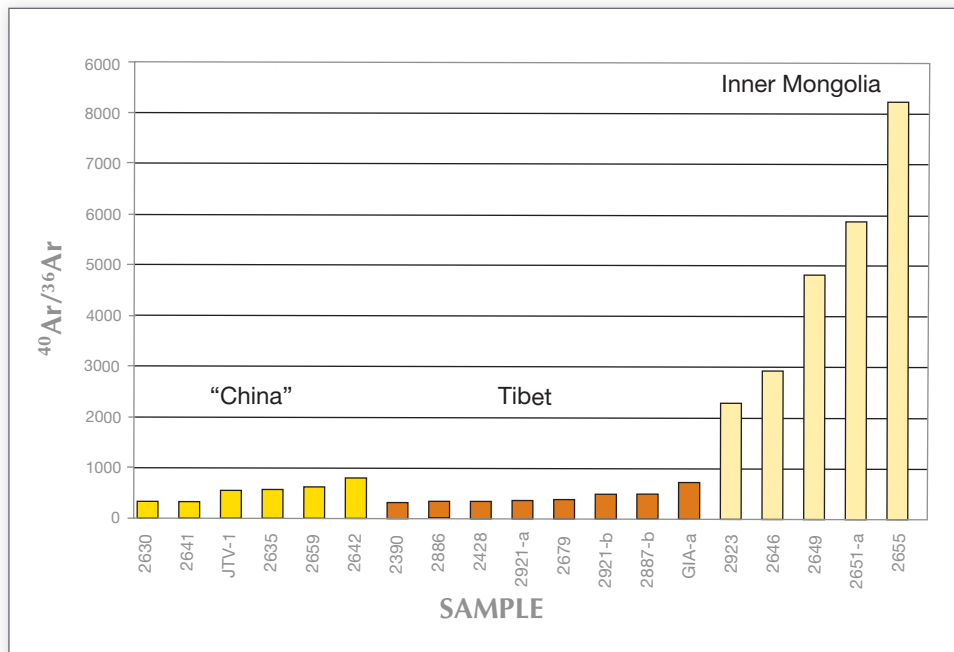
Figure 11. Argon-release experiments conducted on red and green andesine reportedly from Tibet and "China," and on pale yellow andesine from Inner Mongolia, showed significant differences in the ratio of radiogenic ^{40}Ar to ^{36}Ar, which indicate that the Tibetan and "Chinese" samples were depleted of their radiogenic argon by recent exposure to high temperatures. Samples of yellow rough originally stated to be from "China" are placed in the Inner Mongolia results.

rough from Inner Mongolia, which had high ratios of ^{40}Ar to ^{36}Ar, and the red Tibetan/"Chinese" rough and faceted stones, which all had values near atmospheric or slightly above. It was clear the red samples recently had been heated to high temperature.

Scanning Electron Microscopy. SEM study of a red andesine from the 2008 GAAJ expedition revealed smooth areas on the sample that resembled the fused glass on the treated Inner Mongolian andesine. Chemical analyses of one such area showed that it was high in potassium and contained copper, much like the glass observed on the treated andesine. Furthermore, small particles of copper sulfide and a copper-iron-zinc alloy were attached to the surface of the stone (figure 12). The argon isotopic ratio (sample 2921-b) indicated that the sample recently had been heated to high temperature.

Additional Isotopic Analyses. A pale yellow Inner Mongolian rough from Andegem and two Tibetan stones from JTV (obtained on the 2008 expedition to the Bainang mine) were dissolved under clean-laboratory conditions and examined with solution ICP–mass spectrometry. The analyses mainly targeted lead isotopes that form from the decay of naturally radioactive thorium and uranium. Thorium-232 has a half-life of about 14 billion years and decays to lead-208. Uranium-238 has a half-life of about 4.5 billion

TABLE 4. Isotope ratios for andesine samples.

Isotope ratio	Inner Mongolia (yellow)	Tibet (red)
$^{207}Pb/^{208}Pb$	4.0 ± 0.1	4.1 ± 0.1
$^{208}Pb/^{206}Pb$	2.0 ± 0.1	2.1 ± 0.1
$^{88}Sr/^{43}Ca$	13.7 ± 0.1	13.6 ± 0.1
$^{137}Ba/^{43}Ca$	0.13 ± 0.01	0.14 ± 0.01
$^{66}Zn/^{88}Sr$	0.0003 ± 0.00005	0.0004 ± 0.00005

Figure 12. These SEM images show microscopic particles of copper sulfide (left) and a copper-iron-zinc alloy (right) attached to the surface of an andesine sample from the 2008 GAAJ expedition to Tibet. Images by Chi Ma.
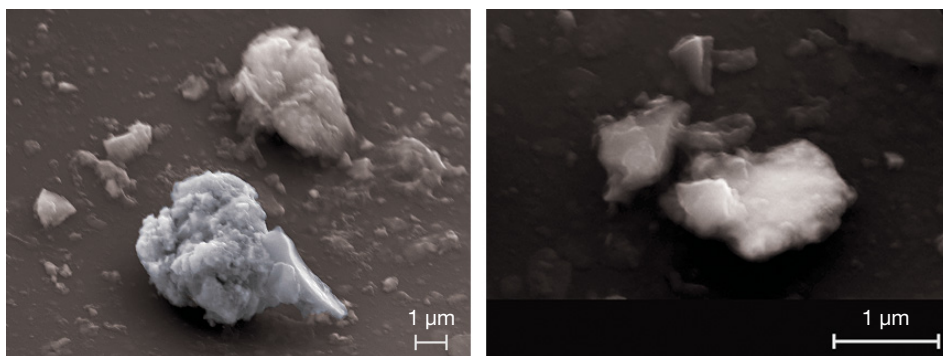
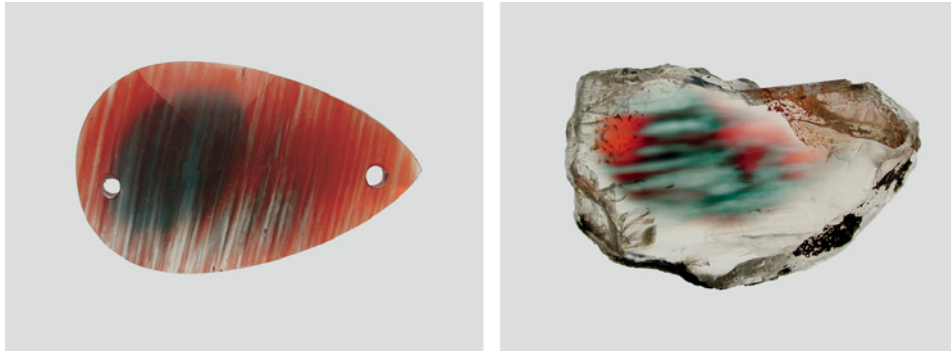*Figure 13. Color bands were seen in much of the andesine reportedly from Tibet and "China" (left, 23 mm wide), but also in some samples from Oregon (right, 19 mm wide, from the Ponderosa mine). Photos by G. R. Rossman.*

years and decays to lead-206, whereas uranium-235 has a half-life of about 700 million years and decays to lead-207. It is extraordinarily unlikely that two deposits of feldspar separated by 2,300 km would have formed with the same geologic age, the same trace concentrations of uranium and thorium, and the same proportions of uranium and lead isotopes.

The results showed the isotopic ratios were essentially identical within measurement error (table 4), suggesting that the samples were from the same source. Some additional isotopic ratios of divalent minor and trace elements measured in the analyses also were strikingly similar in the feldspars from the two localities. The combination of the argon contents, SEM studies, and various isotopic ratios made it very difficult to accept that these samples came from different deposits.

Differences in Appearance. Differences between the Oregon sunstones and the Tibetan/"Chinese" red andesine examined by this author ranged from subtle to obvious. The latter material generally had far fewer copper flakes than the Oregon sunstones. A much larger proportion of the Tibetan/"Chinese" samples contained linear bands of color (again, see figure 3 and figure 13, left), though some banding was also seen in a fraction of the Oregon sunstones (figure 13, right). The pattern of core-to-rim color zoning favors green cores in the Tibetan/"Chinese"

material and red cores in the Oregon sunstones, but exceptions do exist (e.g., figure 14). However, none of these differences offers proof of laboratory treatment. The coloration of both materials appears to be the result of diffusion: natural diffusion in the case of Oregon sunstone, probably occurring during the eruptive event, and laboratory diffusion in the case of the Tibetan/"Chinese" andesine we tested.

The Olympic Games Andesine. In August 2008, the author examined stones that had been internally laser-engraved (Garabedian and Garabedian, 2009) with an image of the Olympic rings and sold as a souvenir of the 2008 Summer Games held in Beijing (figure 15, left). Claims surfaced on the Internet that these were actually Mexican labradorite, diffused and sold as Tibetan/"Chinese" feldspar (James, 2008b). Chemical testing easily distinguished these souvenirs from Mexican material and showed that they were identical in composition to the heated Asian andesine (figure 15, right).

A Mine in the Democratic Republic of the Congo? A single faceted red andesine represented as coming from the Democratic Republic of the Congo was obtained from GemFrance in April 2009. It was subjected to argon-isotopic studies in July 2009, and fell within the same range as samples stated to be from Tibet and China (table 2). Furthermore, its chemical
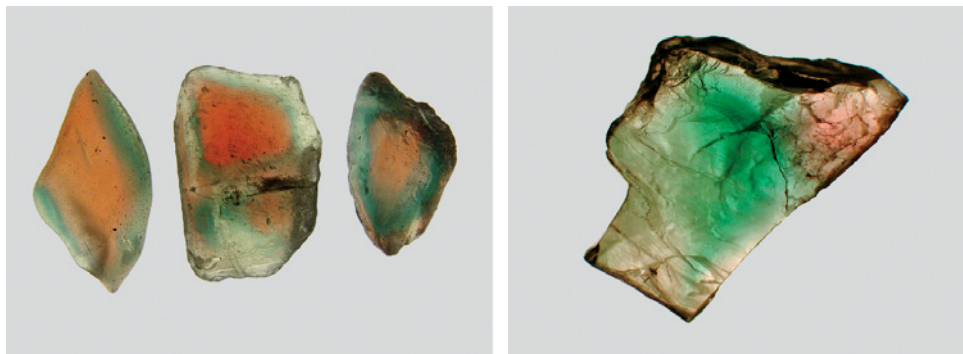

Figure 14. Although green cores are typical of concentrically zoned Tibetan/"Chinese" andesine, some samples contain red cores (left, 1.5–2.3 cm). Likewise, most zoned Oregon labradorites have red cores, but some have green cores (right, 1.8 cm). Photos by G. R. Rossman.

BOX B: FELDSPAR NOMENCLATURE

The common feldspars are a group of minerals that span a range of compositions with varying proportions of sodium, potassium, and calcium in addition to aluminum and silicate. They are classified into *alkali feldspars* and *plagioclase feldspars*.

The alkali feldspars form a continuous solid solution between the sodium feldspar albite and the potassium feldspars—sanidine, orthoclase, and microcline—where the three names reflect the degree of silicon and aluminum ordering on the tetrahedral sites, which in turn determine if the feldspar is monoclinic or triclinic. They tend to have comparatively little calcium in their compositions. Collectively, they are called K-feldspars after the chemical symbol for potassium (K).

The plagioclase feldspars form a continuous solid solution between the sodium feldspar albite and the calcium feldspar anorthite (see table B-1). There can also be minor amounts of potassium replacing some of the sodium and of iron replacing some of the aluminum. Historically, the plagioclase feldspars have been subdivided into six different names depending on the proportions of sodium and calcium in their composition.

Feldspar compositions are commonly plotted on a ternary diagram that indicates the proportions of potassium, sodium, and calcium (figure B-1). On this diagram, the range of analyzed compositions (by electron microprobe analysis) are indicated for feldspars from Tibet/"China," Inner Mongolia, Mexico, and Oregon (from Lake County, and also the Ponderosa mine in Harney County). Because the Asian feldspars occur on both sides of the 50% calcium proportion boundary, some are classified by the nomenclature as *andesine* (less than 50%), and some are *labradorite* (more than 50%).

Feldspar nomenclature can be even more complicated. During growth from a melt in a magma chamber, plagioclase feldspar often changes composition such that the inner portion of the crystal can have a somewhat different composition than the rim. Consequently, a single crystal may have different names depending on the portion analyzed. In this case, the plagioclase nomenclature distinction does not indicate a fundamental difference in the feldspar other than a minor difference in composition.

The Asian feldspars are also displaced vertically from the horizontal axis due to their slightly higher potassium content. It is this potassium that makes the argon isotope analysis possible.

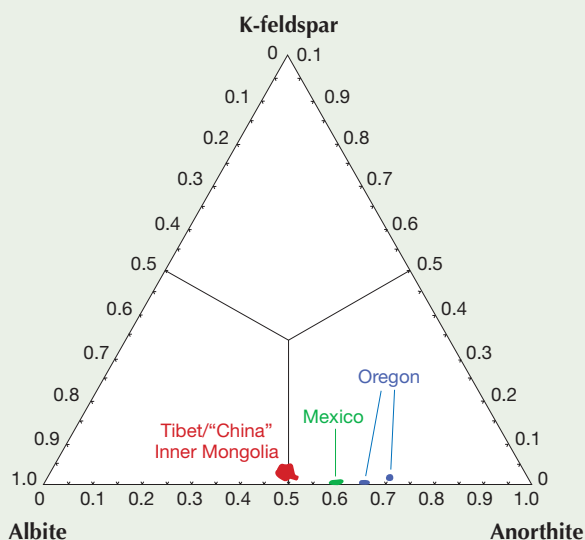*Figure B-1. The chemical composition of plagioclase samples from Tibet/"China," Inner Mongolia, Mexico, and Oregon analyzed by the author are depicted in this ternary diagram.*

TABLE B-1. Plagioclase feldspars.

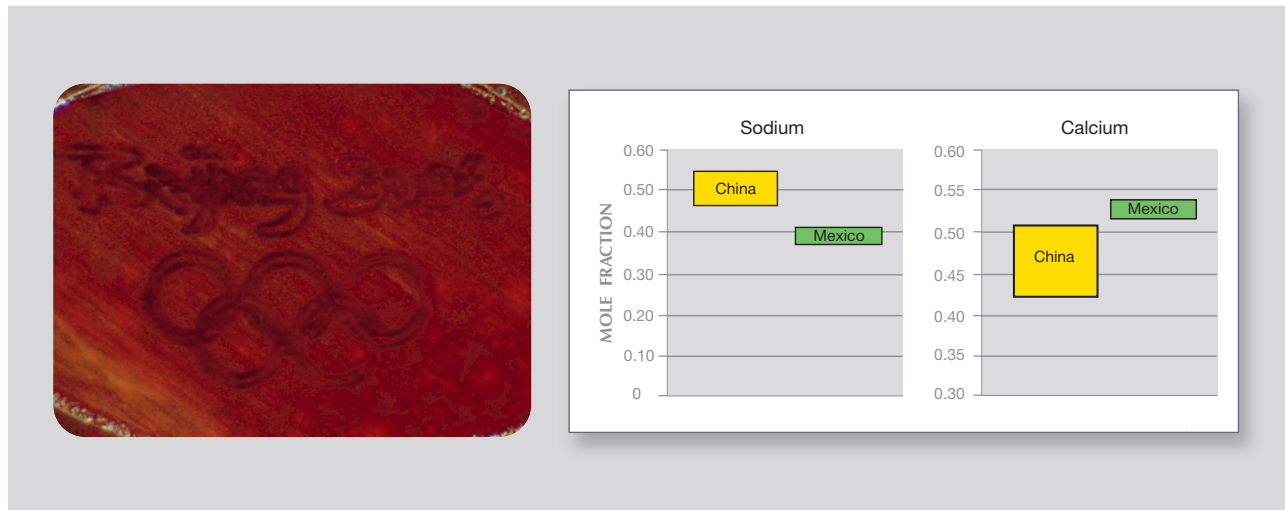|	Na	Ca
Albite	100–90%	0–10%
Oligoclase	90–70%	10–30%
Andesine	70–50%	30–50%
Labradorite	50–30%	50–70%
Bytownite	30–10%	70–90%
Anorthite	10–0%	90–100%

Figure 15. Red laser-engraved andesine in faceted 5 × 7 mm ovals was sold by DSN as souvenirs of the 2008 Beijing Olympics. Comparison of the proportions of sodium and calcium between these samples and Mexican feldspar clearly reveals their differences. The composition of the emblem-engraved stones falls within the range of the heated Asian andesine. Photo by G. R. Rossman.

composition matched the treated Tibetan/"Chinese" feldspar (see *G&G* Data Depository). These results clearly raise doubts that there is a Congolese source of natural red andesine.

SUMMARY THROUGH MID-2009

Andesine from Tibet/"China" (e.g., figure 16) has been surrounded by controversy. Many of the results presented above have already appeared to some extent on the Internet (e.g., "Special issue on red feldspar," 2009) and have been observed independently by various individuals and laboratories worldwide. Rumors of possible treatment were known early in this author's work on the material, but definitive proof was lacking.

The argon-isotope results offer the most compelling evidence of widespread high-temperature treatment of Tibetan/"Chinese" andesine. Coupled with the observation of what appear to be copper-containing fluxes on the surface, and the occasional microscopic bits of copper compounds attached to the stones, the case for copper-diffused andesine from Inner Mongolia is strong. In fact, according to Christina Iu (pers. comm., 2011), it is now freely admitted by some Asian dealers. Nevertheless, this does not eliminate the possibility that there is also a source of natural-color andesine in Tibet, and samples obtained from a subsequent expedition in September 2010 (e.g., Abduriyim and Laurs, 2010) have been the focus of further research that will be reported in a future article.

Figure 16. The source and natural versus treated color origin of "Chinese" andesine continues to be controversial. These stones (5.90–21.45 ct) were cut from material reportedly mined in Tibet. Courtesy of Litto Gems; photo by Robert Weldon.

REFERENCES

Abduriyim A. (2008) Gem News International: Visit to andesine mines in Tibet and Inner Mongolia. *G&G*, Vol. 44, No. 4, pp. 369–371.

Abduriyim A. (2009) A mine trip to Tibet and Inner Mongolia: Gemological study of andesine feldspar. News from Research, www.gia.edu/research-resources/news-from-research/andesine-mines-Tibet-Inner-Mongolia.pdf, Sept. 10.

Abduriyim A., Kobayashi T. (2008) Gem News International: Gemological properties of andesine collected in Tibet and Inner Mongolia. *G&G*, Vol. 44, No. 4, pp. 371–373.

Abduriyim A., Laurs B.M. (2010) Additional field research on Tibetan andesine. *G&G*, Vol. 46, No. 4, pp. 310–311.

Amidon W.H., Farley K.A. (2010) Mass spectrometric ^{3}He measurements in ^{4}He-rich phases: Techniques and limitations for cosmogenic ^{3}He dating of zircon, apatite, and titanite. *Geochemistry Geophysics Geosystems*, Vol. 11, No. 10, Art. Q10004 [9 pp.].

Anderson O. (1917) Aventurine labradorite from California. *American Mineralogist*, Vol. 2, p. 91.

Armstrong J.T. (1995) CITZAF: A package of correction programs for the quantitative electron microbeam X-ray analysis of thick polished materials, thin films, and particles. *Microbeam Analysis*, Vol. 4, pp. 177–200.

Cao Y. (2006) Study on the feldspar from Guyang County, Inner Mongolia, and their color enhancement. Master's thesis, China University of Geosciences, Beijing [in Chinese].

Capatina C. (2005) The study of copper ruby glass. *Ceramics-Silikáty*, Vol. 49, No. 4, pp. 283–286.

Emmett J., Douthit T. (2009) Copper diffusion of plagioclase. News from Research, www.gia.edu/research-resources/news-from-research/Cu-diffusion-Emmett.pdf, Aug. 21.

Federman D. (2006) Gem Profile: Andesine feldspar. *Modern Jeweler*, www.modernjeweler.com/print/Modern-Jeweler/Andesine-Feldspar/1$52, March.

Fritsch E. (2002) Gem News International: Red andesine feldspar from Congo. *G&G*, Vol. 38, No. 1, pp. 94–95.

Furuya M. (2008) Copper diffusion treatment of andesine and a new mine in Tibet. *JGGL Gem Information*, Vol. 37–38, pp. 1–11 [in Japanese].

Garabedian A.C., Garabedian M. (2009) *Method for Introducing Inclusion Image into Gemstone.* United States Patent Application US 2009/0269702 A1.

Hofmeister A.M., Rossman G.R. (1985) Exsolution of metallic copper from Lake County labradorite. *Geology*, Vol. 13, pp. 644–647.

House M.A., Farley K.A., Stockli D. (2000) Helium chronometry of apatite and titanite using Nd-YAG laser heating. *Earth and Planetary Science Letters*, Vol. 183, No. 3-4, pp. 365–368.

Hughes R.W. (2010) Hunting Barack Osama in Tibet: In search of the lost andesine mines. www.ruby-sapphire.com/tibet-andesine.htm, Nov. 3.

James R. (2008a) Sunrise over Oregon. www.yourgemologist.com/ISGForumsBoard/showthread.php?t=5566, Apr. 17.

James R. (2008b) ISG report on the diffusion treatment of andesine! www.yourgemologist.com/ISGForumsBoard/showthread.php?t=5569, Jul. 23.

Johnston C.L., Gunther M.E., Knowles C.R. (1991) Sunstone labradorite from the Ponderosa mine, Oregon. *G&G*, Vol. 27, No. 4, pp. 220–233.

Kratochvil G. (2008) The Great andesine scam. www.jewelcutter.com/articles/andesine_scam.htm, May 17.

Krzemnicki M.S. (2004) Red and green labradorite feldspar from the Congo. *Journal of Gemology*, Vol. 29, No. 1, pp. 15–23.

Laurs B.M. (2005) Gem News International: Gem plagioclase reportedly from Tibet. *G&G*, Vol. 41, No. 4, pp. 356–357.

Laurs B.M., Rockwell K., Breeding C.M. (2006) Gem News International: Labradorite from Chihuahua, Mexico. *G&G*, Vol. 42, No. 4, pp. 274–275.

Li H. (1991) Discovery of feldspar type moonstone gem in Inner Mongolia. *Bulletin of Geological Science and Technology*, Vol. 11, pp. 136–137 [in Chinese].

Li H. (1992) Preliminary study of labradorite-moonstone from Inner Mongolia. *Jewellery*, Vol. 1, No. 6, pp. 45–47 [in Chinese].

Nakai I., Numako C., Hosono H., Yamasaki K. (1999) Origin of the red color of Satsuma copper-ruby glass as determined by EXAFS and optical absorption spectroscopy. *Journal of the American Ceramic Society*, Vol. 82, No. 3, pp. 689–695.

O'Meny C. (2002) Interview de Laurent Sikirdji. www.abc-luxe.com, Sept. 13.

Petrov A. (2010) Anorthite and native brass from Miyake-Jima, Tokyo. www.mindat.org/article.php/976/Anorthite+and+Native+Brass, July.

Pouchou J.-L., Pichoir F. (1991) Quantitative analysis of homogeneous or stratified microvolumes applying the model "PAP." In K.F.J. Heinrich and D.E. Newbury, Eds., *Electron Probe Quantitation*, Plenum Press, New York.

Rossman G.R. (2010) Pierre de soleil de l'Oregon et feldspath rouge de Chine, la controverse. *Revue de Gemmologie a.f.g.*, No. 172, pp. 5–10.

Special issue on red feldspar (2009). News from Research, www.gia.edu/research-resources/news-from-research/special-issue-homepage.html, Aug. 21.

UV-Vis-NIR Reflectance Spectroscopy of Natural-Color Saltwater Cultured Pearls from *Pinctada Margaritifera*

Stefanos Karampelas, Emmanuel Fritsch, Jean-Pierre Gauthier, and Thomas Hainschwang

Natural-color saltwater cultured pearls from *Pinctada margaritifera* were studied by diffuse reflectance UV-Vis-NIR spectroscopy to identify the absorption features associated with their various colors. Nine patterns observed in the visible range demonstrated that individual colors are caused not by one pigment but by a mixture of pigments.

O ver the past 30 years, colored cultured pearls have become very popular (see Komatsu and Akamatsu, 1978; Shor, 2007; and references therein). Until the late 1990s, however, cultured pearl strands were marketed only in single colors: "golden," black, and so forth. Since that time, multi-colored ensembles, some even using cultured pearls from different mollusks, began to see strong demand (figure 1; Elen, 2003; Shor, 2007; Shigley et al., 2010).

Saltwater cultured pearls (SWCPs) from the *Pinctada margaritifera* mollusk are principally grown in French Polynesia, but also in the Cook Islands, Fiji, and other localities (see Shigley et al., 2010). The vast majority of the SWCPs produced are bead-nucleated, and marketed as Tahitian, "black" South Sea, or simply "black" cultured pearls. They have a variety of bodycolors, most commonly black to light gray to white, as well as yellow to green, brown, gray-red, gray-blue, and gray-green. They can also contain strong overtones (i.e., secondary colors), including pink and purple. Combinations of body-colors and overtones give *P. margaritifera* SWCPs a wide range of color appearances (again, see figure 1).

The origin of their color is still under investigation, and a better understanding will help separate natural-color cultured pearls from their treated-color counterparts. This study presents spectral characteristics in the ultraviolet/visible/near-infrared (UV-Vis-NIR) region of natural-color SWCPs from *P. margaritifera*, in an effort to better characterize the mechanisms of their coloration.

MATERIALS AND METHODS

For this study, we selected 21 undrilled SWCPs from *P. margaritifera* in a wide range of colors. The samples ranged from 9.3 to 13.4 mm in diameter (for details on their color and size, see table 1). They were obtained from reputable sources (see acknowledgments) and represented as natural color.

Diffuse reflectance UV-Vis-NIR spectra were obtained at the IMN (Institut des Matériaux Jean Rouxel) for the 250–1600 nm range (only 250–900 nm is presented here because this is the range containing color-related absorption bands) with a Cary 5G spectrometer fitted with a Varian diffuse reflectance accessory. The data sampling interval and spectral bandwidth of each measurement were set at 0.7 nm to achieve a high resolution, and the relatively slow scan rate of 60 nm/minute permitted a satisfactory signal-to-noise ratio. Matte black sample holders with various hole sizes (4–10 mm in diameter) were used so that the sample could be

Figure 1. This bracelet features 32 multicolored round cultured pearls (represented as having natural color) from P. margaritifera, ~10 mm in diameter. Photo © Autore, Sydney, Australia.

positioned for maximum exposed measurement surface (with as homogeneous a color as possible), producing a more intense signal. For samples with inhomogeneous color distribution (again, see table 1), separate spectra were taken from areas of different color. Before each measurement, background spectra were taken using white MgO powder (for 100% reflectance) and matte black card (0%) references. The measurements, which took about 25 minutes each, were repeated at least twice on each sample to confirm the repeatability of the results.

RESULTS

Figures 2 through 5 present the diffuse reflectance UV-Vis-NIR spectra of nine representative natural-color SWCPs. Each spectrum revealed a decrease in diffuse reflectance (i.e., increase in absorption) at about 280 nm, regardless of the sample's color. Figure 2 shows that nearly all the light from the visible part of the spectrum (390–780 nm) is transmitted, consistent with the samples' white bodycolor. Sample SK-208 showed weak absorptions at about 405 and 700 nm, while sample SK-224 had a small absorption from 330 to 460 nm (consisting of two different bands at 330–385 nm and 385–460 nm). However, these weak absorptions did not produce any eye-visible color. Sample SK-223 had small bands at 700 nm and at 330–460 nm (although less intense than in SK-224), as well as a weak absorption that gradually cut through the visible region with a maximum in the near-infrared region at ~820 nm.

This absorption was responsible for the sample's very light gray coloration.

Figure 3 shows the UV-Vis-NIR spectra of the inhomogeneously colored SWCP SK-206, in the grayish yellow and black parts of the sample. As

TABLE 1. Color and size of saltwater cultured pearl samples from *P. margaritifera* used in this study.

| Sample no.	Bodycolor	Size (mm)
SK-205	Light gray	9.6
SK-206	Grayish yellow/Black	11.0
SK-207	Green-yellow/Yellow	10.2
SK-208	White	10.2
SK-209	Black	13.0
SK-210	Blue-black/ Green-blue-black	13.4
SK-212	Green-black	10.9
SK-213	Grayish green-yellow	11.7
SK-214	Red-black	13.2
SK-216	Gray-green/Gray-red	11.0
SK-217	Orange-red-black	10.5
SK-218	Gray-blue/Gray-red	9.3
SK-219	Gray-blue/ Gray-green-yellow	10.0
SK-220	Grayish green-yellow	12.3
SK-221	Grayish greenish yellow	11.4 × 9.2
SK-223	White (slightly gray)	11.6 × 10.5
SK-224	White	12.6 × 8.5
SK-228	Dark gray	10.0
SK-230	Green-black	10.4
SK-231	Red-black	9.6 × 9.4
SK-232	Gray-green-yellow	10.2

UV-Vis-NIR Spectra
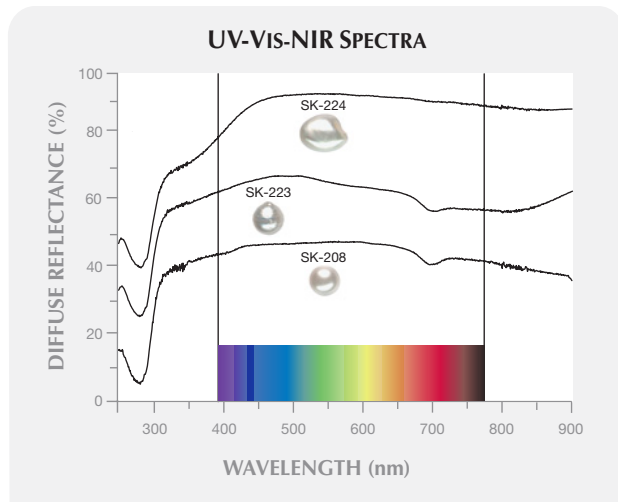
Figure 2. These diffuse reflectance spectra are from three P. margaritifera *SWCPs with a white or very light gray bodycolor. A weak continuous absorption that extends through the visible region with a maximum in the near-infrared region (at about 820 nm) is responsible for sample SK-223's slight coloration; none of the bands in the other spectra produce visible hues. The spectra of SK-223 and SK-208 are shifted down by 15% and 35% for clarity.*

UV-Vis-NIR Spectra
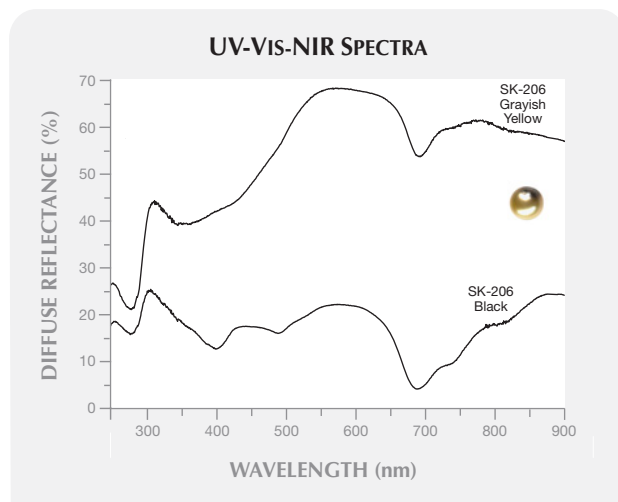
Figure 3. The grayish yellow part of SK-206 shows an intense absorption from 330 to 460 nm, as well as other weak bands and continuous absorption with a maximum at about 820 nm. The black part of the sample (spectrum shifted downward 5% for clarity) shows the same absorptions as the yellow part, and has an additional band at about 530 nm. The absorptions have equal intensity, giving the sample its black color.

expected, the two spectra were different in the visible range. The grayish yellow part had a band from 330 to 460 nm, as well as at 405 and 700 nm, and continuous absorption with a maximum in the near infrared at ~820 nm, similar to the spectra in figure 2. These features were more intense than those of the whitish samples in figure 2. Two additional weak bands at 495 and 745 nm were observed. The yellow color is due to the relatively stronger absorption from the UV-to-blue range; a grayish color is probably due to the continuous absorption. The spectrum from the black part of the sample shows the same bands observed in the yellow area, as well as an additional absorption at about 530 nm. The black color occurs because all the absorptions are equally intense.

The spectra of black (SK-209) and dark gray (SK-228) cultured pearls are presented in figure 4. The same absorptions seen in the black portion of sample SK-206 are observed, along with two additional barely visible bands at about 585 and 625 nm. The two spectra taken from black surface areas presented in figures 3 and 4 vary due to the different relative intensities of the same bands.

Figure 5 shows the spectra of three natural

NEED TO KNOW

- Reflectance spectra collected from natural-color *P. margaritifera* cultured pearls show various absorptions according to bodycolor.

- The diversity of absorptions suggests that the cultured pearls' coloration is due to combinations of several pigments.

- Uroporphyrin has been confirmed as one of the pigments, but additional research is needed to identify the exact nature of the others.

SWCPs of other colors: the blue-black portion of SK-210, orange-red-black sample SK-217, and red-black sample SK-231. Bands occur at the same wavelengths as in the previous spectra, but with different relative intensities. The spectrum taken from the blue-black sample showed a spread of absorptions across the visible range that produced the black color. A diffuse reflectance maximum (i.e., transmission maximum) was also observed in the blue range

UV-Vis-NIR Spectra

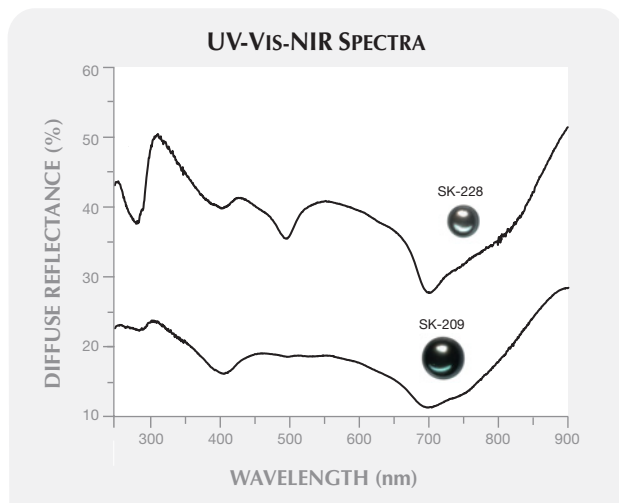*Figure 4. The diffuse reflectance spectra of a a dark gray (SK-228) and black (SK-209) SWCP from* P. margaritifera *are similar to those of the black portion of SK-206. The absorptions from the black bodycolors (SK-206 and SK-209) are more intense than those observed in the dark gray sample (SK-228). The SK-209 spectrum is shifted downward by 5% for clarity.*

from ~450 to 490 nm. The spectrum taken on the orange-red-black SWCP showed absorptions across the visible range that are responsible for the black coloration. The bands in the orange-red portion, from about 580 to 780 nm, are less intense than elsewhere in the spectrum, and this caused the orange-

Figure 5. A series of absorptions in the reflectance spectra for the blue-black portion of sample SK-210, orange-red-black SK-217, and red-black SK-231, at the same wavelengths as in the previous spectra, explains their black coloration.

UV-Vis-NIR Spectra
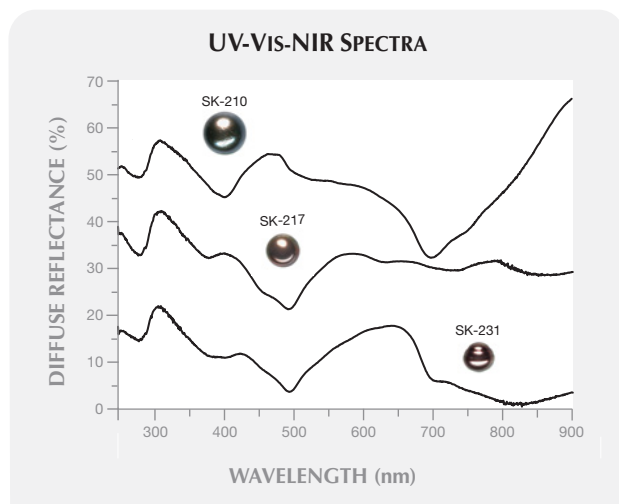
red coloration. The spectrum on the red-black sample showed bands across the visible range causing the black coloration, and a diffuse reflectance window in the red portion with a maximum at about 650 nm that caused the red bodycolor.

DISCUSSION

Nine visible-range absorption features were observed in the spectra of natural-color SWCPs from *P. margaritifera*: a continuous band extending through the visible range with a maximum in the near infrared (at ~820 nm), an absorption from the ultraviolet to blue portion of the spectrum (330–460 nm, consisting of two bands at 330–385 nm and 385–460 nm); two others in the blue region (at 405 and 495 nm); three absorptions in the green-yellow-orange region (at 530, 585, and 625 nm); and two in the red (at 700 and 745 nm).

Some of these bands have been documented previously in natural-colored SWCPs from *P. margaritifera*: those at 405, 495, and 700 nm (Cuif et al., 1993; Dauphin and Cuif, 1995; Elen, 2003; Huang, 2006; Wang et al., 2006) and from 330 to 460 nm (Elen, 2003). Slight differences in band position between the present study and earlier ones are probably due to the different parameters we used for the measurements (i.e., higher-resolution spectra). In other studies, some of the bands seen in SWCPs from *P. margaritifera* were also found in similarly colored SWCPs from *Pteria sterna* (Kiefert et al., 2004). However, some bands present in spectra from *P. margaritifera* are absent from those of *P. sterna*, and vice versa (authors' unpublished research).

The particular color shown by SWCPs from *P. margaritifera* depends on the relative intensity of several absorptions, which are probably due to various combinations of pigments. Applying a tentative simplified approach, there should be as many absorptions bands as there are pigments in any sample (i.e., up to nine). To our knowledge, only the cause of the 405 nm band has been identified; it is attributed to a kind of porphyrin called uroporphyrin (Iwashi and Akamatsu, 1994). Porphyrins are a type of tetrapyrrole, composed of four modified pyrrole (C_4H_4N) rings interconnected via methine bridges. A combination of melanins (Caseiro, 1993) as well as other tetrapyrroles could produce some of the other patterns observed in the visible region of the spectrum. A study of the precise relationship between the samples' optical absorption and photoluminescence characteristics and a comparison with isolated natural pigments is ongoing.

Figure 6. These two necklaces show the diversity of color (here represented as natural) in cultured pearls from P. margaritifera (10–14 mm in diameter on the left, and 8–9 mm on the right). Courtesy of Armand Asher Pearls, New York; photo by Robert Weldon.

CONCLUSION

SWCPs from *P. margaritifera* feature a variety of natural bodycolors (figures 1 and 6). UV-Vis-NIR spectroscopy reveals that their specific color is due to the relative intensity of several absorption features (probably up to nine). Uropor-phyrin is the only pigment that has been conclusively identified so far. Further research using other spectroscopic methods on different natural-color SWCPs from *P. margaritifera* and on isolated natural pigments is needed to identify other factors involved in their coloration.

REFERENCES

Caseiro J. (1993) La Nacre Noire de Polynésie. PhD thesis, Université Claude Bernard, Lyon, France, 386 pp.

Cuif J-P., Dauphin Y., Stoppa C., Beeck S. (1993) Forme, structure et couleurs des perles de Polynésie. *Revue de Gemmologie a.f.g.*, No. 115, pp. 9–11.

Dauphin Y., Cuif J-P. (1995) Trichromatic characterization of the "black pearls" from aquaculture centers of French Polynesia. *Aquaculture*, Vol. 133, No. 2, pp. 113–121.

Elen S. (2003) Identification of yellow cultured pearls from the black-lipped oyster *Pinctada margaritifera*. *G&G*, Vol. 38, No. 1, pp. 66–72.

Huang Y.L. (2006) Visible absorption spectrum representation of Tahitian black pearls and treated pearls. *Journal of Gems and Gemmology*, Vol. 8, No. 1, pp. 5–8.

Iwahashi Y., Akamatsu S. (1994) Porphyrin pigment in black-lip pearls and its application to pearl identification. *Fisheries Science*, Vol. 60, No. 1, pp. 69–71.

Kiefert L., Moreno D.M., Arizmendi E., Hänni H.A., Elen S. (2004) Cultured pearls from the Gulf of California, Mexico. *G&G*, Vol. 40, No. 1, pp. 26–39.

Komatsu H., Akamatsu S. (1978) Differentiation of black pearls. *G&G*, Vol. 16, No. 1, pp. 7–15.

Shigley J.E., Laurs B.M., Janse A.J.A., Elen S., Dirlam D.M. (2010) Gem localities of the 2000s. *G&G*, Vol. 46, No. 3, pp. 188–216.

Shor R. (2007) From single source to global free market: The transformation of the cultured pearl industry. *G&G*, Vol. 43, No. 3, pp. 200–226

Wang W., Scarratt K., Hyatt A., Shen A.H.-T., Hall M. (2006) Identification of "chocolate pearls" treated by Ballerina Pearl Co. *G&G*, Vol. 42, No. 4, pp. 222–235.

For online access to all issues of **GEMS & GEMOLOGY** from 1981 to the present, visit:

gia.metapress.com

BROWNISH RED ZIRCON FROM MULING, CHINA

Tao Chen, Hao Ai, Mingxing Yang, Shu Zheng, and Yungui Liu

Gem-quality brownish red zircon occurs in alluvium derived from Tertiary alkali basalt at Muling in the northeast Chinese province of Heilongjiang. Rough and cut samples were characterized using standard gemological methods, electron microprobe, LA-ICP-MS, and Raman and UV-Vis-NIR spectroscopy. Internal features consisted of melt inclusions, apatite, magnetite, fluid inclusions, and color zones. The samples contained abundant rare-earth elements, but showed only slight radiation damage and properties consistent with "high" zircon. Although it has yet to be mined commercially, the Muling deposit is a promising source of gem zircon.

Zircon ($ZrSiO_4$) is a common accessory mineral, occurring in a wide variety of sedimentary, igneous, and metamorphic rocks (Finch and Hanchar, 2003). Often appearing as small, rounded grains, zircon also can form large (up to a centimeter or more), well-formed prismatic crystals. Zircon has long been used as a gem material because of its high dispersion and relatively high refractive index (Faulkner and Shigley, 1989). Major sources of gem zircon are Sri Lanka, Madagascar, Cambodia, and Tanzania (Shigley et al., 2010). The present study provides a detailed characterization of brownish red zircon from Muling, China (e.g., figure 1).

LOCATION AND GEOLOGIC BACKGROUND

Muling is a city of more than 300,000 in the northeastern Chinese province of Heilongjiang (figure 2). It lies in the mid-northern section of the Dunhua-Mishan fault, which forms the northern branch of the Tanlu fault (Qiu et al., 2007). Zircon is known from three main deposits within the city limits—at Gangouzi, Fusheng, and Hanchangou—where it occurs in alluvium derived from weathered Tertiary alkali basalt. The gems have been recovered from areas measuring up to 1700 m long and 20–200 m wide, at depths of 0.3–1.2 m. Associated heavy minerals in the alluvium include yellow, blue, pink, and colorless sapphire; garnet; and spinel (with some of these three in gem quality); enstatite, olivine, and chromite also occur. All of these minerals were probably originally transported to the earth's surface as megacrysts in the alkali basalt. U-Pb age dating indicates the zircon has a crystallization age of 9.39 ± 0.4 million years.

The Muling deposits were discovered in 1985, but mining is still limited. So far, it has consisted of informal surface digging by local people, who extract the gems by hand after washing the alluvial material. Zircon is more common than corundum, and it has been recovered as a byproduct of sapphire mining. The commercial potential of the deposits has not been evaluated, nor have the source rocks for the gems been located.

MATERIALS AND METHODS

The materials examined were either recovered on site by author HA or purchased from local miners. The samples consisted of 17 rough pieces, 3 faceted stones, and 23 polished plates (~1 mm thick). Most of the plates were cut in specific orientations—that is, parallel (11 plates) or perpendicular (10 plates) to the c-axis. The rough zircons ranged from 4 × 2 × 2 mm to 17 × 6 × 5 mm, and the faceted stones weighed 0.40–1.33 ct (see, e.g., figure 3). Refractive indices on small crushed fragments (<0.5 mm) derived from five pieces of rough were measured using immersion oil

---

Figure 1. Muling, in northeastern China, is the source of these brownish red zircons (1.90–3.33 ct). Photo by Robert Weldon.

and the Becke line method. Other standard gemological properties (pleochroism, SG, fluorescence, and absorption spectrum with the hand spectroscope) were obtained from the rough samples and nine of the polished plates. All of the polished plates were observed for microscopic features.

Chemical composition was measured on five of the polished plates (cut from four samples). Major elements were analyzed by electron microprobe using a JEOL JXA-8100 instrument. The analyzed elements included Mg, Ca, Mn, Al, Zr, Fe, Si, and Hf. Trace-element concentrations, including rare-earth elements (REE), were measured by laser ablation–inductively coupled plasma–mass spectrometry (LA-ICP-MS). Laser sampling was performed using a MicroLas Geolas 2005 system equipped with a 193 nm ArF-excimer laser. Helium was selected as the carrier gas to enhance transport efficiency of the ablated material. Argon was used as the makeup gas and mixed with the carrier gas before entering the ICP. An Agilent 7500a ICP-MS was utilized to acquire ion-signal intensities. Sampling pits had a
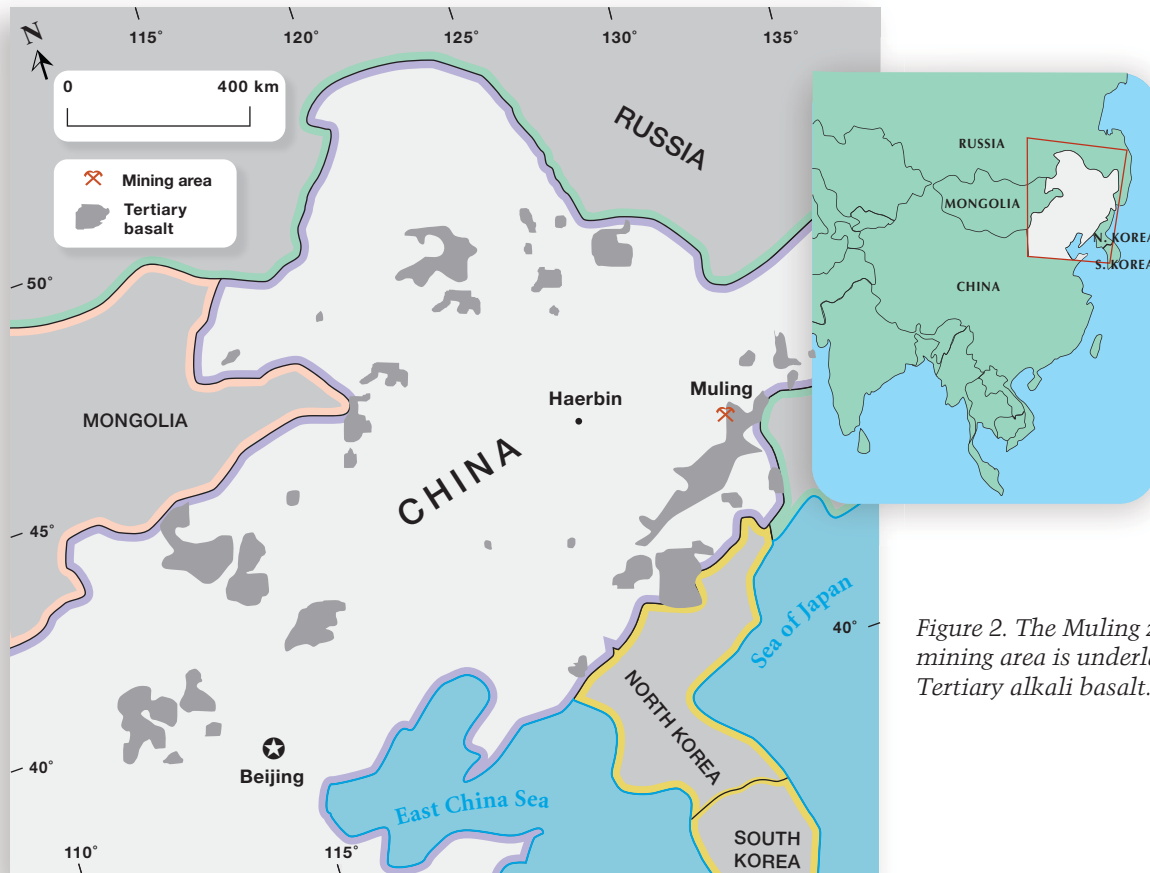

Figure 2. The Muling zircon mining area is underlain by Tertiary alkali basalt.
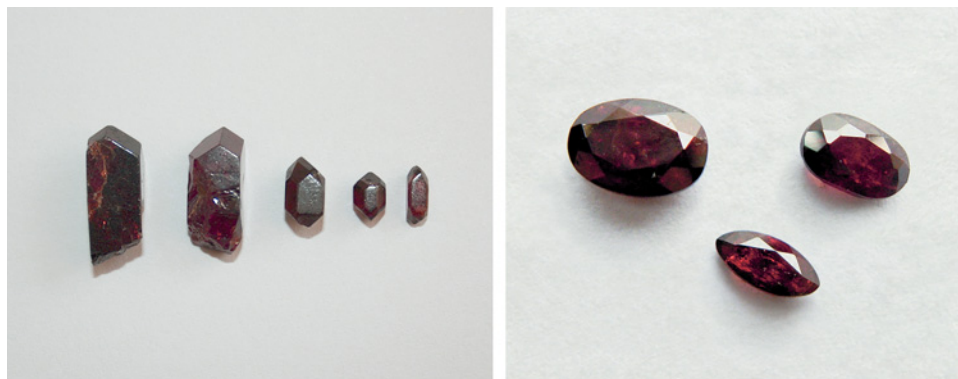
Figure 3. These rough (left, 0.07–0.84 g) and faceted (right, 0.40–1.33 ct) zircons are some of the samples examined for this report. Photos by T. Chen.

diameter of about 60 μm. Each analysis included an approximately 20 second background acquisition followed by 50 seconds of data acquisition. Calibration was performed using NIST SRM 610 glass as an external standard in conjunction with internal calibration using Si following the methods of Longerich et al. (1996) and Günther et al. (1999). The SRM 610 standard was selected because it contains concentrations of certain elements that are close to those in the zircon samples of this study. Analyses of USGS rock standards (BIR-1G and BHVO-2G) indicated that the precision (1σ, relative standard deviation) was better than 10% for trace elements.

Raman spectra of the zircon and its inclusions were recorded with a Renishaw MKI-1000 spectrometer coupled to an argon-ion laser (514.5 nm). In each experiment, three scans were collected and averaged. Polarized UV-Vis-NIR absorption spectra were measured using a Shimadzu UV-1601 spectrophotometer in the 200–800 nm range, with a step interval of 0.5 nm and scan speed of 2.64 nm/second. Both types of spectra were recorded from nine oriented polished plates.

Three reddish brown and two dark brownish red zircon crystals were chosen for heat treatment experiments. Heating was carried out in air using a YFX 9/13Q-YC furnace. The samples were placed in quartz sand in a corundum crucible and heated from room temperature to 1100°C at a rate of 5°C/minute. After annealing at the target temperature for 24 hours, the samples were cooled for 6 hours. The furnace door was opened slightly when the temperature cooled to about 150°C, and the samples were removed at approximately room temperature.

RESULTS AND DISCUSSION

Gemological Properties. The crystals showed a combination of tetragonal prismatic and pyramidal faces. The samples ranged from red to brownish red, and were generally transparent to translucent with some cracks. Their refractive indices (>1.81) and specific gravity values (4.57–4.69) were consistent with "high" zircon (e.g., O'Donoghue, 2006). The hand spectroscope showed no absorption features except for faint lines below 600 nm in some samples; no characteristic absorption lines in the red region were noted.

Melt inclusions were common, occurring individually and in groups. These inclusions were cap-

NEED TO KNOW

- Brownish red zircon is produced as a byproduct of artisanal mining for basalt-derived sapphires at Muling in northeastern China.

- The zircon is only slightly metamict, with properties that are consistent with "high" zircon.

- The brownish red coloration is due to radiation damage, and the stones can be lightened by heating in air.

tured during crystal formation and record the conditions present during their growth. Glass melt inclusions formed dark ovoids, as seen previously in zircon by Thomas et al. (2003). Some melt inclusions, ranging from ~10 to 50 μm, consisted of metamict zircon surrounded by a decrepitation halo; each metamict zircon typically contained one or two internal voids (figure 4). Two apatite inclusions were observed, one a short semitransparent crystal and the other a long colorless transparent prism (figure 5). A group of dark brownish red crystals in one sample (figure 6) were identified as magnetite. Parallel color zones, fractures, and fluid inclusions also were observed in some samples.

Chemical Composition. Trace-element signatures in igneous zircons are linked to their source-rock type and crystallization environment. Table 1 lists the
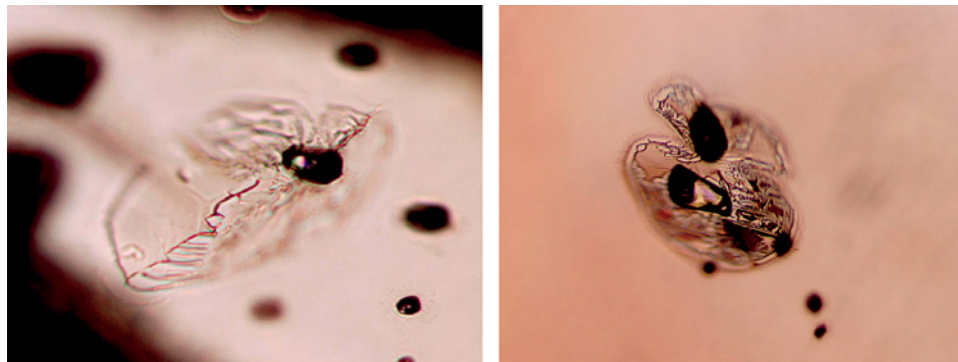
Figure 4. Metamict zircon inclusions in the zircon samples often contain one or two voids and have halos of small decrepitated melt inclusions surrounding them. Photomicrographs by T. Chen; magnified 200× (left) and 100× (right).
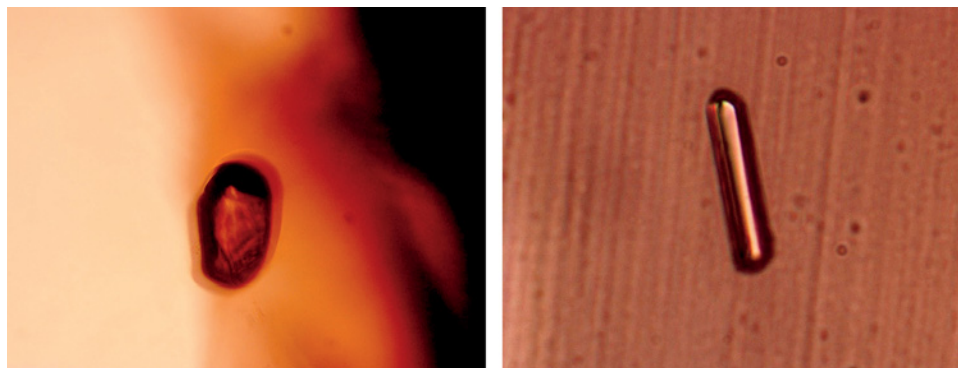
Figure 5. Apatite inclusions were observed as high-relief stubby crystals (left, 66 μm long) and colorless prisms (right, 110 μm long). Photomicrographs by T. Chen.

major- and trace-element composition of four zircons from Muling. The predominant impurities were Hf, Al, Mg, Ca, Y, REE, P, Th, and U. The concentrations of Th (355–2440 ppm) and U (341–871 ppm) were high enough that they would be expected to cause metamictization of zircon over time. The relatively high concentration of rare-earth elements (again, see table 1) indicates that the Muling zircons came from mafic rocks (Fan et al., 1998).

Raman Spectroscopy. Figure 7 shows the polarized Raman spectra of four representative samples of Muling zircon. Some of the main features include the internal modes at 1005 cm^{-1} (Si–O ν_3 stretching), 973 cm^{-1} (Si–O ν_1 stretching), and 438 cm^{-1} (Si–O ν_2 bending). The assignments of the bands at 393 and 356 cm^{-1} are still the subject of debate, and have been described as internal or external modes. The three bands at 224, 213, and 201 cm^{-1} are generally considered lattice modes, such as vibrations involving SiO$_4$ tetrahedrons and Zr ions (Hoskin and Rodgers, 1996; Nasdala et al., 2003). The reason for variations in the relative intensity of the most prominent bands at 1005 and 356 cm^{-1} has not yet been well explained.

Nasdala et al. (1998) showed that Raman spectra of slightly to moderately metamict zircons have the same band pattern as crystalline zircon; however,

the full width at half maximum (FWHM) of the intense mode at about 1000 cm^{-1} increases as a function of radiation damage (Nasdala et al., 1998). In well-crystallized zircon, the ν_3 FWHM is less than 5 cm^{-1}, while partially metamict zircon commonly has a FWHM value greater than 10 cm^{-1}. In this study, ν_3 FWHM values ranged from 5.15 to 5.56 cm^{-1}, indicating well-crystallized material (i.e.,

Figure 6. This group of magnetite inclusions in zircon occurred as short, parallel prisms. Photomicrograph by T. Chen; magnified 200×.

Figure 7. Polarized Raman spectra of oriented polished plates of Muling zircon show different relative band intensities. The most intense band in samples C-5 and P-10 is at 1005 cm⁻¹, whereas the strongest band in P-7 and P-9 is at 356 cm⁻¹.

to f-f transitions (movement of electrons between atomic f orbitals of different energies) related to REEs and elements such as U and Th (actinides and lanthanides). As in most natural zircon, these sharp lines are weak and faint (Nasdala et al., 2003).

Heat Treatment. Figure 9 shows five zircons before (top) and after (bottom) heating to 1100°C. After the experiment, their tone significantly lightened and

Figure 8. These polarized UV-Vis-NIR absorption spectra were obtained from two polished plates (~1 mm thick) cut from the same crystal.

"high" zircon). The FWHM value of ν_3 measured from the zircon inclusions (figure 4) was 9.47 cm⁻¹, indicating they were partially metamict.

UV-Vis-NIR Spectroscopy. Zircon coloration depends on transition metal content and the presence of radiation-induced color centers (Nasdala et al., 2003). Polarized UV-Vis-NIR absorption spectra from one sample are shown in figure 8. The spectra are similar to that of a brownish red zircon from Chanthaburi, Thailand, which is believed to be colored by radiation damage (see minerals.caltech.edu/files/visible/zircon/index.htm). The characteristic absorption spectra, consisting of sharp lines below 600 nm, are attributed
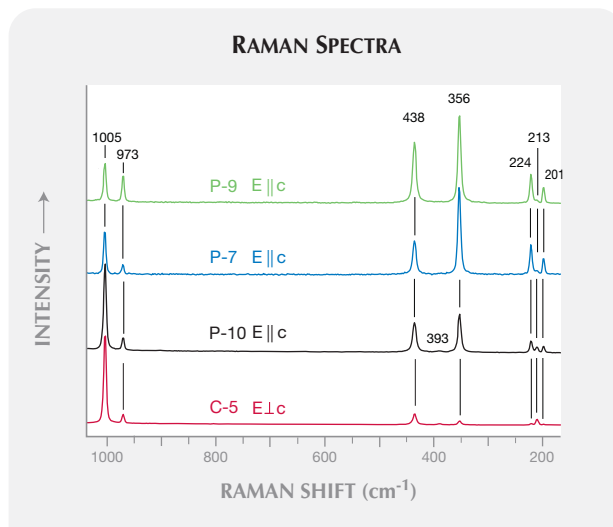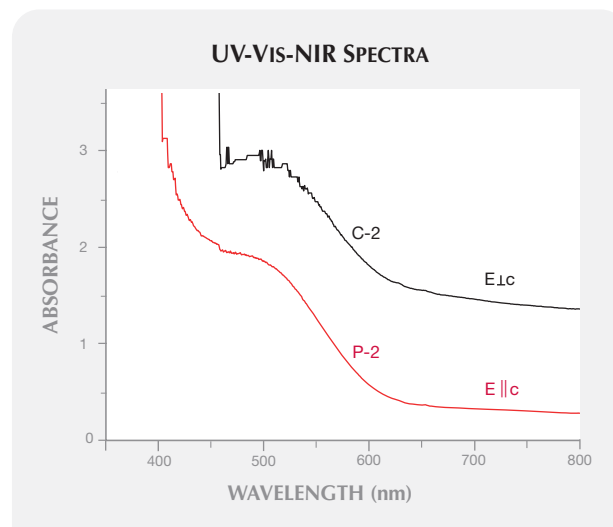
much of the red hue was removed. The color changes seemed to be less related to the original hue than to the amount of inclusions in the sample; heating caused the more transparent zircons to become more colorless. However, some orange areas were seen around cracks in the heated samples. We expect that more commercially desirable colors can be obtained by heating for shorter durations and/or at lower temperatures.

CONCLUSION

Alluvial deposits at Muling, in northeastern China, host gem-quality brownish red zircon crystals that show a combination of tetragonal prismatic and pyramidal faces. Melt inclusions are common, and trace-element content indicates a mafic source. Raman spectroscopy suggests they underwent very little radiation damage. Polarized UV-Vis-NIR absorption spectra showed weak sharp lines caused by f-f transitions related to actinides and lan-

Figure 9. These Muling zircon samples (0.49–0.77 g), shown before and after heating, became significantly lighter after heat treatment. Photos by Y. Liu.

thanides. This locality shows potential as a commercial source of gem zircon.

ABOUT THE AUTHORS

Dr. Chen (summerjewelry@163.com) is a research scientist, Dr. Yang is a gemologist and dean, and Mr. Liu is a graduate student at the Gemmological Institute, China University of Geosciences, Wuhan. Mr. Ai is a graduate student at the State Key Laboratory of Ore Deposit Geochemistry, Chinese Academy of Sciences, Guiyang. Mr. Zheng is a researcher at the State Key Laboratory of Geological Processes and Mineral Resources, China University of Geosciences, Wuhan.

REFERENCES

Fan A.N., Liu R.X., Li H.M., Li N., Sui J.L., Lin Z.R. (1998) Zircon chronology and REE geochemistry of granulite xenolith at Hannuoba. *Chinese Science Bulletin*, Vol. 43, No. 18, pp. 1510–1515.

Faulkner M.J., Shigley J.E. (1989) Zircon from the Harts Range, Northern Territory, Australia. *G&G*, Vol. 25, No. 4, pp. 207–215.

Finch R.J., Hanchar J.M. (2003) Structure and chemistry of zircon and zircon-group minerals. In J.M. Hanchar, Ed., *Zircon, Reviews in Mineralogy and Geochemistry*, Vol. 53, Mineralogical Society of America and Geochemical Society, Washington, DC, pp. 1–25.

Hoskin P.W.O., Rodgers K.A. (1996) Raman spectral shift in the isomorphous series $(Zr_{1-x}Hf_x)SiO_4$. *European Journal of Solid State and Inorganic Chemistry*, Vol. 33, pp. 1111–1121.

Longerich H.P., Jackson S.E., Günther D. (1996) Inter-laboratory note. Laser ablation inductively coupled plasma mass spectrometric transient signal data acquisition and analyte concentration calculation. *Journal of Analytical Atomic Spectrometry*, Vol. 11, pp. 899–904.

Nasdala L., Pidgeon R.T., Wolf D., Irmer G. (1998) Meta-mictization and U-Pb isotopic discordance in single zircons: A combined Raman microprobe and SHRIMP ion probe study. *Mineralogy and Petrology*, Vol. 62, pp. 1–27.

Nasdala L., Zhang M., Kempe U., Panczer G., Gaft M., Andrut M., Plöze M. (2003) Spectroscopic methods applied to zircon. In J.M. Hanchar, Ed., *Zircon, Reviews in Mineralogy and Geochemistry*, Vol. 53, Mineralogical Society of America and Geochemical Society, Washington, DC, pp. 427–466.

O'Donoghue M., Ed. (2006) *Gems*, 6th ed. Butterworth-Heinemann, Oxford, UK.

Qiu Z.L., Yany J.H., Yang Y.H., Yang S.F., Li C.Y., Wang Y.J., Lin W.P., Yang XX. (2007) Trace element and hafnium isotopes of Cenozoic basalt-related zircon megacrysts at Muling, Heilongjiang Province, northeast China. *Acta Petrologica Sinica*, Vol. 23, No. 2, pp. 481–492.

Shigley J.E., Laurs B.M., Janse A.J.A., Elen S., Dirlam D.M. (2010) Gem localities of the 2000s. *G&G*, Vol. 46, No. 3, pp. 188–216.

Thomas J.B., Bodnar R.J., Shimizu N., Chesner C.A. (2003) Melt inclusions in zircon. In J.M. Hanchar, Ed., *Zircon, Reviews in Mineralogy and Geochemistry*, Vol. 53, Mineralogical Society of America and Geochemical Society, Washington, DC, pp. 63–87.

AQUAMARINE FROM THE THUONG XUAN DISTRICT, THANH HOA PROVINCE, VIETNAM

Le Thi-Thu Huong, Wolfgang Hofmeister, Tobias Häger, Nguyen Ngoc Khoi,
Nguy Tuyet Nhung, Wilawan Atichat, and Visut Pisutha-Arnond

Vietnamese aquamarine is notable for its attractive color and well-formed crystals. Commercially significant deposits are known only from the Thuong Xuan District in Thanh Hoa Province, where the aquamarine (as well as topaz) have been mined from granitic pegmatites and associated eluvial deposits. Rough and cut samples were investigated by standard gemological methods, Raman and IR spectroscopy, and electron microprobe and LA-ICP-MS chemical analysis. The samples were characterized by a low concentration of alkalis and relatively high amounts of iron and cesium. Raman and IR spectroscopy showed the presence of CO_2 and type I H_2O in the beryl structural channels.

Gem-quality aquamarine has been produced mainly from Brazil and Africa (Bank et al. 2001; Webster, 2002), as well as Pakistan, Russia, Myanmar, China, India, Ukraine, and the United States (Shigley et al., 2010). Aquamarine was discovered in Vietnam in 1985 at the village of Xuan Le (Thuong Xuan District in Thanh Hoa Province) during geological mapping by the government. While known for more than 25 years, this attractive aquamarine has been described in only a few brief reports (Pham Van et al., 2004; Huong et al., 2008; Atichat et al., 2010; Laurs, 2010). According to local

dealers, ~100–150 kg of gem material were recovered by local people annually during the past decade, and in 2010 some 300–400 kg were produced. A limited number of gemstones have been faceted so far (e.g., figure 1), and sold mainly into the Vietnamese market. This article describes the geologic setting, gemological properties, and spectroscopic characteristics of Thuong Xuan aquamarine.

LOCATION, GEOLOGY, AND MINING

The Thuong Xuan aquamarine deposits lie ~70 km west of the provincial capital, Thanh Hoa City (figure 2). While Thuong Xuan is the only commercially significant aquamarine locality in the country, the adjacent Que Phong District in Nghe An Province has produced small amounts of aquamarine from eluvial deposits.

The Thuong Xuan region is cross-cut by a group of mainly northwest-trending faults. The aquamarine is hosted by pegmatites distributed mostly within the Ban Chieng and Ban Muong granite complexes, which together cover an area of 100 km² (figure 3). The pegmatite bodies typically form lenses or veins, ranging from 10 to 30 cm thick and a few meters in length to 4–5 m thick and tens of meters long. According to unpublished research by one of the authors (NNK), the pegmatites consist of quartz (38–48%), K-feldspar (~35%), plagioclase (18–24%), muscovite (2.3–3.5%), and biotite (0–2%). Quartz, feldspar, aquamarine, topaz, tourmaline, fluorite, and (rarely) zircon are found in miarolitic cavities. Although the topaz is of gem quality, it is not hosted by the same pegmatites as the aquamarine.

Many eluvial occurrences of aquamarine are known, of which four—Ban Pang, Lang Ben, Non Na

Figure 1. These faceted aquamarines (2.40–7.65 ct) from Vietnam's Thuong Xuan District were studied for this report. Photo by L. T.-T. Huong.

Ca, and Ban Tuc—are the most productive; all are derived from pegmatites intruding the Ban Chieng granite. Most of the recent production has come from these deposits, which typically contain aquamarine of very good gem quality together with

Figure 2. The Thuong Xuan aquamarine deposit is located in north-central Vietnam, not far from the border with Laos.

quartz, topaz, and cassiterite. So far there has been no organized mining; the crystals are simply gathered by hand from the eluvial deposits or recovered from shallow workings in the pegmatites using rudimentary tools. The crystals have a prismatic hexagonal shape, variable hue and saturation, and are transparent to translucent. They typically range from 5 to 20 cm long and 1–6 cm in diameter.

MATERIALS AND METHODS

Six aquamarine crystals from eluvial deposits (up to 4.5 cm long; figure 4) and four faceted stones (2.40–7.65 ct; again, see figure 1) representative of the current production from Thuong Xuan were examined using standard gemological techniques. These samples were purchased from local dealers, except for one crystal that was found in an eluvial deposit by one of the authors (NTN). All samples were tested with a dichroscope, Schneider refractometer, hydrostatic Shimadzu balance, UV lamp, and Schneider immersion microscope with Zeiss optics.

Raman spectroscopy was used to investigate H_2O and CO_2 molecules in the beryl structural channels, as these can show differences between aquamarine from different sources, and to identify inclusions in selected samples. The spectra were collected with a Jobin Yvon LabRam HR 800 spectrometer coupled with an Olympus BX41 optical microscope and an Si-based CCD (charge-coupled device) detector; samples were excited by a 514 nm green Ar^+ ion laser. Raman microspectroscopy of inclusions was performed in confocal mode, facilitating analysis at the micron scale (2–5 µm).
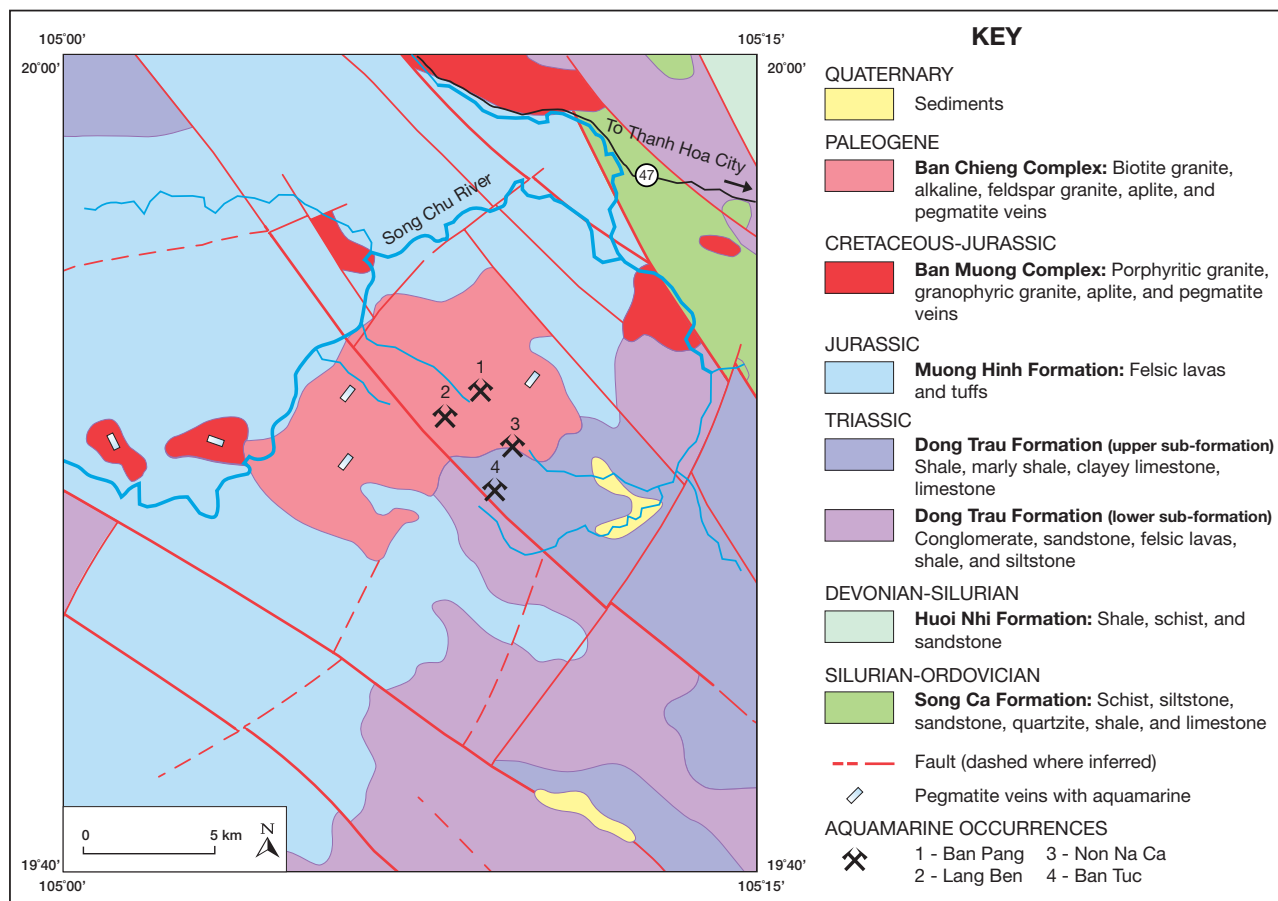
Figure 3. The primary and eluvial occurrences of aquamarine in the Thuong Xuan area are associated with granitic rocks. Modified after Bach and Quan (1995).

To study the characteristics of H_2O in the beryl channels, we recorded IR spectra from portions of two crystals using the KBr pellet method (2 mg of powdered sample mixed with 200 mg of KBr) in the range of 4000–500 cm^{-1} with a Perkin Elmer FTIR 1725X spectrometer.

Three of the crystals were partially polished for chemical analysis by electron microprobe and by laser ablation–inductively coupled plasma–mass spectrometry (LA-ICP-MS). Microprobe analyses were performed with a JEOL JXA 8900RL instrument equipped with wavelength-dispersive spectrometers, using 20 kV acceleration voltage and 20 nA filament current. Silicon was analyzed by microprobe, and wollastonite was used as the standard. LA-ICP-MS data for all elements except Si were obtained using an

Figure 4. These aquamarine crystals (up to 4.5 cm long) were characterized for this study. Photo by L. T.-T. Huong.
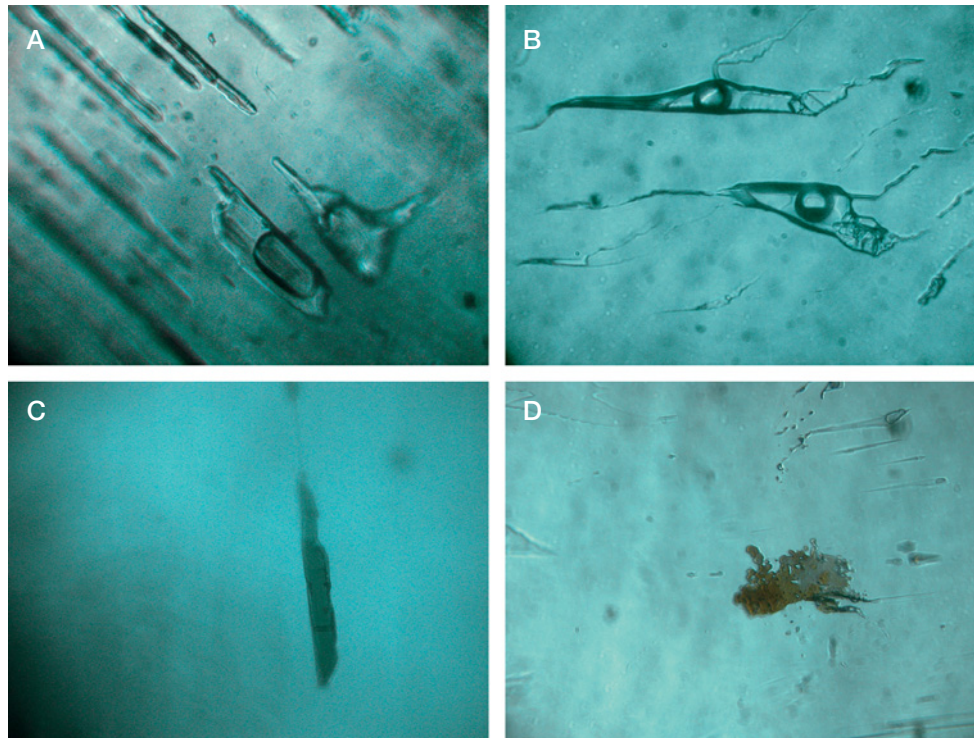
Figure 5. Inclusions documented in the Thuong Xuan aquamarine included growth tubes and two-phase inclusions (A), three-phase inclusions with calcite and albite (B), and mineral inclusions of hematite (C) and biotite (D). Photomicrographs by L. T.-T. Huong; magnified 50×.

Agilent 7500ce ICP-MS in pulse counting mode, and ablation was achieved with a New Wave Research UP-213 Nd:YAG laser ablation system, using a pulse repetition rate of 10 Hz, an ablation time of 60 seconds, a dwell time of 10 milliseconds per isotope, a 100 μm crater diameter, and five laser spots averaged for each sample. Be was calibrated using the NIST 612 glass standard, and BCR2G glass was also analyzed as a reference material.

RESULTS AND DISCUSSION

Visual Appearance and Gemological Properties. The six crystals were translucent to transparent, and light to medium blue. They consisted of well-formed hexagonal prisms {10$\overline{1}$0}, {01$\overline{1}$0}, and {$\overline{1}$100}, while the basal pinacoids {0001} were typically broken or rounded. The four cut samples were fairly clean to the naked eye, with fractures visible in some samples. They were light to medium blue with moderate saturation, and showed obvious pleochroism when viewed with the dichroscope. The refractive indices were n_o = 1.572–1.579 and n_e = 1.569–1.573. SG values varied between 2.66 and 2.70. All samples were inert to long- and short-wave UV radiation.

Internal Features. Microscopic observation revealed growth tubes and angular or elongated two-phase (liquid and gas, figure 5A) fluid inclusions in all the samples. Multiphase (liquid, gas, and crystal) inclu-

sions were seen less frequently. The liquid and gas phases were identified by Raman spectroscopy as H_2O and CO_2. Transparent crystals in the multiphase inclusions within one sample were identified as calcite and albite (figure 5B). Hematite and biotite were found as mineral inclusions in one sample (figures 5C,D).

Chemical Composition. The chemical composition of the three analyzed samples is presented in table 1. The Thuong Xuan aquamarines were characterized by a relatively high concentration of Fe (up to 1.50 wt.% Fe_2O_3; compare to Adamo et al. [2008] and Viana et al. [2002]) and low amounts of Na (up to 0.048 wt.% Na_2O) and K (up to 0.007 wt.% K_2O).

TABLE 1. Chemical composition of aquamarine from Thuong Xuan, Vietnam.[a]

Chemical composition	Sample 1	Sample 2	Sample 3
Oxides (wt.%)			
SiO_2	65.42	65.87	66.41
Al_2O_3	18.13	17.80	18.55
Fe_2O_3	1.50	1.42	1.37
Sc_2O_3	0.005	0.005	0.005
BeO	13.40	13.52	12.59
MnO	0.012	0.009	0.011
MgO	0.046	0.058	nd[b]
CaO	0.046	0.030	0.027
Na_2O	0.025	0.048	0.037
K_2O	0.007	0.003	0.006
Li_2O	0.009	0.001	0.002
Cs_2O	0.193	0.126	0.132
Total	98.79	98.89	99.14
Trace elements (ppm)			
B	1.87	2.82	2.33
P	49.5	17.6	40.2
Ti	6.18	3.07	2.24
V	0.525	0.477	0.198
Cr	2.06	1.52	2.53
Co	0.247	0.134	0.082
Ni	1.9	5.0	0.8
Ga	71.4	71.2	70.0
Ge	0.850	0.630	1.06
Rb	58.1	54.9	55.7
Sr	0.047	0.125	0.510
Y	0.042	0.018	0.046
Zn	0.130	0.123	0.060
Nb	0.027	0.027	0.037
Mo	0.082	0.103	0.223
Ba	0.178	0.152	0.780
La	0.024	0.033	0.019
Ta	0.022	0.011	0.030

[a] Si was analyzed by electron microprobe, and the others by LA-ICP-MS. Elements typically reported in beryl analyses were converted to oxides for ease of comparison with the published literature.
[b] Abbreviation: nd = not detected.

The Cs contents were very high compared to aquamarine from other sources (Adamo et al., 2008; Viana et al., 2002), with up to 0.193 wt.% Cs_2O. Also present were small but significant amounts of Mg, Mn, Ca, Sc, Li, Ga, Rb, and P, as well as traces of several other elements (again, see table 1).

Spectroscopic Investigation. *Raman.* The main Raman bands of the beryl group, shown in figure 6, are due to ring vibrations (e.g., Kim et al., 1995;

Charoy et al., 1996) and Si-O stretching vibrations (Adams and Gardner, 1974; Huong, 2008). In addition, a band at 1243 cm⁻¹ present in all samples is related to the vibration of CO_2 molecules in the beryl structural channels (Charoy et al., 1996). It was seen only in the E∥c orientation, because the only possible orientation of CO_2 molecules in the channel is with the symmetry axis parallel to the c-axis. While CO_2 has been previously documented as a channel constituent in beryl (e.g., Aines and Rossman, 1984), to our knowledge it has not been ascribed to aquamarine from a particular locality.

Figure 7 shows a representative Raman spectrum of Thuong Xuan aquamarine in the 3700–3500 cm⁻¹ range, which corresponds to the energy of H_2O vibrations in beryl. A band at 3608 cm⁻¹—related to type I H_2O and not associated with alkalis (e.g., Huong et al., 2010)—was observed in all samples. Conversely, a band at 3598 cm⁻¹—related to type II H_2O and associated with alkalis—was almost undetectable. This is consistent with the chemical data showing low contents of alkalis (sodium and potassium), which are associated with type II H_2O in the structural channels of beryl.

Infrared. Various bands consistent with those typically seen in aquamarine were observed in the IR spectra of the Thuong Xuan aquamarines (figure 8). Those recorded in the range 1300–800 cm⁻¹ have

Figure 6. In addition to typical Raman features for beryl, the aquamarine showed a peak at 1243 cm⁻¹ in the E∥c orientation that is due to CO_2.

RAMAN SPECTRA
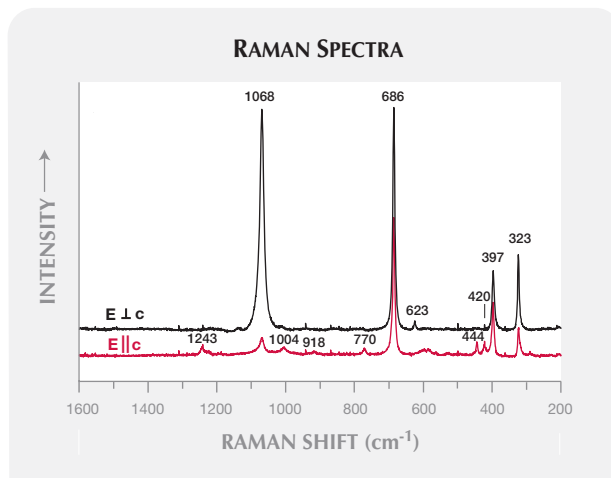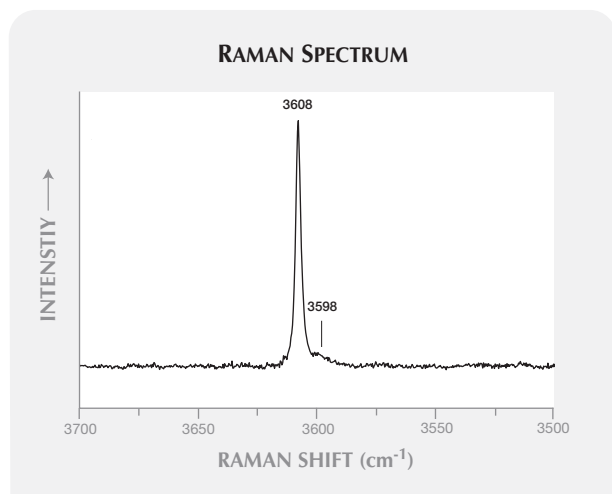
RAMAN SPECTRUM

Figure 7. Raman spectra of the aquamarine showed a band at 3608 cm⁻¹ that is associated with type I H₂O. This indicates a very low alkali content.

IR TRANSMITTANCE SPECTRUM
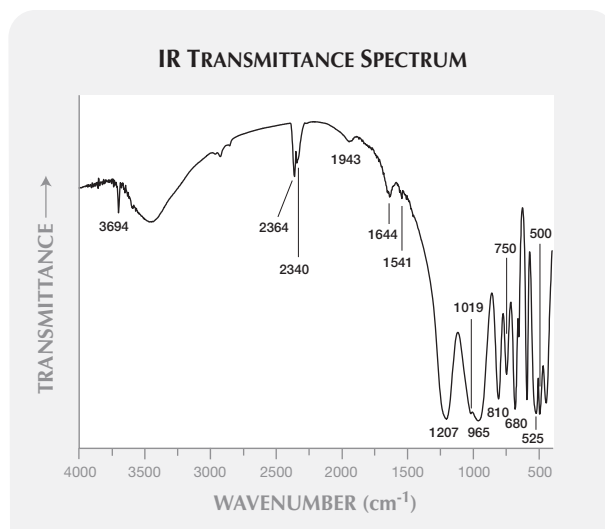
Figure 8. Infrared spectra of the Vietnamese aquamarine showed a band related to type I H₂O at 3694 cm⁻¹ and a doublet at 2364 and 2340 cm⁻¹ that is due to CO_2.

been assigned to internal Si-O vibrations (Gervais and Pirou, 1972; Adams and Gardner, 1974; Hofmeister et al., 1987; Aurisicchio et al., 1994). Bands appearing at ~750 and 680 cm⁻¹ were ascribed to the Be-O cluster by Hofmeister et al. (1987). The two bands at 525 and 500 cm⁻¹ correlate to Si-O-Al stretching (Plyusnina, 1964). The doublet at 2364 and 2340 cm⁻¹ is due to carbon dioxide (Leung et al., 1983).

Features in the 1700–1500 cm⁻¹ and 3800–3500 cm⁻¹ ranges are generated by different types of H₂O (Wood and Nassau, 1967). In the latter range, the Thuong Xuan aquamarines showed only one band at 3694 cm⁻¹. This correlates to type I H₂O (Schmetzer and Kiefert, 1990), and is consistent with the Raman analyses and very low alkali contents of this aquamarine.

CONCLUSION

Since the early 2000s, a significant amount of gem-quality aquamarine has been recovered from the Thuong Xuan area by local people, and more production is expected in the future. Some of the aquamarine has been mounted into jewelry (figure 9) for distribution mainly into the Vietnamese market. This aquamarine contains low concentrations of alkali ions, and relatively high amounts of iron and cesium. The low alkalis were revealed by chemical analysis and by the sole presence of type I H₂O in

Raman and IR spectra. In addition, the presence of CO_2 molecules in structural channels was indicated by Raman spectroscopy.

Figure 9. A limited amount of Vietnamese aquamarine has been faceted and mounted into jewelry, such as the 6.5 ct stone shown in this gold ring. Courtesy of Duong Anh Tuan, Doji Gold & Gems Group, Hanoi; photo by L. T.-T. Huong.

REFERENCES

Adamo I., Pavese A., Prosperi L., Diella V., Ajo D., Gatta G.D., Smith C.P. (2008) Aquamarine, Maxixe-type beryl, and hydrothermal synthetic blue beryl: Analysis and identification. *G&G*, Vol. 44, No. 3, pp. 214–227.

Adams D.M., Gardner I.R. (1974) Single-crystal vibrational spectra of beryl and dioptase. *Journal of the Chemical Society, Dalton Transactions*, Vol. 1974, No. 14, pp. 1502–1505.

Aines R.D., Rossman G.R. (1984) The high temperature behavior of water and carbon dioxide in cordierite and beryl. *American Mineralogist*, Vol. 60, pp. 319–327.

Atichat W., Khoi N.N., Pisutha-Arnond V., Wathanakul P., Sriprasert B., Sutthirat C., Leelawattanasuk T., Tay T.S., Saejoo S., Naruedeesombat N., Rochd C., Makakum C., Pttharapanich W. (2010) Properties of aquamarine from central Vietnam. *5th International Workshop on Provenance and Properties of Gems and Geo-Materials*, October 17–24, Hanoi, pp. 135–139.

Aurisicchio C., Grubessi O., Zecchini P. (1994) Infrared spectroscopy and crystal chemistry of the beryl group. *Canadian Mineralogist*, Vol. 32, pp. 55–68.

Bach L.D., Quan T.D. (1995) *Geology and Mineral Resources of Vietnam*. Thanh Hoa sheet (E-48-IV), scale 1:200,000, Vietnam Department of Geology and Minerals, Hanoi.

Bank F., Bank H., Villa E. (2001) Santa Maria aquamarine. *Journal of Gemmology*, Vol. 27, No. 5, pp. 257–258.

Charoy B., De Donato P., Barres O., Pinto-Coelho C. (1996) Channel occupancy in an alkali-poor beryl from Serra Branca (Goias, Brazil): Spectroscopic characterization. *American Mineralogist*, Vol. 81, pp. 395–403.

Gervais F., Piriou B. (1972) Étude des spectres de réflexion infrarouge du beryl dans les région 280-1400 cm^{-1}. *Comptes Rendus de l'Académie des Sciences Paris*, Vol. 274, pp. 252–255.

Hofmeister A.M., Hoering T.C., Virgo D. (1987) Vibrational spectroscopy of beryllium aluminosilicates: Heat capacity calculation from band assignments. *Physics and Chemistry of Minerals*, Vol. 14, pp. 205–224.

Huong L.T.-T. (2008) Microscopic, Chemical and Spectroscopic Investigations on Emeralds of Various Origins. PhD dissertation, Johannes-Gutenberg University, Mainz.

Huong L.T.-T., Khoi N.N., Nhung N.T., Häger T., Hofmeister W. (2008) A study on aquamarine from Thuong Xuan deposit, Thanh Hoa Province, Vietnam. *Proceedings of the 2nd International Gem and Jewelry Conference*, March 9–12, 2009, Bangkok.

Huong L.T.-T., Häger T., Hofmeister W. (2010) Confocal micro-Raman spectroscopy: A powerful tool to identify natural and synthetic emeralds. *G&G*, Vol. 46, No. 1, pp. 36–41.

Kim C., Bell M.I., McKeown D.A. (1995) Vibrational analysis of beryl (Be$_3$Al$_2$Si$_6$O$_{18}$) and its constituent ring (Si$_6$O$_{18}$). *Physica B: Condensed Matter*, Vol. 205, No. 2, pp. 193–208.

Laurs B.M. (2010) Gem News International: Aquamarine and heliodor from Indochina. *G&G*, Vol. 46, No. 4, pp. 311–312.

Leung C.S., Merigoux H., Poirot J.P., Zecchini P. (1983) Sur l'identification des pierres fines et de synthèse par spectroscopie infrarouge. *Revue de Gemmologie a.f.g.*, Vol. 75, pp. 14–15.

Pham Van L., Giuliani G., Garnier V., Ohnenstetter D. (2004) Gemstones in Vietnam—A review. *Australian Gemmologist*, Vol. 22, No. 4, pp. 162–168.

Plyusnina I.I. (1964) Infrared absorption spectra of beryls. *Geokhimiya*, Vol. 1, pp. 31–41 [in Russian].

Schmetzer K., Kiefert L. (1990) Water in beryl—A contribution to the separability of natural and synthetic emeralds by infrared spectroscopy. *Journal of Gemmology*, Vol. 22, No. 4, pp. 215–223.

Shigley J.E., Laurs B.M., Janse A.J.A., Elen S., Dirlam D.M. (2010) Gem localities of the 2000s. *G&G*, Vol. 46, No. 3, pp. 188–216.

Viana R.R., Jordt-Evangelista E.H., Magela da Costa E.G., Stern W.B. (2002) Characterization of beryl (aquamarine variety) from pegmatites of Minas Gerais, Brazil. *Physics and Chemistry of Minerals*, Vol. 29, No. 10, pp. 668–679.

Webster R. (2002) *Gems: Their Sources, Descriptions and Identification*, 5th ed. Rev. by P.G. Read, Butterworth-Heinemann, Oxford, UK.

Wood D.L., Nassau K. (1967) Infrared spectra of foreign molecules in beryl. *Journal of Chemical Physics*, Vol. 47, No. 7, pp. 2220–2228.

For online access to all issues of **GEMS & GEMOLOGY** from 1981 to the present, visit:

gia.metapress.com

G&G
Lab Notes

EDITORS

Thomas M. Moses | **Shane F. McClure** | *GIA Laboratory*

DIAMOND

Large HPHT-Treated Cape Diamond

Since the early 2000s, high-pressure, high-temperature (HPHT) treatment has been used extensively to improve the color of diamonds. In the early stages, the typical starting material was brown type IIa diamond, which was processed to achieve a colorless to near-colorless stone. In recent years, we have also seen brown type IaB diamonds HPHT-treated to near-colorless (J. Van Royen et al., "HPHT treatment of type IaB brown diamonds," Fall 2006 *G&G*, pp. 86–87). The treatment can also change the bodycolor of colored diamonds, such as gray type IIb stones that are altered to blue. On rare occasions, the GIA Laboratory has seen light yellow cape diamonds HPHT-treated to vivid yellow.

The New York lab recently received a 28.65 ct brownish yellowish orange emerald-cut diamond (figure 1) for grading. Microscopic examination revealed few inclusions, and the stone showed a good polish except for one facet with a frosted surface, which suggested HPHT treatment (figure 2). The diamond was inert to both long- and short-wave UV radiation. Infrared spectroscopy revealed that it was type Ia with a spectral pat-

Figure 1. This 28.65 ct Fancy Deep brownish yellowish orange diamond is HPHT treated. The starting material was probably a typical cape diamond with light yellow or brownish yellow color.

tern typical of cape diamonds, which was inconsistent with the brownish orange color. The UV-Vis absorption spectrum, however, did not show a cape spectrum. Instead, we observed an increase in absorption from 700 nm to higher energies (attributed to isolated nitrogen) and a weak absorption from the H2 optical center (zero-phonon line at 986.2 nm).

These gemological and spectroscopic properties indicated that this large brownish yellowish orange diamond was HPHT treated. The starting material probably had a light yellow or brownish yellow bodycolor. Instead of becoming intense yellow, HPHT treatment produced a strong yellowish orange hue with a brownish modifier,

which could be attributed to a relatively high concentration of isolated nitrogen as well as the size of the stone.

Jason Darley

A Very Large Colorless HPHT-Treated Diamond

Over the past year, the laboratory has observed an influx of large HPHT-treated diamonds, both type I and type II (see Lab Notes: Spring 2010, pp. 50–51; Winter 2010, p. 298; and the previous entry in this issue). This trend has continued in 2011.

Among the HPHT-annealed diamonds we have identified recently, one was exceptional. This cushion-cut diamond weighed 38.59 ct (24.37 × 18.69 × 10.22 mm; figure 3) and was graded F color with a clarity of VVS_1. Microscopic examination revealed internal graining in a few orientations, and strong internal strain was seen with crossed polarizers. Such fea-

Figure 2. The diamond in figure 1 had a frosted surface along the girdle, a good indication of HPHT treatment. Magnified 40×.
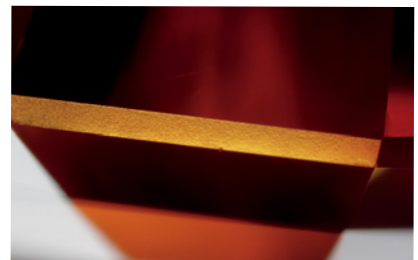
Figure 3. This 38.59 ct cushion-cut diamond proved to be HPHT treated.

tures are common in HPHT-treated type IIa diamonds (T. M. Moses et al., "Observations on GE-processed diamonds: A photographic record," Fall 1999 *G&G*, pp. 14–22).

The IR absorption spectrum revealed a typical type IIa diamond, with no detectable nitrogen- or hydrogen-related features. The UV-Vis spectrum also showed no isolated nitrogen-related absorptions. However, photoluminescence spectroscopy collected at liquid-nitrogen temperature with laser excitations of varying wavelength confirmed HPHT annealing, consistent with the graining and strain patterns seen with the microscope.

This is one of the largest HPHT-treated diamonds the GIA Laboratory has ever identified. Treating diamonds this size is risky, and we suspect that not all facilities have the equipment to anneal them, as the capsule normally used in HPHT presses will not accommodate such a large stone. It is also possible that such diamonds take longer to process.

Gem diamonds of this size and quality are extremely rare. The increasing number of large HPHT-treated diamonds seen in the laboratory underscores the importance of proper disclosure and reliable gem identification.

Wuyi Wang and Tom Moses

Thermoluminescence from Type IaB Diamonds

The luminescence properties of diamond are widely documented in the scientific literature. Analysis of fluorescence, phosphorescence, cathodoluminescence, and photoluminescence (PL) reactions has proven extremely valuable to gemological laboratories in identifying natural, lab-grown, and color-treated diamonds. Thermoluminescence (TL), the reemission of stored energy as light in response to heating, has also been observed in diamond, though its value to gemologists has been limited at best.

During PL testing of near-colorless diamonds in the Carlsbad laboratory, we observed an interesting TL response from certain stones. After exposure to 325 nm laser excitation while cooled to liquid-nitrogen temperature (~77 K), many pure type IaB diamonds briefly luminesced when they were removed from the cryogenic vessel and allowed to warm to room temperature (figure 4). We did not notice this behavior in diamonds of other types observed under the same conditions. Pure type IaB diamonds are dominated by B-aggregated nitrogen impurities (~1175 cm^{-1} in FTIR spectra; figure 5) and are relatively uncommon among nitrogen-containing diamonds. Their observed

Figure 4. This colorless type IaB diamond (~0.75 ct) was cooled in a liquid-nitrogen bath during 325 nm laser PL analysis. When the stone was removed and warmed to room temperature, it briefly displayed a blue thermoluminescence emission.

TL emissions were short-lived (<2 seconds), mostly blue, and varied from strong to very weak. A few samples showed green emission.

To determine the lattice defect responsible for the luminescence, we measured the TL emission using a portable CCD spectrometer. The diamonds showing blue TL displayed a broad luminescence band from ~410 to 510 nm. PL spectra collected from the same stones using 325 nm laser excitation showed a very strong N3 defect (415 nm), which is likely the cause of the blue TL emission (figure 6). One diamond displaying green TL had a luminescence band from ~490 to 550 nm, which we attributed to H3 defects (503.2 nm) recorded in the PL spectrum of the sample.

While the TL behavior is apparently restricted to nearly pure type IaB diamonds, the reason for this remains unclear. The B-aggregate of nitrogen is associated with lattice vacancies that may somehow play a role. Additionally, it is well known that A-aggregated nitrogen impurities tend to quench luminescence. We did notice that as the A-aggregate became more abundant, the TL emission disappeared, even in stones with high concentrations of B-aggregates. While there is no obvious explanation for the link between this TL behavior and pure type IaB diamonds, the luminescent effect is a fascinating byproduct of laboratory testing.

David Nelson and Christopher M. Breeding

Two Diamonds Cut to Exhibit Inclusions

The New York lab recently observed two striking examples of hydrogen- and etch-related features in diamonds that had been manufactured to highlight their inclusions. Hydrogen-related features often take the form of well-defined symmetrical clouds that are usually dark-colored or gray (W. Wang and W. Mayerson, "Symmetrical clouds in diamond—The hydrogen connection," *Journal of Gemmology*, Vol. 28, No. 3, 2002, pp. 143–152).

FTIR Absorption Spectrum

1175

ABSORBANCE

WAVENUMBER (cm⁻¹)
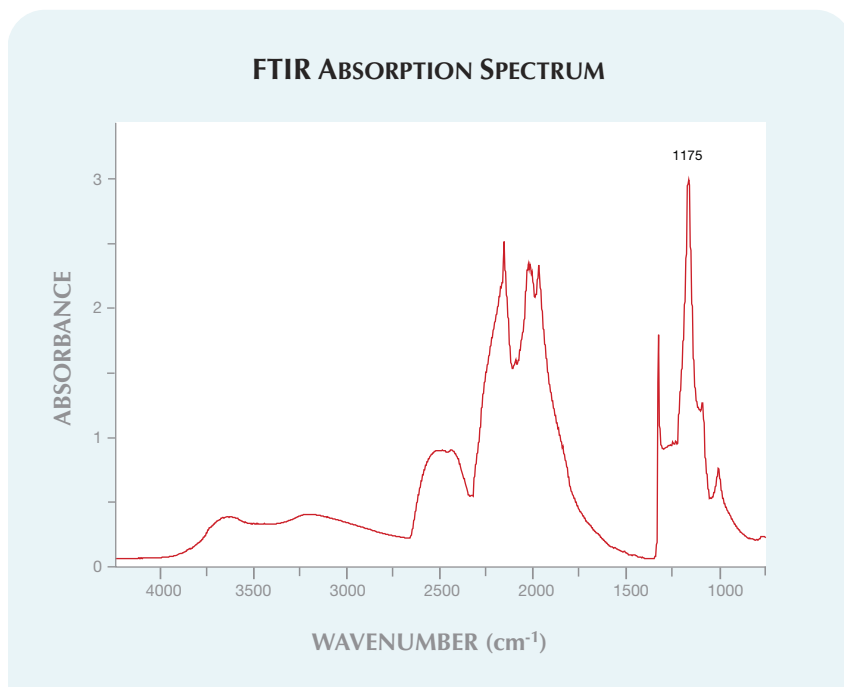
Figure 5. FTIR spectroscopy demonstrated that the diamonds showing TL emission were nearly pure type IaB, as indicated by the band at 1175 cm⁻¹.

Such clouds are often obscured by a diamond's faceting, but that was not the case with these specimens.

The first, a 1.05 ct Fancy gray–greenish yellow octahedron (figure 7), had been polished to preserve the original rough shape. Clearly visible in the interior was a cloud with an elaborate structure that was well-aligned with the polished faces. Such formations could be related to octahedral growth and variations in the crystallization environment. Viewed through the large triangular facets, the cloud resembled a Star of David hexagram.

The other diamond, a 4.51 ct Fancy greenish yellow-brown round brilliant (figure 8), contained a hydrogen cloud composed of six roughly oval-shaped arms aligned to a central point and extending along the [100] axes. Even more conspicuous were bundles of needle-like etch channels that converged in the diamond's center (see also Fall 2009 Lab Notes, pp. 209–210). These channels result from corrosive fluids in the magma that transport diamonds from deep within the earth to near-surface environments. Under certain conditions, the

fluids can dissolve deep into the interior of the diamond, following directions of weakness in the crystal structure. It is very common to see etch channels along the [111] directions, as in this example. These channels had a brown color from natural radiation staining.

The varying appearance of hydrogen clouds is not fully understood. One possible explanation is that a cloud tends to be concentrated in the {100} growth sector due to the diamond's higher surface energy during growth. If growth paused for any reason, the cloud could have spread along the crystal edges, forming an octahedral outline once growth resumed.

Rather than follow the conventional approach to cutting, which seeks to minimize inclusions for the sake of market value, these unusual diamonds accentuated the natural beauty of their growth features, making them truly one-of-a-kind.

Jon Neal, Jason Darley, and Vinny Cracco

Figure 6. PL analysis of type IaB diamonds with blue TL emission showed a prominent N3 defect (415 nm peak), which is likely the cause of the TL behavior.

PL Spectrum

415
N3

INTENSITY

WAVELENGTH (nm)
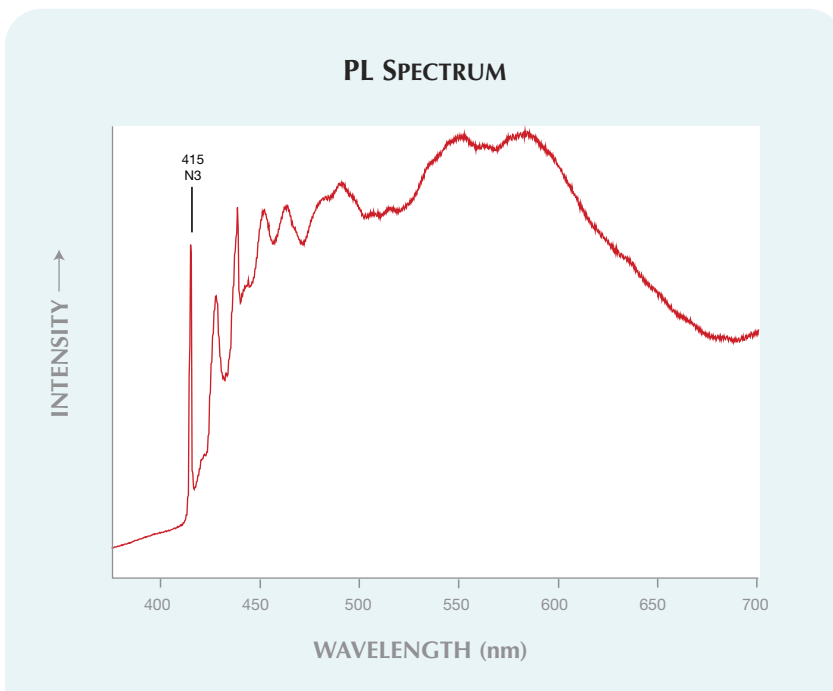
Figure 7. This 1.05 ct Fancy gray–greenish yellow diamond contains a cloud with an octahedral structure that matches that of the polished faces.

HALITE
Submitted for Identification

A 13.25 g near-colorless piece of rough was recently submitted to the Carlsbad laboratory for identification (figure 9). Initial examination showed a rounded surface with one large flat side that was obviously a cleavage, as its stepped appearance in some areas indicated it had been broken rather than sawn. Dissolution tubes extended into the stone in three directions at right angles.

Figure 8. In this 4.51 ct Fancy greenish yellow-brown round brilliant, bundles of needle-like etch channels converge at the center, dividing the six oval-shaped clouds (only four of which are visible here).

The RI of the cleavage surface was around 1.55, though the unpolished surface yielded a rather indistinct reading. The optic character, observed with a polariscope, was singly refractive. The specimen fluoresced weak yellow to long-wave UV radiation and was inert to short-wave UV. Given the dissolved appearance of the surface, the author was hesitant to measure the sample's hydrostatic specific gravity. Water-soluble minerals have been used as gems (e.g., the hanksite described in the Spring 2010 Gem News International [GNI], pp. 60–61), and immersing such a specimen might cause damage.

While there were no obvious external clues to the morphology of the specimen other than its perfect cleavage, microscopic examination proved more revealing. With magnification, numerous planes of fluid-filled cubic negative crystals were visible (figure 10, left). The cubic crystal system was consistent with the singly refractive character. Most of the negative crystals contained a brown to colorless liquid with a gas component, but a few contained a green fluid with several daughter crystals (figure 10, right). Both types of fluid inclusions were indicative of a natural material.

Further testing with energy-dispersive X-ray fluorescence (EDXRF) spectroscopy indicated that the major elements were sodium and chlorine. The ionic combination of these two elements is familiar to us as halite, or common table salt. Raman analysis confirmed this identification.

Although halite is not rare or durable enough to be considered a gem material, this proved to be an interesting exercise in identification. Because the surface provided so little crystallographic information, most of the clues could only be gathered from microscopic features. A solid foundation in crystallography and microscopy is essential for any gemologist, who may be called on to identify even non-gem-related materials.

Nathan Renfro

Three Similar-Appearing Green Stones: JADEITE, OMPHACITE, and HYDROGROSSULAR

The New York laboratory recently received several green cabochons for identification over the period of a few days (e.g., figure 11). They all had a saturated green color, and microscopic observation revealed similar microcrystalline textures. Observation with a dichroscope showed very weak or no pleochroism, which is common for fine-textured aggregates. In the desk-model spectroscope, all of the cabochons displayed chromium lines near 690 nm, and all but one also had a line near 437 nm, as seen in jadeite and omphacite. The samples were inert to long- and short-wave UV radiation. Their SG values, however, varied from 2.90 to 3.34. In addition, all but one of the cabochons had refractive indices of 1.66–1.68—typical values for jadeite and omphacite—while the other stone (also with the highest SG value) had an RI of 1.72.

Raman spectroscopy identified the stone with the highest RI and SG values as hydrogrossular (hibschite). This identification was further supported by infrared spectroscopy, based on distinct hydroxyl absorption bands in the 4000–3000 cm^{-1} region. EDXRF spectroscopy indicated major amounts of calcium, aluminum, and silicon, with minor chromium, consistent with hydrogrossular's formula of $Ca_3Al_2(SiO_4)_{3-x}(OH)_{4x}$ (x = 0.2–1.5)

Figure 9. The rounded surface of this 13.25 g piece of halite was the result of dissolution. The cleavage plane indicates the specimen had been cleaved after dissolution.
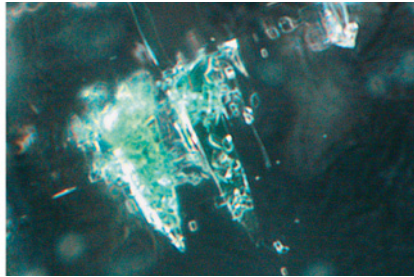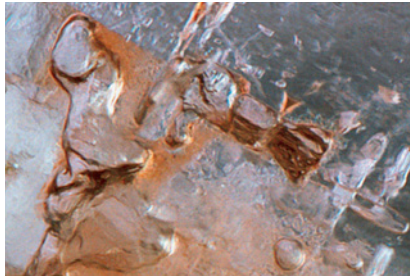
Figure 10. The cubic habit of these fluid-filled negative crystals reveals the halite's crystal structure (left, magnified 60×). A few of them hosted a green fluid and multiple daughter crystals (right, magnified 100×).

and the stone's green color. Hydrogrossular occurs in green colors when trace amounts of chromium are present, and variations in hydroxyl content cause differences in physical properties such as RI and SG (W. A. Deer et al., *Rock-Forming Minerals—Orthosilicates*, Vol. 1A, 2nd ed., Longman Group Ltd., London, 1982).

The other cabochons were identified as jadeite or omphacite, using the same techniques. Omphacite [(Ca,Na)(Mg,Fe,Al)Si_2O_6] is a clinopyroxene that forms a solid solution with jadeite (NaAlSi_2O_6). Both minerals have similar properties—such as overlapping RI values—and they were differentiated by Raman spectroscopy. Further confirmation was provided by EDXRF, which revealed the presence of Ca and Fe in omphacite, and the absence of these elements in jadeite.

Positive identification of jadeite can be difficult because other minerals also exhibit similar fine aggregate texture, SG and RI ranges, hardness, UV reaction (if not impregnated), and/or chromium-related UV-Vis absorption

bands; amphibole (nephrite) and serpentine-group minerals are some of the better-known examples. Proper identification requires careful observation and testing.

Ren Lu

Beryllium- and Tungsten-Bearing SAPPHIRES from Afghanistan

In March 2010, the Bangkok laboratory received a rough parcel of 175 blue sapphires reportedly from a relatively new deposit near the lapis lazuli mines in the Kokcha Valley of Afghanistan's Badakhshan Province. The pieces ranged from ~0.2 to 4 g (figure 12), and about half the parcel was gem quality. During a trip to Afghanistan in July 2010 (see Winter 2010 GNI, pp. 319–320), one of us (VP) obtained six additional samples said to be from this deposit, consisting of blue sapphires on a matrix of bluish green and yellowish brown crystals (identified as dravite and phlogopite by Raman and laser ablation–inductively

coupled plasma–mass spectrometry [LA-ICP-MS] analysis, respectively).

Of the 181 samples, most had strong hexagonal blue color zoning surrounding a yellow core that displayed a six-rayed star pattern when viewed with transmitted light (figure 13). Common inclusions were negative crystals (sometimes associated with healed fissures), corroded zircon crystals, twin planes, and crystals of corundum. Most of the sapphires were sector zoned with colorless areas associated with the basal pinacoid.

EDXRF analysis detected iron, gallium, vanadium, and surprisingly, tungsten (an element typically associated with synthetics). LA-ICP-MS showed similar amounts of gallium and vanadium in both the blue and colorless areas. However, the colorless areas were higher in magnesium and lower in iron, while titanium was nearly absent. Significant levels of beryllium (up to 20 ppma), as well as niobium, tin, tantalum, zirconium, hafnium, and tungsten (30–700 ppma) were found in the colorless areas but not in the blue portions. Though not common, beryllium (in association with niobium and tantalum) has been reported in some untreated blue sapphires from Madagascar (V. Pardieu, "Beryllium discovered in unheated sapphires," *InColor*, Fall-Winter 2007-2008, p. 41) and Tasmania (B. M. McGee, "Characteristics and origin of the Weldborough sapphire, NE Tasmania," bachelor's thesis, School of Earth Sciences, University of Tasmania, 2005).

UV-Vis spectroscopy showed strong absorptions at 580 and 700 nm (o-ray) and ~700 nm (e-ray) that are typical of metamorphic/metasomatic-type blue sapphires. Very weak iron-related absorptions were visible at 377, 388, and 450 nm, and the spectrum cutoff tended to be very low (around 300 nm). The FTIR spectra (figure 14) showed strong absorption between 3700 and 3100 cm^{-1} (probably due to molecular water) as well as features related to diaspore (lines at 2120 and 1990 cm^{-1} and broad bands around 3020 and 2880 cm^{-1}) and mica

Figure 11. These three similar-looking stones were identified (left to right) as jadeite (23.90 ct), omphacite (8.12 ct), and hydrogrossular (13.90 ct).

Figure 12. These sapphire crystals (~0.2–4 g) are reportedly from Afghanistan's Badakhshan Province. Most are tabular prisms, with a colorless area (that appears grayish here) on the top and bottom of each crystal.

(lines in the ~3700–3620 cm⁻¹ region) in most samples. A band at 3163 cm⁻¹ was also observed in most of the sapphires, along with some unusual absorptions: a broad band at 3428 cm⁻¹, a sharp feature at 3387 cm⁻¹, and a series of four broad bands at ~4450, 4306, 4200, and 4100 cm⁻¹.

The presence of such distinctive chemical and spectral features in these sapphires, combined with their reported origin near the historic Afghan lapis mines, makes them a very interesting addition to the marketplace.

Vincent Pardieu, Sudarat Saeseaw, Kamolwan Thirangoon, and Pantaree Lomthong

Figure 13. Microscopic examination of this sapphire with transmitted light shows hexagonal blue bands surrounding a yellow core that displays a star pattern. The high-relief inclusion in the core is a negative crystal. Magnified 40×.
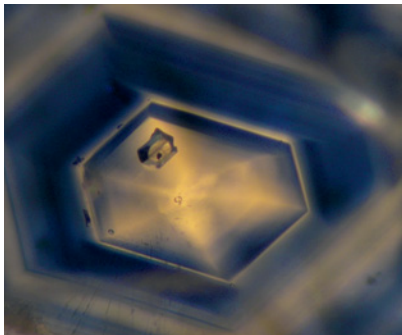
Aggregate of Black SYNTHETIC MOISSANITE and Crystalline SILICON

The Carlsbad laboratory recently received a 1.35 ct black submetallic round brilliant for an identification and origin report. It had an SG of 3.06, an over-the-limit RI, and was opaque to strong fiber-optic light. These properties suggested synthetic moissanite, although the SG was lower than the 3.22 previously reported for this material (K. Nassau et al., "Synthetic moissanite: A new diamond simulant," Winter 1997 *G&G*, pp. 260–275). Curiously, the sample displayed a granular structure in reflected light, which seemed to be an intergrowth of a higher-luster metallic material with a duller, darker matrix (figure 15). Raman spectroscopy identified the matrix as synthetic moissanite and the interstitial metallic material as crystalline silicon. The abundance of silicon in this sample accounted for its low SG.

Silicon inclusions in black syn-

thetic moissanite were described recently by Haibo et al. (Winter 2009 GNI, p. 308), though the intergrowth in this stone was much more extensive than the isolated silicon blebs in that report. Like the samples examined by Haibo et al., though, this black synthetic moissanite appeared to be a product of the physical vapor transport (PVT) technique. Silicon inclusions have not been reported in synthetic moissanite grown by seeded sublimation, but they are known in PVT material grown in China (Z. Chen et al., "Growth of large 6H-SiC single crystals," *Journal of Inorganic Materials*, Vol. 17, No. 4, 2002, pp. 685–690).

Alethea Inns

SYNTHETIC STAR SPINEL Imitation of Moonstone

The Carlsbad laboratory recently examined a translucent white round cabochon that initially appeared to be

Figure 14. These FTIR spectra of a Badakhshan sapphire (sample 668563702, 1.35 ct and ~4 mm thick) reveal strong absorption between 3700 and 3100 cm⁻¹ (probably due to molecular water), as well as mica-related bands and some unusual features.

FTIR ABSORPTION SPECTRA
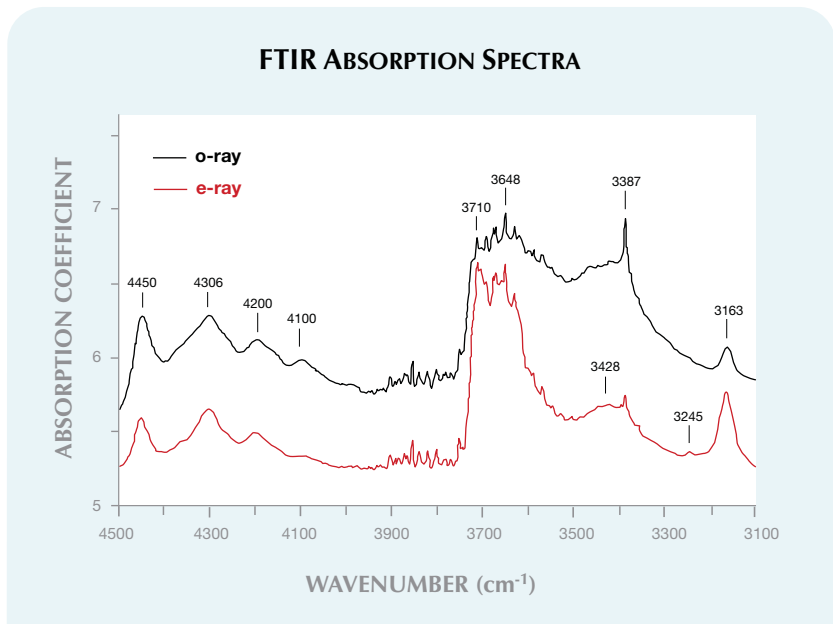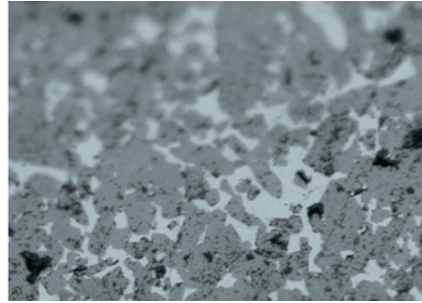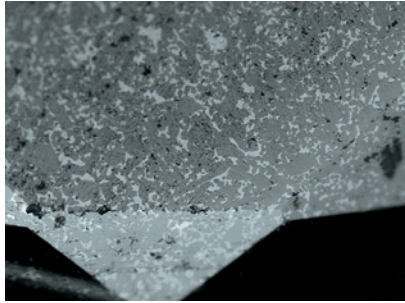
Figure 15. Reflected light shows the aggregate structure of the synthetic moissanite (which appears dark gray here, with darker pits) and the bright-reflecting crystalline silicon. Magnified 30× (left) and 112× (right).

Figure 17. Dense stringer-like dislocations throughout the synthetic star spinel, viewed here at 60× magnification, produced the asterism.

a moonstone (figure 16). The sample showed a pronounced bluish adularescence in diffused lighting. When viewed with a direct light source such as fiber-optic illumination, however, it displayed a pronounced star (figure 16, right). This star contained four pairs of rays, a somewhat unusual configuration.

Gemological testing revealed properties consistent with synthetic spinel, including a spot RI reading of 1.72 and strong green fluorescence to short-wave UV radiation. Microscopic examination uncovered a dense network of dislocation stringers, oriented crystallographically throughout the gem (figure 17). In cross-polarized light, these dislocation networks displayed considerable strain. Also observed with magnification was a blue metallic coating on the back of

the cabochon. In reflected light, there were obvious areas where the coating had chipped off (figure 18). This coating was apparently added to create an effect resembling the blue adularescence seen in moonstone.

Because the mounting prevented additional tests such as specific gravity measurement, advanced testing was needed to confirm the identity of this cabochon. EDXRF spectroscopy showed Al and Mg as the only major elements, consistent with the expected composition of spinel. Minor trace elements were iron, titanium, and chromium.

The crystallographically oriented dense network of dislocations is the presumed source of the asterism, and the four-rayed pattern is consistent with the synthetic spinel's cubic crystal structure. This contributor had

Figure 18. Defects in the metallic blue coating on the back of the synthetic star spinel were obvious in reflected light at 100× magnification.

never seen a synthetic star spinel, much less one that imitated moonstone. Given moonstone's wide availability and typically modest price, it is unlikely that there are many such specimens in the market. Nevertheless, buyers should be aware that imitations can occur at any price level. And even though this cabochon proved to be a synthetic imitation, it can be appreciated as an interesting specimen in its own right.

Nathan Renfro

Figure 16. This ~5 ct synthetic star spinel made a convincing moonstone imitation in diffused lighting, but in direct lighting it showed a pronounced star.

2011 TUCSON

Figure 1. Among the Vietnamese spinels seen at this year's Tucson shows was the 2.59 ct cobalt blue gem on the left (courtesy of Palagems.com, Fallbrook, California; photo by Robert Weldon). The rare väyrynenite from Pakistan on the right weighs 2.41 ct (photo and stone courtesy of The Gem Trader, Surprise, Arizona).

Many dealers at this year's Tucson gem and mineral shows were surprised by better-than-expected sales on the heels of the global economic downturn. The success was apparently due to the need to restock inventories after buying was curtailed during the past two years, as well as enthusiasm for an improved economic outlook. Some of the gem and mineral standouts included Vietnamese spinel (see figure 1 left and report on pp. 60–61 of this issue), rare stones that are also quite attractive (e.g., the väyrynenite in figure 1 right), and some large pieces of gem rough (e.g., the morganite in figure 2). Several additional notable items seen in Tucson are described in the following pages and will also be documented in future issues of *G&G*.

The theme of this year's Tucson Gem and Mineral Society show was "Minerals of California," which featured many displays of particular interest to gemologists such as pegmatite gems and benitoite. The theme of the 2012 TGMS show will be "Minerals of Arizona" in honor of Arizona's Centennial.

G&G appreciates the assistance of the many friends who shared material and information with us this year, and also thanks the American Gem Trade Association for providing space to photograph these items during the AGTA show.

COLORED STONES AND ORGANIC MATERIALS

Faceted cavansite. Cavansite is a rare calcium vanadium phyllosilicate that occurs primarily as fibrous ball-shaped aggregates. Most cavansite on the market is recovered from cavities in basaltic rocks near Pune, India, that are part of the famous Deccan Traps (see M. F. Makki, "Collecting cavansite in the Wagholi quarry complex,

Figure 2. This semi-transparent morganite from Brazil weighs an impressive ~22.4 kg, and was part of an even larger crystal. The stone's pleochroism is easily visible when viewed from different directions. Photos by Eric Welch; courtesy of BC Gemas do Brasil, Governador Valadares, Brazil.

Figure 3. These bright blue stones (1.45–2.45 ct) are faceted examples of the rare mineral cavansite. Photo by Robert Weldon.

Pune, Maharashtra, India," *Mineralogical Record*, Vol. 36, No. 6, 2005, pp. 507–512). Though its bright saturated blue color has made it sought-after by mineral collectors, it has not seen use as a gemstone because of its low hardness (Mohs 3.5) and durability.

At the Gem & Jewelry Exchange (GJX) show, Mauro Panto of The Beauty in the Rocks, Perugia, Italy, offered numerous pieces of faceted cavansite (e.g., figure 3). Most stones weighed 1–5 ct, rarely up to 10 ct. He said that about 500 carats have been faceted so far, all showing the typical bright blue to greenish blue coloration of cavansite.

As would be expected, faceting cavansite is very difficult, since the fibrous crystals are prone to splitting. According to Mr. Panto, the material is faceted by a proprietary process that does not involve stabilization or treatment of any kind. Because of the aggregate nature of the material, the cut stones typically contain small cavities, and only top-quality pieces show no pits or nicks. It is always translucent.

Though it is intended as a collectors' stone, Mr. Panto reported that a few designers have set faceted cavansite in jewelry. Because production of cavansite is limited and good-quality pieces suitable for faceting are rare and expensive, only limited amounts of the cut material are expected to be available in the future.

Thomas W. Overton (toverton@gia.edu)
GIA, Carlsbad

New find of green grossular at Merelani, Tanzania. While in Tucson for the gem and mineral shows, Bill Larson (Palagems.com, Fallbrook, California) and Steve Ulatowski (New Era Gems, Grass Valley, California) showed this contributor some newly mined green grossular from Tanzania that was impressive for its transparency and good color. They said it was produced in mid-December 2010 from Block D at the Merelani tanzanite mines. All the new production reportedly came from a single pocket that yielded ~0.5 kg of grossular crystals and did not contain any tanzanite. The crystals were lustrous and very well formed (e.g., figure 4); some had only a small attachment point with the graphite matrix. The presence of graphite on the base of some crystals gave them a dark appearance when viewed in some directions. Several gemstones have been cut from this grossular, reportedly up to nearly 100 ct, and they display a more intense color than typical "mint" green garnet from this deposit (e.g., figure 5).

Brendan M. Laurs

Blue quartz colored by trolleite and lazulite inclusions. At the Pueblo Gem & Mineral Show, Leonardo Silva Souto (Cosmos Gems, Teófilo Otoni, Brazil) displayed blue quartz colored by crystalline inclusions. He stated that the material was mined in the northern part of Minas Gerais

Figure 4. These grossular crystals (1.49–26.82 g) were recovered in mid-December 2010 from Merelani, Tanzania. Courtesy of Palagems.com; photo by Robert Weldon.

Figure 5. Compared to typical "mint" green garnet (center, 10.62 ct) from Tanzania, the new production shows a more intense color (left and right, 8.67 and 17.13 ct). Courtesy of New Era Gems; photo by Jeff Scovil.

State in Brazil. His company acquired a 70–80 kg rough parcel in Teófilo Otoni in August 2010, which was polished into approximately 3,500 carats of translucent to opaque cabochons weighing 10–30 ct (e.g., figure 6). The color was mostly homogeneous, though a few stones were zoned in blue to greenish blue.

Three opaque cabochons (~20 ct each) were donated to the Mineralogy Museum at the University of Rome "La Sapienza," and examined for this report. They were characterized by standard gemological techniques, and also by a Cameca SX-50 electron microprobe at the Italian National Research Council's Institute of Environmental Geology and Geoengineering (IGAG-CNR) in Rome. The gemological properties were consistent with quartz, and microscopic examination revealed diffuse and interconnected wispy blue areas. Microprobe analyses of the blue inclusions identified both trolleite and lazulite (see the G&G Data Depository at gia.edu/gandg), which are aluminum phosphates.

Colored by mineral inclusions rather than trace elements or color centers, natural blue quartz is always

Figure 6. These blue quartz cabochons (~10–30 ct) are colored by trolleite and lazulite inclusions. Photo by M. Campos Venuti.

either translucent or opaque. Quartz with blue inclusions of dumortierite, riebeckite, tourmaline, gilalite, lazulite, ajoite, and papagoite are well known in the literature. To the best of our knowledge, however, this is the first documented case of blue quartz colored by trolleite and lazulite.

According to Mr. Souto, additional production of this quartz is expected in the future. The trolleite and lazulite inclusions are not particularly attractive on their own, making this material an unlikely candidate for the inclusion collector's market. Nevertheless, the homogeneous blue color and the availability in calibrated sizes give this quartz interesting potential for jewelry.

Michele Macrì (michele@minerali.it) and Adriana Maras
Department of Earth Sciences
University of Rome "La Sapienza"

Marcello Serracino and Marco Albano
IGAG-CNR, Rome

Spectral interference in quartz from India. At the Pueblo Gem & Mineral Show, an interesting variety of quartz was being marketed under the name "Anandalite" by Nirvana Stone (Tokyo and Osaka, Japan). To the casual observer, this material appeared to be ordinary quartz crystal clusters, but closer inspection under direct lighting revealed a distinct phenomenon: spectral interference colors under minor rhombohedral faces. These clusters came in a wide

Figure 7. This quartz from India (46 g cluster and 0.29 ct faceted stone) shows spectral interference colors due to lamellar twinning. Photo by Robert Weldon.
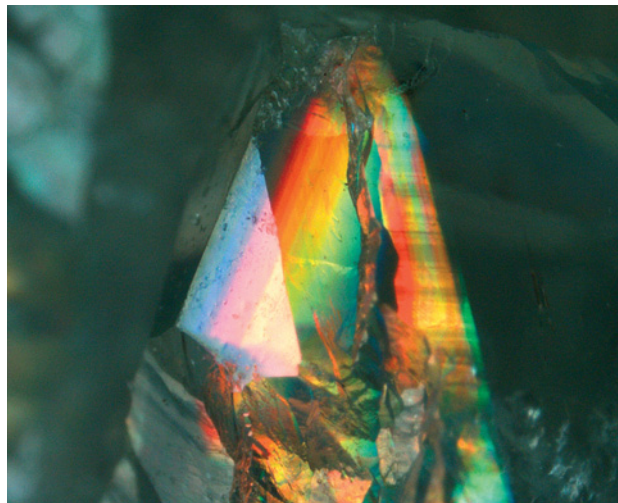
Figure 8. The subsurface location of the interference colors shows that the feature is a natural phenomenon in the quartz and not the result of a coating. Photomicrograph by N. Renfro; magnified 20×.

Figure 9. This attractive yellow scapolite is reportedly from the southern Indian state of Tamil Nadu. Courtesy of John Taylor (27 × 11 mm crystal) and Dudley Blauwet Gems (5.27 ct cut stone); photo by Robert Weldon.

variety of sizes, from a few grams to hundreds of grams (e.g., figure 7). Most of the individual quartz crystals were on the order of ~5 mm long, with some specimens featuring crystals up to ~15 mm long. The quartz ranged from colorless to very pale purple; faceted stones were also available in sizes up to several carats. The dealer stated that the source was India, but did not specify an exact locality.

This phenomenon in quartz is known as the "Lowell effect," after gem dealer Jack Lowell, who first observed it in amethyst from Artigas, Uruguay. The effect has also been seen in quartz and amethyst from Orissa, India, and Washington state (E. G. Gübelin and J. I. Koivula, *Photoatlas of Inclusions in Gemstones*, Vol. 2, Opinio Verlag, Basel, Switzerland, 2005, pp. 568 and 644). The cause appears to be lamellar twinning along the minor rhombohedral faces (figure 8). The twinning likely results from a modification in the growth environment during the late stages of formation, given the fact that so many of the crystals in a single cluster show the phenomenon at the same stage of growth.

While this is not the first time such material has been reported, this does appear to be the first time it has been mined in marketable quantity. Since this phenomenon resembles the much more common iridescence from air-filled cracks, it is possible that such phenomenal quartz has been overlooked in the past.

Nathan Renfro (nrenfro@gia.edu) and John I. Koivula
GIA Laboratory, Carlsbad

Scapolite from India. At the AGTA show, Dudley Blauwet (Dudley Blauwet Gems, Louisville, Colorado) exhibited rough and cut yellow scapolite from a relatively new find in India (figure 9). According to his supplier, the crystals came from a pegmatite located ~10 km from Karur in the southern Indian state of Tamil Nadu. The scapolite reportedly was mined from seams between layers of feldspar.

Mr. Blauwet first encountered the rough material at the September 2009 Denver Gem and Mineral Show. Since then, one of his part-time employees (John Taylor of Bloomington, Illinois) purchased four lots of terminated crystals from the Indian supplier, and in September 2010 Mr. Blauwet obtained a parcel of gem rough (broken crystals) from the same supplier. Nineteen stones have been faceted, 76.14 carats in total, ranging from 3.11 to 5.27 ct. These consisted of matched sets, pairs, and suites of similar-sized stones, cut with the table oriented perpendicular to the c-axis for the best color. He reported that all of the stones except one had an RI range of 1.537–1.556. This corresponds to an intermediate composition between marialite and meionite (W. A. Deer et al., *Rock-Forming Minerals—Framework Silicates*, Vol. 4, Longman, London, 1963, pp. 321–337). The stones fluoresced intense pink-orange to short-wave UV radiation and (with one exception) lavender to long-wave UV.

Despite numerous buying trips to India over the past 30 years, Mr. Blauwet has never encountered gem-quality Indian scapolite. A review of the literature yielded only one reference to such material (U. Henn, "Scapolite cat's-eyes from India," *Gemmologie: Zeitschrift der Deutschen Gemmologischen Gesellschaft*, Vol. 54, No. 1, 2005, pp. 55–58), but the samples documented in that article were chatoyant and typically brownish orange to yellowish brown. Mr. Blauwet stated that the top-quality material from the new locality has a lighter but more consistent color than fine scapolite from Dodoma, Tanzania.

Stuart D. Overlin (soverlin@gia.edu)
GIA, Carlsbad

Figure 10. At Lang Chap in northern Vietnam, miners dig through mud in search of spinel while local buyers observe the digging from above (photo by D. Blauwet). The Lang Chap spinels in the inset weigh 1.71–3.18 ct (photo by Robert Weldon).

Spinel from northern Vietnam, including a new mine at Lang Chap. The year 2010 saw impressive production of spinel from Yen Bai Province in northern Vietnam (see, e.g., Summer 2010 Gem News International [GNI], pp. 151–153). This material was widely available in Tucson, including at this contributor's booth at the AGTA show. In May, June, and October, this author visited all of the deposits reviewed here except for Bai Son and Trum Chan.

A new mine at **Lang Chap** (figure 10) was discovered in mid-April in a remote bamboo jungle about 20 km west-southwest of Luc Yen (Yen The) at 22°05′86″N, 104°34′83″E. By late May, some 350 people were working secondary deposits to a depth of ~2 m in a steep narrow valley. Waterworn pieces of "maroon" (dark purplish red) spinel up to 3 cm across were found, along with excellent red-pink to pinkish red-orange gem rough. By October,

though, the number of workers at Lang Chap had dwindled to about 30, and less rough material was available. For more information on this mine, see D. Blauwet, "La mine de spinelle de Lang Chap, au Nord du Vietnam," *Revue de Gemmologie A.F.G.*, No. 173, 2010, pp. 11–15.

The most important of Vietnam's spinel deposits, Cong Troi (Gateway to the Sun) at **An Phu**, has been mined since the mid-1990s and had another good year in 2010. In addition to well-formed crystals embedded in marble, the production included rough material from alluvial traps in the weathered marble. This locale is known for its variety of spinel colors (figure 11, left), consisting mainly of maroon to purple, pink, and padparadscha-like stones. In addition, the mine has produced dark blue to grayish blue, light bluish gray, and "lavender" to purple spinel, along with a rare variety that is lavender in daylight and pink under incandescent light.

Elsewhere in Yen Bai Province, "cobalt" blue spinel (figure 11, right) was still available from the **Bai Son** mine near An Phu. Some of this violetish blue spinel changes to violet-purple under incandescent light (see also J. B. Senoble, "Beauty and rarity—A quest for Vietnamese blue spinels," *InColor*, Summer 2010, Issue 14, pp. 18–23). Large pieces of rough (8–20 g) were seen in local markets in June, though clean material was very rare. Bai Son also yields a rare "sky" blue spinel, some of which turns lavender under incandescent light. Cobalt blue spinel was also obtained from mines located about 10 km from Luc Yen, at **Bai Gau** (dark blue) and **Trum Chan** (light to medium blue). Some of the lighter blue spinel from Trum Chan turns light lavender under incandescent light. A 370 g color-zoned (light "aqua" blue to a medium "sky" blue) specimen containing transparent areas was discovered at Trum Chan in June. Other colors include light pink, smoky pink, pink-red to red-orange (figure 12, center-right stone), and various shades of lavender and maroon.

Bai Linh, located 10 km northeast of Luc Yen near the corundum deposit of Lieu Do, produces orange-red spinel

Figure 11. The Cong Troi mine at An Phu produces a wide range of spinel colors (left, 0.97–6.07 ct). Other mines in the An Phu–Luc Yen area yield "cobalt" blue spinel (right, 1.83–7.78 ct). Photos by Robert Weldon.

Figure 12. These pink to red to red-orange spinels come from Tan Huong (three stones on left, 2.05–6.00 ct), Minh Tien (top right, 4.20 ct), Trum Chan (center right, 2.10 ct), and Bai Linh (bottom right, 0.62 ct). Composite photo by Robert Weldon.

Figure 13. These four samples (the tabular crystal weighs 0.6 g) are the rare mineral zektzerite. Photo by Brad Payne.

(figure 12, bottom right). A limited amount of pink to purplish pink spinel (figure 12, top right) comes from alluvial workings between An Phu and the noted tourmaline locale of **Minh Tien** several kilometers to the north. Only a few pieces offered in local markets were identified as being from this area, but all of them were relatively large (3+ g).

In the Yen Bai area, pink to dark purplish red stones (figure 12, left group) have been produced from **Tan Huong**, a noted star ruby locality ~80 km south of Luc Yen. Cut spinels from this area range up to 6 ct.

Production of spinel from Yen Bai Province is expected to continue during the 2011 mining season.

Dudley Blauwet (mtnmin@q.com)
Dudley Blauwet Gems, Louisville, Colorado

Gem zektzerite. Rare minerals occasionally find their way to the hands of a lapidary, where they are transformed into gems. This was the case with a small parcel of zektzerite recently loaned to GIA for examination by Brad Payne, who also offered this material at the 2011 Tucson Gem & Mineral Show.

Zektzerite, $LiNaZrSi_6O_{15}$, is an orthorhombic mineral in the tuhualite group. It was named in honor of geologist Jack Zektzer, who first initiated a study of this material at the Smithsonian Institution's Department of Mineral Sciences in 1975. His samples originated from the Golden Horn batholith in Okanogan County, Washington, the same source as the old stock that Mr. Payne recently acquired and faceted.

Six faceted samples (0.21–1.54 ct) and a 0.6 g tabular pseudohexagonal crystal were examined at the GIA Laboratory in Carlsbad. With the exception of one light purplish pink gem, the faceted stones had a light brownish yellowish orange color (figure 13). Standard gemological testing revealed RIs of 1.580–1.583. The average SG, determined optically using a Sarin device, was 2.81. All of the samples were inert to long-wave UV-radiation, and fluoresced weak to moderate yellow to short-wave UV. These characteristics are consistent with those reported for zektzerite in mineralogy textbooks. Raman analysis confirmed this identification.

Magnification revealed liquid "fingerprint" inclusions and cleavages throughout the stones (figure 14, left). One sample also contained numerous dark blue pleochroic elongated crystals (figure 14, right), but their depth precluded Raman analysis.

A review of the literature found no published reports of faceted zektzerite. Given the rarity of this material, it would seem to have a niche as a collector's stone.
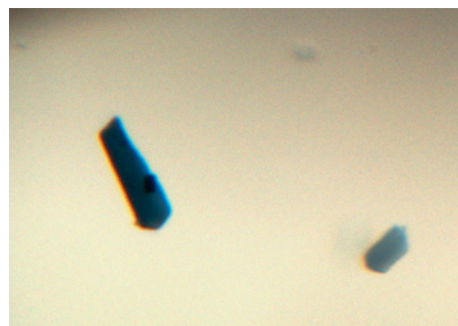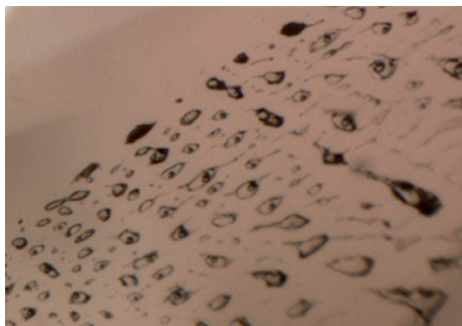
Nathan Renfro

Figure 14. Inclusions in the zektzerite consisted of fluid fingerprints composed of numerous negative crystals with communication tubes (left), as well as dark blue pleochroic crystals (right). Photomicrographs by N. Renfro; magnified 110×.

SYNTHETICS AND SIMULANTS

"Coral Sea" agate. At the AGTA show, Bill Heher (Rare Earth Mining Co., Trumbull, Connecticut), had some new doublets that were marketed as Coral Sea agate (figure 15). Formed of natural lace agate from Oregon on a reconstituted turquoise backing, the polished slab had scenes resembling a coral reef. The concept was developed by lapidary Fred Graupp (Robesonia, Pennsylvania).

Sizes ranged from 18 × 13 mm ovals up to free-form pieces of 70 mm or larger. Mr. Heher stated that he has sold over 200 pieces, but supplies are limited because the production process is very labor intensive.

Thomas W. Overton

Figure 16. *The profile view of this 16 × 25 mm agate doublet reveals its quartz cap. Composite photo by Robert Weldon.*
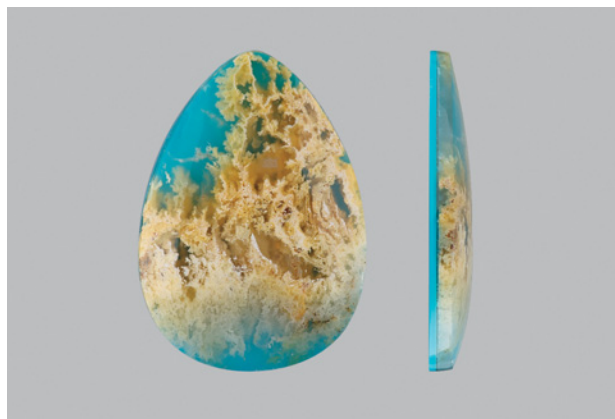
Figure 15. *Doublets of lace agate and reconstituted turquoise, sold as Coral Sea agate, often resemble coral reef scenes. The piece shown here weighs 37.40 ct; its assembled structure is apparent when viewed along the edge. Composite photo by Robert Weldon.*

Dendritic agate in doublets, inlays, and jewelry. The Fall 2008 GNI section (pp. 262–263) reported on a large selection of dendritic agate from central India. The stones were fashioned by Indus Valley Commerce (Ghaziabad, India) to reveal an array of colors and patterns, in a clarity range of transparent to translucent. At the Arizona Mineral and Fossil Show, the company exhibited some attractive new applications of the material, in the form of doublets, inlays, and pendant jewelry.

The doublets are produced by bonding a cap of clear quartz to a typically thin layer of agate, giving it a beveled appearance (figure 16). According to company director Tarun Adlakha, the museum-grade epoxy and two-week curing process ensure strength and color stability, even under UV exposure. The inlays (figure 17) offer other interesting design possibilities, with dendritic agate discs framed inside of other gem materials such as rock crystal, jasper, chrysoprase, obsidian, tiger's-eye, and banded agate. The agate pendants (e.g., figure 18) are made by hand and combine Mogul-inspired floral motifs with garnet, spinel, emerald, sapphire, and old-cut diamond accents. The agates

in the inlay and jewelry pieces range from 6 to 50 mm.

The 2008 GNI report noted that Indus Valley Commerce had planted cucumbers and other deep-rooting vines to loosen the alluvium along the Narmada River and draw the agate nodules to the surface. While that method is still used to some extent, most of the mining is now done by conventional digging, in pits as deep as 50–60 feet (15–18 m). Current production totals 7,000–8,000 finished pieces annually.

Stuart D. Overlin

Figure 17. *This ensemble shows dendritic agate inlaid in chrysoprase (left, 22 × 35 mm), snowflake obsidian (center, 31 × 37 mm), and agate (right, 30 mm). Photo by Robert Weldon.*

Figure 18. This Mogul-style pendant features a 51 ct dendritic agate set in gold with flat-cut diamonds and a carved garnet drop. The adjustable cord is strung with garnet beads and shellac-filled 22K gold spacers. Photo by Jeff Scovil.

GNI REGULAR FEATURES

DIAMONDS

Artisanal diamond mining in Liberia. Since the early 1900s, northwest Africa has been an important source for diamonds, almost all of them alluvial. Sierra Leone, Guinea, Ivory Coast, and Liberia (figure 19) are the main diamond sources in this region. The deposits are mainly worked by artisanal miners, who continue to prospect new fields in the area.

Liberia's Mano River basin is located in Grand Cape Mount County and forms part of the border with Sierra Leone. It is underlain by the Mano Craton of West Africa. Small diggings in this field commonly produce 0.5–4 ct yellow diamonds (figure 20), as well as some gray and brown stones. Very rarely recovered are light green, blue, and pink diamonds in the ~0.5–1.5 ct range. Although it is impossible to know the exact production from the Mano River basin, the monthly yield (including industrial-quality stones) is likely a few hundred carats, with ~10% or less being gem quality.

A less significant source of Liberian diamonds is the

Figure 19. The Mano River basin and the Ganta field are sources of diamond in Liberia.

Ganta field in Nimba County, located near the border with Guinea. This area is less populated and has fewer miners, but it has an alluvial structure similar to that of the Mano River basin. This contributor saw many different qualities and colors of diamonds during a visit in November 2010 (figure 21). Most of the stones weighed 0.5–8 ct and were heavily included (industrial quality), showing macle and ballas (fibrous spherical) morphology.

Makhmout Douman (makhmout@arzawagems.com)
Arzawa Mineralogical Inc., New York

COLORED STONES AND ORGANIC MATERIALS

Update on emerald mining at Kagem, Zambia. In January 2011, these contributors spent three days at the Kagem emerald mine in the Kafubu area of northern Zambia.

Figure 20. Miners dig for diamonds along the Mano River near the town of Lofa. The yellow Mano River diamonds in the inset weigh 4.38 and 0.68 ct. Photos by M. Douman.
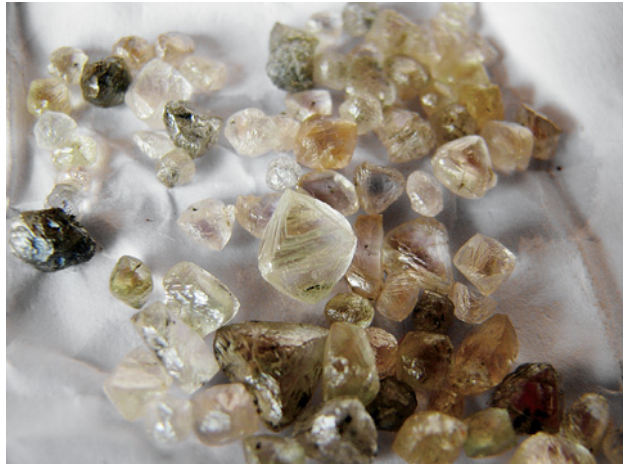
Figure 21. A wide range of quality is exhibited by diamonds (here, 0.4–6 ct) from the Ganta area of Liberia. Photo by M. Douman.

Kagem, owned and managed by Gemfields (London), is located 35 km south of Kitwe, near the border with the Democratic Republic of Congo. Our visit was led by Gemfields geologist Robert Gessner.

The Kagem mine (figure 22) is located on the eastern 2 km of the Fwaya-Fwaya belt, which runs east to west over 8 km and is one of the world's richest emerald deposits. Production takes place year-round, though it slows during the rainy season. The gems are found in a biotite-phlogopite schist reaction zone (10 cm to 1 m thick) that mainly formed between subvertical quartz-tourmaline veins and the host ultramafic talc-magnetite-schist. The emeralds are recovered by "chiselers" using hand tools. (For more on the geology and mining of Zambian emeralds, see J. C. Zwaan et al., "Emeralds from the Kafubu area, Zambia," Summer 2005 *G&G*, pp. 116–148; and Winter 2009 GNI, pp. 298–299.) The mineralized material surrounding the hand-mined areas is transported to a washing plant and separated into low- and high-grade piles for processing. After the material has been crushed and washed, the emeralds are hand-picked from conveyor belts. Automated optical sorting is not feasible, as the emeralds are often still embedded in the schist. After trimming/cobbing, the emeralds are soaked in mineral oil and sorted by color, clarity, and size (e.g., figure 23). The stones range up to 5–6 cm long, and good-quality emeralds measuring 4–5 cm are not uncommon.

Kagem has traditionally been an open-pit mine. The huge excavation we witnessed during our visit (again, see figure 22) was dug since 2007 (and Gemfields' arrival in 2008), and resulted from merging three pits (Chama, Fwaya-Fwaya, and F10). Most of the current production is coming from that excavation. However, because the emerald-bearing zone dips 16° south-southeast, large amounts of waste material must be removed to reach it. In February 2009, Gemfields began a feasibility study for underground exploitation. At the time of our visit, a mining project located in the former F10 pit area had reached a depth of 135 m, with 43 m comprised by an inclined tunnel. Along the tunnel there were 70 m of exploratory workings. The company plans to extend the tunnel 130 m deeper.

The authors also visited a new open pit that is being explored by Gemfields at Lushingwa, located 1.5 km southeast of the Fwaya-Fwaya pit. Since the geology varies considerably over the area, core drilling is being done to gain a better understanding of the emerald mineralization.

Gemfields has an efficient, well-run operation in place. The biggest challenges are profitably producing good-quali-

Figure 22. Gemfields' Chama/Fwaya-Fwaya/F10 pit at the Kagem mine is one of the largest colored stone excavations in the world. Photo by V. Pardieu.

Figure 23. A small amount of the production from Kagem consists of top-grade emeralds such as those shown here (up to 2 cm long). Some of the crystals are partially covered by a thin layer of biotite-phlogopite from the host schist. Photo by V. Pardieu.

ty rough while preventing theft and illegal mining from such a large (46 km^2), thickly forested area. The company is concerned about the safety and living conditions of its workers and supports social projects in the area, particularly education.

Flavie Isatelle (flavie.isatelle@gmail.com)
Centre de Recherche Gemmologique
University of Nantes, France

Vincent Pardieu
GIA Laboratory, Bangkok

Pargasite from Tanzania. G. Scott Davies (American-Thai Trading, Bangkok) recently donated eight specimens of transparent yellowish brown pargasite to GIA (figure 24). The five rough stones ranged from 0.3 to 1.67 g, and the three faceted samples weighed 1.23, 1.25, and 1.39 ct. All are reportedly from the Dodoma region in central Tanzania. Mr. Davies said that he obtained 700 grams of rough in

Figure 24. These five rough and three faceted pargasite samples from Tanzania range from 1.23 to 8.36 ct. Gift of American-Thai Trading, GIA Collection nos. 38317–38324. Photo by G. Scott Davies.

Bangkok in late 2007, but has not encountered any additional rough material since then. The stones faceted from this material were medium-to-dark slightly yellowish brown, and the largest stone he cut weighed just over 3 ct; perfect cleavage makes cutting larger stones a challenge.

The rough and cut samples were examined at the GIA Laboratory in Bangkok. All of the crystals exhibited perfect cleavage in one direction parallel to the prism. Three had cleaved surfaces on two parallel sides, while two others showed one cleaved surface, with the opposite parallel surface appearing natural in form; one of those faces possessed distinct etch marks. Standard gemological testing of the rough and faceted samples gave the following properties: color—orangy brown to yellowish brown, with pronounced pleochroism (greenish yellow and brown); RI (from the faceted stones)—n_α = 1.628, n_β = 1.633, and n_γ = 1.648; optic sign—positive; birefringence—0.020; hydrostatic SG—3.09 (with two of the rough pieces registering 3.07 and 3.08); Chelsea filter reaction—none; fluorescence—inert to long-wave UV radiation, and moderate to strong chalky yellow to short-wave UV; and no diagnostic absorption features visible with a handheld spectroscope. Microscopic examination revealed numerous fine oriented tubes and pinpoints throughout the stones, as well as some planar fluid inclusions (related to incipient cleavage). Some of the rough samples exhibited distinct two-phase inclusions containing an unidentified metallic crystal. Other than the SG, these properties are close to those of a pargasite sample from Myanmar described in the Fall 2004 GNI section (pp. 254–256). However, the SG still falls within the range reported for pargasite in mineralogy textbooks.

Pargasite is a member of the amphibole group and has the chemical formula $NaCa_2[(Mg,Fe^{2+})_4Al](Si_6Al_2)O_{22}(OH)_2$. Energy-dispersive X-ray fluorescence (EDXRF) spectroscopy of the samples detected major Si, Ca, Al, Mg, and Fe—as would be expected from pargasite's formula (Na is not detectable by this method)—as well as traces of Ti and K. Raman analysis produced a match to the pargasite reference spectra in GIA's Raman database. To the best of our knowledge, this is the first report of gem-quality pargasite from Tanzania.

Nick Sturman (nsturman@gia.edu)
GIA Laboratory, Bangkok

Scapolite from Afghanistan. In February 2010, GIA received some colorless scapolite from Dudley Blauwet that was notable for its fluorescence and inclusions. According to his supplier, it came from the Chilmak mine, which is located above Kiran village ~10 km from the historic lapis lazuli mines (Lajuar Madan) in the Kokcha Valley, Sar-e-Sang District of Afghanistan. Mr. Blauwet first saw matrix specimens of this material in 2005. In mid-December 2009, he purchased a 1.3 kg rough parcel in Peshawar, Pakistan, which consisted of broken fragments and some complete crystals. The majority of the material was semitranslucent; less than 100 g was translucent to transparent, and some of this contained small but conspic-
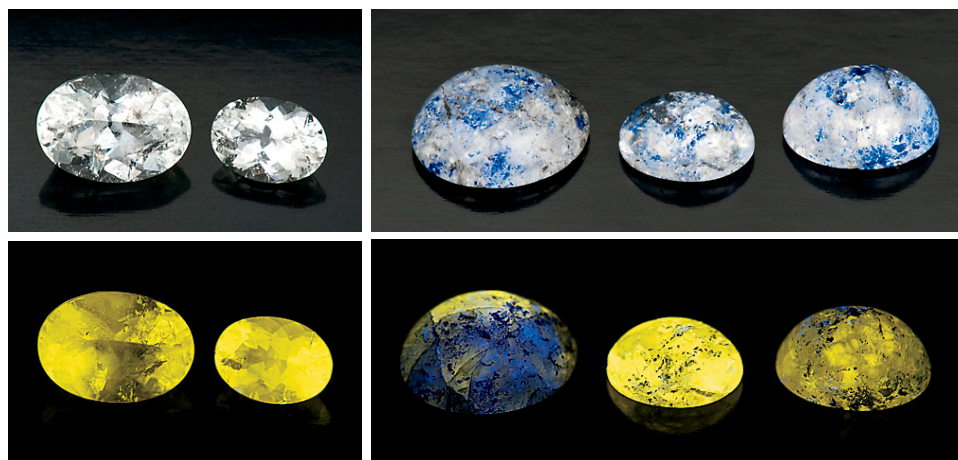
Figure 25. These faceted (0.66 and 1.59 ct) and cabochon-cut (1.48–3.06 ct) scapolites are from Afghanistan. They fluoresced yellow when exposed to UV radiation (bottom, long-wave UV). Photos by Robert Weldon.

uous inclusions of a bright blue mineral. He offered a few faceted stones for the first time at the 2010 Tucson gem show. In November 2010, he purchased 1.7 kg of similar material in Peshawar, with 5–10% being transparent enough to facet into clean stones or translucent cabs with the blue inclusions. As of April 2011, he had cut 19 stones that ranged up to 3.98 ct (most weighed ~1.5 ct); he predicted a total of 120 carats when the cutting is complete.

Five polished scapolite samples from Mr. Blauwet (figure 25, top) were examined at GIA: two faceted stones (0.66 and 1.59 ct) and three cabochons (1.48, 2.36, and 3.06 ct). All were colorless with varying degrees of transparency; the cabochons had numerous eye-visible blue inclusions. Standard gemological testing yielded the following properties: RI—1.539–1.549; birefringence—0.005–0.009; and hydrostatic SG—2.55 and 2.59 for the faceted stones and 2.49–2.59 for the cabochons. These properties are consistent with published values for scapolite-group minerals. In addition, scapolite is known to have strong UV fluorescence. The faceted stones fluoresced very strong yellow to long-wave UV radiation (figure 25, bottom) and moderate yellow to short-wave UV. The heavily included cabochons showed weaker reactions.

Scapolite is a solid-solution series with marialite ($Na_4Al_3Si_9O_{24}Cl$), meionite ($Ca_4Al_6Si_6O_{24}CO_3$), and silvialite ($Ca_4Al_6Si_6O_{24}SO_4$) end members (M. Superchi et al., "Yellow scapolite from Ihosy, Madagascar," Winter 2010 *G&G*, pp. 274–279). EDXRF spectroscopy indicated that all the samples contained Na, Al, Si, S, K, Ca, Cl, Br, and

Sr. Laser ablation–inductively coupled plasma–mass spectrometry analysis confirmed most of these elements except Cl and Br; additionally, it also identified the presence of Li, Be, and B, as well as Rb, Ba, and Pb. Quantitative data reduction for one sample indicated it was mainly marialite with a very small silvialite component. This result was consistent with the RI and SG measurements, which indicated a nearly pure marialite composition.

Typical inclusions in the faceted stones were feathers and numerous tiny crystals, some of which had a blue color similar to that seen in the cabochons (figure 26, left). These blue crystals were identified as lazurite by Raman microspectroscopy. One of the faceted stones contained two elongated euhedral crystals, one of which had a sharp termination. Raman spectroscopy identified them as apatite (figure 26, right).

Although similar yellow fluorescence has been reported in scapolite from Tanzania (J. E. Arem, *Color Encyclopedia of Gemstones*, 2nd ed., Van Nostrand Reinhold, New York, pp. 166–167), the inclusions in this Afghan material are distinctive.

Andy H. Shen (andy.shen@gia.edu)
GIA Laboratory, Carlsbad

Tourmaline finds at Mt. Marie, Paris, Maine. Some notably bright colors of tourmaline have recently been produced from the Mt. Marie quarry in Oxford County, Maine. The site is located 7 km east of South Paris and 6.5 km southeast of the famous Mount Mica pegmatite (see

Figure 26. Inclusions of blue lazurite (left) and prismatic apatite (right) were seen in the scapolites. Photomicrographs by A. H. Shen; image widths 3.7 mm (left) and 2.1 mm (right).
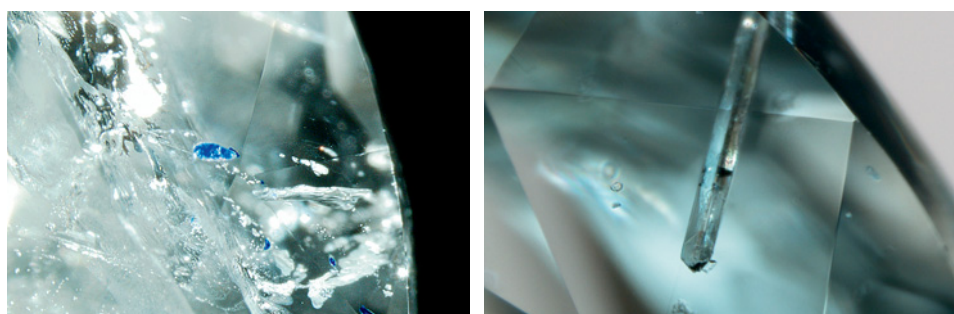
W. B. Simmons et al., "Mt. Mica: A renaissance in Maine's gem tourmaline production," Summer 2005 *G&G*, pp. 150–163). The quarry was originally opened in 1901 by the Mt. Marie Mineral Company in the search for feldspar for industrial use (J. C. Perham, *Maine's Treasure Chest: Gems and Minerals of Oxford Co.*, 2nd ed., Quicksilver Publications, West Paris, Maine, 1987). Mining continued sporadically at Mt. Marie throughout the last century and resulted in numerous quarries and small exploratory pits in the large granite pegmatite. This dike is part of the Oxford pegmatite field of western Maine and is geochemically classified as an LCT-type pegmatite (i.e., relatively enriched in lithium-cesium-tantalum). The portion of the pegmatite that most frequently bears miarolitic cavities ("pockets") is 3–5 m thick, ~30 m wide on an approximate east-west strike, and dips south at ~16°.

The quarry is currently owned by Mt. Marie LLC, and is under lease to Mt. Marie Mining LLC; one of these authors [DD] has mined the site since 1993. Between 1993 and the end of the 2008 field season, the mine produced several sub-meter-sized pockets that contained ~4,000 carats of facet-grade gem tourmaline in a broad range of colors, including pink, reddish orange, green to greenish blue, and blue (e.g., figure 27). There were also uncommon finds of facetable black tourmaline (schorl), colorless to light pink cesium beryl, and smoky quartz.

In May and June of 2009, two pockets (e.g., figure 28) produced 2,000 carats of bluish green to blue facet-grade tourmaline. About 500 carats of this material, including a 13.4 g crystal section (figure 29, left), was blue when viewed perpendicular to the c-axis and intense blue when viewed down the c-axis. About 60 carats of faceted stones weighing 1.0–5.5 ct have been cut from this material to date. Most of the remaining 1,500 carats is a more typical bluish green (darker when viewed down the c-axis). A few bicolored crystal sections were produced that exhibit both bluish green and greenish blue to blue colors.

From mid-2009 through October 2010, efforts were primarily directed at improving mine access and removing additional hanging wall from the productive zone. Mining resumed in November 2010—yielding an attractive yellowish green crystal (figure 29, right)—and will continue in the 2011 field season.

Dennis Durgin (dennisd@megalink.net)
Mt. Marie Mining LLC, Hebron, Maine

Jim Clanin
JC Mining, Bethel, Maine

The origin of color in tourmaline from Mt. Marie, Maine. In September and December 2010, Dennis Durgin sent this author two fragments of recently mined Mt. Marie tourmaline for color-origin investigation. The samples were yellowish green (GRR 2016, 19 × 12 × 9 mm) and dark blue (GRR 2924, 15 × 15 × 6 mm). The green piece displayed a prism face and was polished into a 6.06-mm-thick wafer. The blue fragment was sliced parallel to the c-

Figure 27. These tourmalines (1.05–4.10 ct) are representative of material produced from Mt. Marie in Oxford County, Maine, since 1993. Photo by Jeff Scovil.

axis and polished into a 1.25-mm-thick wafer. Absorption spectra were collected in the 350–1100 nm range using a silicon diode-array microspectrometer with a calcite polarizer, and in the 1000–2000 nm region with a Nicolet Magna 860 FTIR spectrometer with a CaF_2 beam splitter, a deuterated triglycine sulfate detector, a tungsten-halogen lamp, and a $LiIO_3$ crystal polarizer.

When viewed down the c-axis of the samples, the absorption behavior was governed by the light polarized perpendicular to the c-axis (i.e., E⊥c). Both the blue and green colors of Mt. Marie tourmaline showed strong absorption below 350 nm in the UV region and a transmission window in the violet-to-yellow wavelengths (400–600 nm; figure 30). Both also had a broad Fe^{2+}

Figure 28. The Mt. Marie quarry has recently produced some exceptional blue to greenish blue tourmaline. Mine owner Dennis Durgin is shown here with one of the pockets opened in 2009. Photo by Hugh Durgin.

Figure 29. Both pleochroic colors can be seen in the blue 13.4 g Mt. Marie tourmaline on the left. The 27.8 g yellowish green crystal on the right was recovered in November 2010. Photos by Jeff Glover (left) and Hugh Durgin (right).

absorption centered near 710 nm in the deep red region and an additional Fe^{2+} absorption in the near-infrared from 1000 to 1500 nm. Sharp absorption from hydroxyl groups occurred in the 1400–1500 nm range, predominantly parallel to the c-axis.

Figure 30. These UV-Vis-NIR absorption spectra of green (top) and blue (bottom) tourmaline from Mt. Marie (plotted for 1.0 cm thickness) illustrate the features that are responsible for their respective colors.

UV-VIS-NIR ABSORPTION SPECTRA
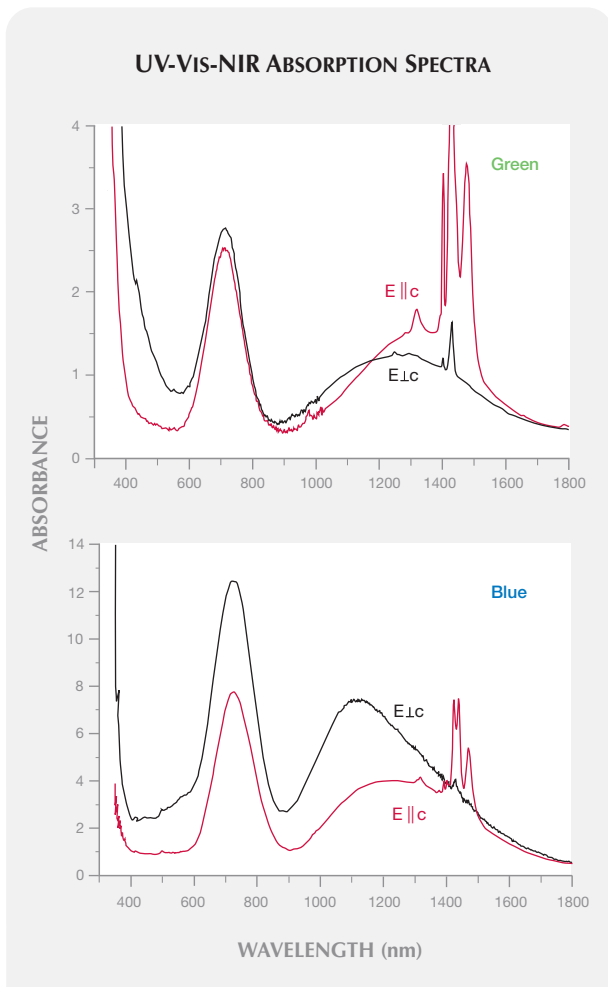
The green material (figure 30, top) had the maximum transmission in the yellow-green portion of the spectrum (~572 nm) and significant transmission in the green region, but with increasing absorption toward the blue and violet (400–500 nm); the combined effect of these produced the yellowish green color. The blue material lacked absorption in the blue-violet region and therefore transmitted a greater proportion of that light, resulting in the blue color. The higher overall absorption of the blue sample in the $E\perp c$ direction was due to a small amount of titanium interacting with iron in what is known as Fe^{2+}-Ti^{4+} intervalence charge transfer (S. M. Mattson and G. R. Rossman, "Fe^{2+}-Ti^{4+} charge transfer in stoichiometric Fe^{2+},Ti^{4+}-minerals." *Physics and Chemistry of Minerals*, Vol. 16, 1988, pp. 78–82).

Compared to the green sample, the greater intensity of the 710 nm band in the blue tourmaline (figure 30, bottom) in the spectrum taken with $E\parallel c$ polarization indicates that it had a higher concentration of iron. The intensity of this absorption in the $E\perp c$ polarization was noticeably higher. This occurs when there is Fe^{3+} interacting with the Fe^{2+} (S. M. Mattson and G. R. Rossman, "Fe^{2+}-Fe^{3+} interactions in tourmaline," *Physics and Chemistry of Minerals*, Vol. 14, 1987, pp. 163–171). Therefore, an "open" (not overly dark) appearance when looking down the c-axis occurs when there is only a limited amount of Fe^{2+}-Fe^{3+} interaction.

In summary, the blue color resulted from the presence of Fe^{2+} and the absence of Ti^{4+}, coupled with a small amount of Fe^{3+}. The green color resulted from Fe^{2+} (with little or no Fe^{3+}) interacting with a small amount of Ti^{4+}. These color mechanisms are typical of blue and green gem tourmaline.

George R. Rossman (grr@gps.caltech.edu)
California Institute of Technology, Pasadena

SYNTHETICS AND SIMULANTS

Trapiche emerald imitation. Two interesting samples resembling trapiche emerald were recently brought to our attention by gem dealer Farooq Hashmi (Intimate Gems, Jamaica, New York). They had been cut from the same "crystal," which closely resembled a natural trapiche emerald. The "crystal" was obtained on a mid-2010 trip to Colombia from a seller who was not initially aware he had acquired an imitation. To better expose the assembled

Figure 31. These two "trapiche emeralds" (5.17 and 3.53 ct) are actually clever assemblages. They were sliced from the same piece of rough by gem cutter Lain Murphy (Clifton, Colorado). Photo by Robert Weldon.

Figure 32. The continuity of inclusions across the separation planes in the green beryl assemblage suggest that the original crystal was drilled through the center and then sawn into six equal sections. Photomicrograph by R. Befi; magnified 15x.

nature of the item, Mr. Hashmi had it sliced and polished into the pieces shown in figure 31.

The samples weighed 5.17 and 3.53 ct, and measured ~10–11 mm in diameter. Magnification revealed an unevenly distributed dark substance on the original surface of the rough. The pieces of the assemblage were joined with adhesive that was colorless in some areas and black in others, to better mimic natural trapiche structure. Raman spectroscopy identified the assembled pieces as beryl and the substance holding them together as a polymer. Raman analysis of inclusions in the beryl confirmed the presence of dolomite, calcite, and pyrite. A cylindrical core of slightly darker green beryl was located in the center of the assemblage. The continuity of the inclusions throughout the assembled pieces (except in the core) suggests that the original crystal had been drilled through the middle and then cut into six equal sections (figure 32).

A cabochon cut from a similar "trapiche" assemblage was reported in the Fall 1998 Lab Notes (p. 212). It consisted of a clear core surrounded by a black rim from which black arms extended in six directions (for comparison, see E. J. Gübelin and J. I. Koivula, *Photoatlas of Inclusions in Gemstones*, ABC Edition, Zurich, 1986, p. 253). The present example shows that such assemblages continue to be found in the marketplace, even mimicking rough material.

Riccardo Befi (rbefi@gia.edu)
GIA Laboratory, New York

A new rough nephrite imitation. Nephrite jade has a rich 7,000-year history in Chinese culture. However, imitations made from marble and serpentine are often seen in the Chinese market. In early 2010, a new type of artificial rough nephrite appeared. This material is difficult to identify with the unaided eye, and its market presence continues to grow. To characterize this new imitation, we purchased two samples (3 and 15 kg) from a market in Hetian (Xinjiang Uygur Autonomous Region) in the summer of 2010, and studied their gemological properties using
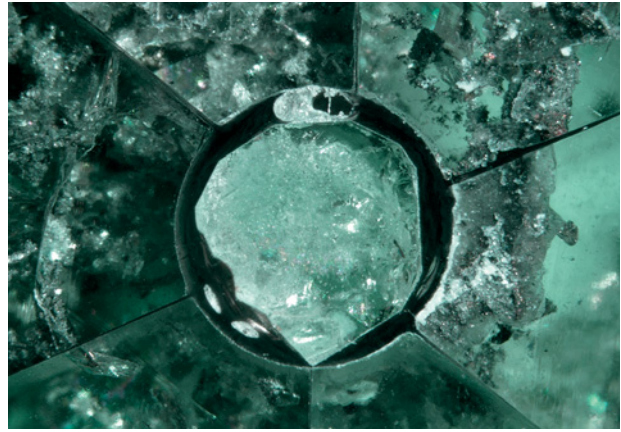
microscopic and spectroscopic techniques at the National Gemstone Testing Center (NGTC) laboratory in Beijing.

The material was white with unevenly distributed orangy brown areas (figure 33). In some areas the color appeared to be applied with a brush, with traces of brushstrokes visible. To imitate the appearance of natural nephrite, pits and cavities had been etched into some areas of the surface. These were larger than those typically seen in natural nephrite, and had a lower luster than the surrounding areas. In addition, polish lines were visible with magnification. Unlike natural nephrite, which can show deep cracks, these samples had few fractures and they rarely extended into the interior. We noted a consistent

Figure 33. When broken open, this imitation nephrite sample (originally 12 x 9 x 6 cm and weighing 3 kg) was found to contain steel disks embedded within the surrounding material. Photo by Y. Zhang.

Figure 34. Infrared spectra of the imitation nephrite showed clear differences from natural material, and identified it as aromatic polyester resin.

Figure 35. This shell specimen (~20.0 mm long) was apparently fashioned to resemble a non-nacreous natural pearl. Photo by T. Hainschwang.

depth of color in and around the fractures, which would also be unusual in natural material. The hardness was very low (approximately Mohs 2.5), and the material was easily scored with a knife.
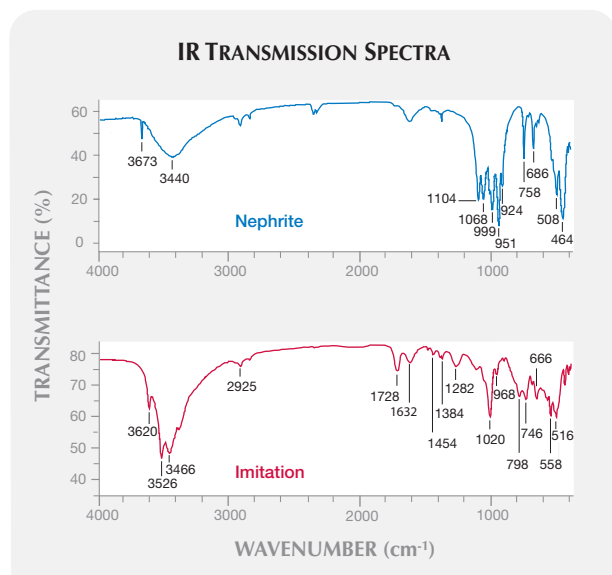
We broke apart the two imitations to observe their internal structures, and both revealed foreign material that was apparently added to increase their heft. One sample contained steel disks (again, see figure 35), while the other held chunks of concrete and stone. Though both of our samples had a lower density than nephrite jade, their heft was close enough to confuse buyers. However, because their internal contents varied and were not tightly held by the surrounding material, different areas produced different sounds when struck. Not surprisingly, the imitation that contained steel disks was attracted to a magnet. As natural nephrite is not magnetic, this is a useful identification criterion when present.

FTIR spectroscopy (KBr pellet method) of the imitations using a Nicolet 6700 infrared spectrometer gave very different results from natural nephrite: a series of bands at 3620, 3526, 3467, 3395, 1728, 1632, and 1020 cm^{-1} that are associated with aromatic polyester resin (figure 34).

As the price of nephrite jade rises and manufacturing technology continues to advance, such imitations are likely to become even more prevalent in the gem market.

Xiaoyan Feng (fengxy@ngtc.gov.cn), Yong Zhang, Maituohuti Abuduwayiti, and Taijin Lu NGTC, Beijing

A skillfully crafted non-nacreous pearl imitation. The current popularity of non-nacreous natural pearls has led to many types of imitations, from sculpted coral and shell to glass and plastic. Non-nacreous white pearls are the most commonly imitated, since the shell of the giant clam (*Tridacna* sp.) is thick enough to allow the creation of large fakes. These are usually easy to identify, since they show a distinctive layered structure when viewed with strong transmitted light.

Figure 36. The engraved pattern and polish lines on the surface of the imitation pearl (left) are distinct from the appearance of non-nacreous natural pearls showing a flame structure (right). Photos by T. Hainschwang.
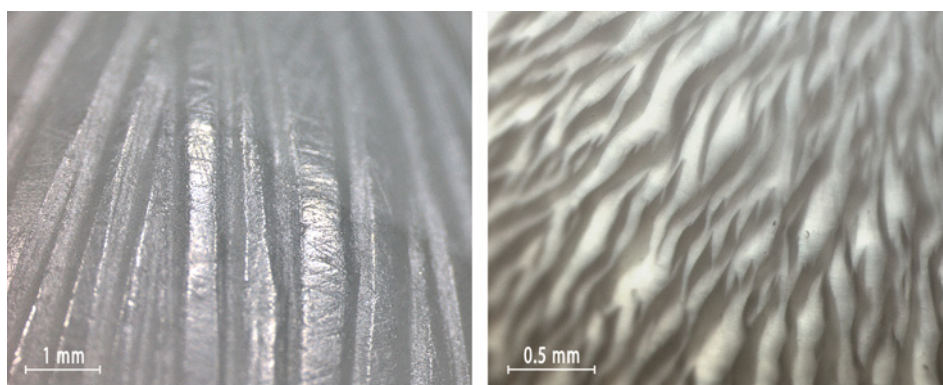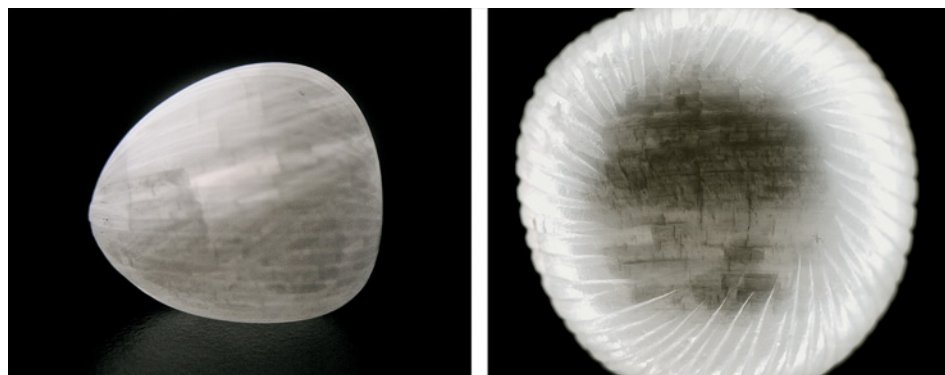
Figure 37. With strong transmitted light, the imitation pearl exhibited the distinct internal banding typical of carved shell. Photos by T. Hainschwang.

This contributor recently received a parcel represented as non-nacreous pearls. At first sight, one 24.64 ct specimen (figure 35) looked like a drop-shaped non-nacreous white pearl with a surface pattern that in some directions might be mistaken for a flame structure. Some white non-nacreous natural pearls display spectacular flame structures due to their fibrous nature. On closer examination, however, it quickly became evident that something was amiss: The "structure" consisted of engraved lines running from top to bottom. When viewed with a microscope, the surface showed obvious polish lines (figure 36, left), and the specimen's appearance bore little resemblance to the flame structure seen in natural non-nacreous pearls (figure 36, right).

Strong transmitted light showed obvious internal parallel banding, oriented in a different direction from the engraved pattern (figure 37). This banding corresponded to the growth layers that are characteristic of shell but never seen in natural pearls. Some natural non-nacreous pearls can show weak diffuse banding, but it appears quite different from that of carved shell material.

This sample was identified as a marine calcareous substance by its chemical composition, which consisted of calcium (plus oxygen) with traces of strontium. The size (~20.0 × 16.5 × 16.3 mm) suggested an imaginatively sculpted piece of *Tridacna* shell. This interesting case offers yet another example of an inventive pearl imitation using inexpensive material.

Thomas Hainschwang
(thomas.hainschwang@gemlab.net)
GGTL Gemlab–Gemtechlab Laboratory
Geneva, Switzerland, and Balzers, Liechtenstein

Plastic-coated quartz, imitating emerald. There are numerous natural, artificial, and treated materials that can imitate emerald quite convincingly. Recently, the Gem Testing Laboratory in Jaipur received for identification a green 73.58 ct drilled briolette measuring 34.10 × 23.14 × 15.68 mm (figure 38). The owner of the stone was certain it was an emerald of Colombian origin.

Although the characteristic green color suggested emerald, the specimen's duller luster gave us some hesitation. We examined it initially with a microscope, as the presence of certain inclusions would have been enough to indicate a natural emerald. Instead we observed elongated two-phase inclusions and reflective liquid films, an inclusion scene not typically associated with Colombian emerald. In addition, gas bubbles (figure 39, left) were present, mainly at or near the surface of the sample. On careful examination, a thick coating was visible; all the gas bubbles were restricted to this layer.

Examining the edges of the drill hole, we observed colorless areas under the thick green coating (figure 39, right). Such areas were also evident on a few facet edges where the coating had chipped off. Hot point testing on an inconspicuous area showed signs of melting. This suggested plastic, which would also explain the sample's dull luster. RI testing revealed a vague shadow edge around 1.54, and the hydrostatic SG was 2.60. The specimen gave a chalky yellow reaction to long-wave UV radiation, and a weak red reaction with the Chelsea filter. With a handheld spectroscope, it displayed a strong band in the red region at around 650 nm, a feature typically associated with green dye. These properties could not reliably identify the colorless base material, but infrared spectroscopy proved it was quartz (rock crystal). The IR spectra also showed an absorption band at 3060–2810 cm^{-1} that may be associated with polymers/plastics, but additional bands expected for the plastic coating could not be resolved due to interfer-

Figure 38. This 73.58 ct briolette, submitted as emerald, was identified as plastic-coated quartz. Photo by G. Choudhary.

Figure 39. Gas bubbles were common at or near the surface of the briolette, suggesting a coating (left, magnified 60×). Chipped areas of coating around the drill hole revealed the colorless quartz underneath (right, magnified 45×). Photomicrographs by G. Choudhary.

ence with other spectral features.

We concluded that this specimen was plastic-coated quartz. In the absence of gemological testing, correct identification would have been problematic, especially for a trader or dealer equipped only with a loupe.

Gagan Choudhary (gtl@gjepcindia.com)
Gem Testing Laboratory, Jaipur, India

TREATMENTS

Lead glass–filled trapiche ruby. Since 2004, the treatment of corundum (particularly ruby) by filling fractures with a lead-based glass has become widespread. There have been several developments since the treatment first appeared, such as glass compositions that do not show the orange/blue "flash effect" and new geographic origins and varieties of filled material (e.g., faceted rubies from Mozambique and star rubies from Madagascar). These contributors recently encountered yet another permutation: lead glass–filled trapiche ruby.

In August 2010, one of us (OS) purchased a 20.37 ct translucent cabochon represented as trapiche ruby at the Chanthaburi gem market in Thailand. The seller indicated the gem came from Mozambique and had been treated

Figure 40. This 20.37 ct trapiche ruby, reportedly from Mozambique, is filled with a lead-based glass. Photo by O. Segura.

with lead glass. To our knowledge, trapiche rubies from Mozambique are rarer but larger than those from Mong Hsu, Myanmar. The sample displayed the classic trapiche pattern with six clearly delineated sectors and the hexagonal growth zones often seen in corundum also were obvious (figure 40).

The gemological properties were typical for ruby, with RIs of 1.755–1.770, a hydrostatic SG of ~3.95, and a standard ruby spectrum with the handheld spectroscope. The material fluoresced strong red to long-wave UV radiation and was inert to short-wave UV.

Viewed with the microscope, the stone showed areas of slightly duller luster in reflected light (figure 41), as is typical of lead glass–filled gems. An abundance of flattened and spherical bubbles of various sizes (e.g., figure 42) indicated widespread filling, possibly in preexisting cavities. This raised the question of whether the gem was a single piece of ruby or a composite. Close examination of the trapiche pattern and orientation of the "silk" in the cabochon demonstrated that it was indeed fashioned from a single crystal, despite the high glass content. Also visible were numerous crystal inclusions with a morphology and relief that suggested apatite (again, see figure 42).

Other traders in Chanthaburi later showed us large (up to 181 ct) untreated trapiche rubies that reportedly came from the Nzérékoré area of southeastern Guinea, an undocumented source for this kind of ruby. Unfortunately, we could not acquire any samples for analysis.

Olivier Segura (oliviersegura@free.fr)
Mandara, Montsoult, France
Emmanuel Fritsch

MISCELLANEOUS

Myanmar Gem Emporium. The mid-year session of the 2010 Myanmar Gem Emporium took place November 17–29. For the first time, the government-run tender was held in the new capital city of Naypyidaw. An estimated 6,750 merchants attended, with more than half of them from mainland China, Hong Kong, and Taipei. The emporium saw record-breaking sales of its jade, pearl, and assorted gem lots, including 7,784 of the 9,157 jade lots offered. In a story published February 14, 2011, China's Xinhua News Agency reported total sales of $1.4 billion.

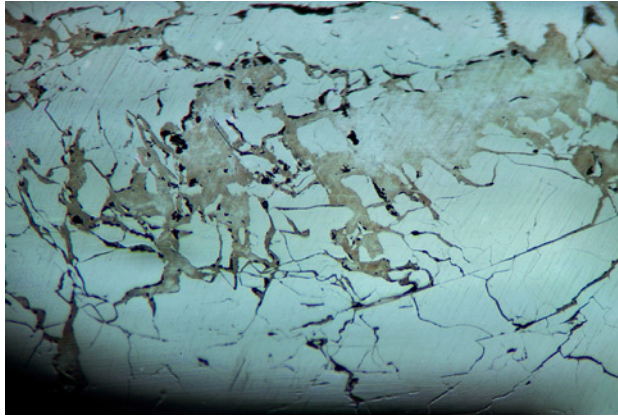The emporium's first session for 2011 was held March

Figure 41. Reflected illumination shows areas filled with a glass-like material of only slightly lower luster than the host ruby. Photomicrograph by O. Segura; magnified 10×.

Figure 42. Trapped bubbles of various sizes demonstrate the extent of lead-glass filling in the trapiche ruby. Dark-colored inclusions, presumably apatite, are visible on the right. Photomicrograph by O. Segura; magnified 20×.

10–22, again in Naypyidaw, with nearly twice as many jade lots offered. According to the *Democratic Voice of Burma*, jade prices were 10 times higher than the previous year, fueled by Chinese demand. Nevertheless, Xinhua reported on March 23 that 13,608 of the 16,939 lots were sold. That same article noted Myanmar's latest production figures. From April through November 2010, the country yielded 27,251 tons of jade and 9.6 billion carats of other gems (including ruby, sapphire, spinel, and peridot), as well as 300 kg of cultured pearls.

U Tin Hlaing
Dept. of Geology (retired)
Panglong University, Myanmar

ERRATUM

The Fall 2010 gem treatments retrospective article by S. F. McClure et al. (pp. 218–240) stated that Schmetzer (2008) had concluded that certain topaz treatment methods were "not diffusion." In fact, Dr. Schmetzer's article reviews the published U.S. patent application by W. B. Yelon et al. (2007/0110924 A1, *Process for Improving the Color of Gemstones and Gemstone Minerals Obtained Thereby*, filed November 14, 2005, published May 17, 2007), which describes the existence of a diffusion layer between topaz and the coating. We thank Dr. Schmetzer for bringing this to our attention.

IN MEMORIAM: KURT NASSAU (1927–2010)

World-renowned scientist Dr. Kurt Nassau, a longtime contributor and review board member for *Gems & Gemology*, died December 18, 2010, at his home in Lebanon, New Jersey. He was 83.

Born in Austria in 1927, Dr. Nassau fled the country with his family in the late 1930s. They settled in England, where he attended school and university before immigrating to the United States after World War II.

Dr. Nassau served as a medical researcher at the Walter Reed Army Medical Center in Washington, DC, before earning a doctorate in chemistry from the University of Pittsburgh. He joined Bell Laboratories (now Lucent Technologies) in 1959 and became known for his research in crystal chemistry and growth.

As a leading expert on the causes of color, especially in minerals and gems, Dr. Nassau began assisting GIA's New York laboratory in the 1960s and served on the GIA Board of Governors from 1975 until 1994. While a member of the Board, he played a key role in facilitating the 1988 purchase of the Sinkankas Library for GIA.

Dr. Nassau was the author of eight books, including the landmark *Gems Made by Man* (1980), *The Physics and Chemistry of Color* (1983), and *Gemstone Enhancement* (1984). He published more than 470 articles and held 17 patents. He was also a major donor of books and crystal specimens to the GIA Collection and the Richard T. Liddicoat Library and Information Center.

Dr. Nassau was a frequent contributor to *G&G* from the 1960s through the 1990s, and served on the journal's Editorial Review Board for more than 20 years, from 1981 until his retirement in 2002. He won the Dr. Edward J. Gübelin Most Valuable Article Award three times, most recently for his Winter 1997 article, "Synthetic Moissanite: A New Diamond Substitute."

✦ *Second Place*

SYNTHETIC GEM MATERIALS IN THE 2000S: A DECADE IN REVIEW

Nathan Renfro, John I. Koivula, Wuyi Wang, and Gary Roskin

Nathan Renfro is a staff gemologist at the GIA Laboratory in Carlsbad. After completing his undergraduate geology studies at Appalachian State University, Mr. Renfro obtained a Graduate Gemologist diploma from GIA. Since joining the laboratory in 2008, he has contributed several articles and Lab Notes to *G&G*. **John Koivula** is chief gemologist at the GIA Laboratory in Carlsbad. A renowned expert on microscopy, photomicrography, and gem inclusions, he is author of *MicroWorld of Diamonds*, co-author of the three-volume *Photoatlas of Inclusions in Gemstones*, and co-author of *Geologica*. He holds bachelor's degrees in chemistry and mineralogy-geology from Eastern Washington State University. **Wuyi Wang** is director of research and development at the GIA Laboratory in New York. He holds a bachelor's degree in geology from Beijing University and a doctorate in geology from the University of Tsukuba. He has spent nearly 20 years studying diamond geochemistry and the treatment of diamonds and other gem materials. **Gary Roskin** is editor of the online magazine *The Roskin Gem News Report*. He was a GIA staff member from 1977 to 1992, serving as an instructor, laboratory supervisor, and alumni association executive director. From 1997 to 2009, he was the gemstone editor of *JCK* magazine.


Nathan Renfro

John I. Koivula


Wuyi Wang

Gary Roskin

✦ *Third Place*

THE WITTELSBACH-GRAFF AND HOPE DIAMONDS: NOT CUT FROM THE SAME ROUGH

Eloïse Gaillou, Wuyi Wang, Jeffrey E. Post, John M. King, James E. Butler, Alan T. Collins, and Thomas M. Moses

Eloïse Gaillou is a postdoctoral fellow at the Smithsonian Institution's National Museum of Natural History and at Carnegie Institution, both in Washington, DC. She obtained her PhD in France in 2006, working on geologic and physical aspects of opals. Her current research focuses on defects in natural diamonds and their influence on physical properties. **Wuyi Wang** was profiled in the second-place entry. **Jeffrey Post** is curator of the U.S. National Gem and Mineral Collection at the Smithsonian Institution's National Museum of Natural History in Washington, DC. He holds bachelor's degrees in geology and chemistry from the University of Wisconsin-Platteville and a PhD in chemistry from Arizona State University. Dr. Post has published numerous articles on mineralogy, gemology, geochemistry, and crystallography. **John King** is chief quality officer of the GIA Laboratory in New York and the editor of *Gems & Gemology in Review: Colored Diamonds*. A noted artist, Mr. King received his master's degree from Hunter College, City University of New York. One of his research areas has been the characterization and color description of colored diamonds. **James Butler** is a consultant in Huntingtown, Maryland, retired from the Naval Research Laboratory. Dr. Butler has published more than 190 papers on experimental chemical physics. He received a bachelor's degree from MIT and a PhD from the University of Chicago, both in chemical physics. **Alan Collins** is emeritus professor of physics at King's College London. He has carried out extensive research on the optical and electronic properties of diamond, much of which has relevance to gemology. He holds PhD and DSc degrees from the University of London. **Thomas Moses** is senior vice president of the GIA Laboratory and Research, New York.
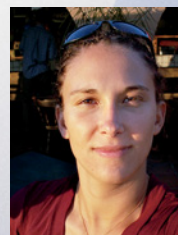
Eloïse Gaillou
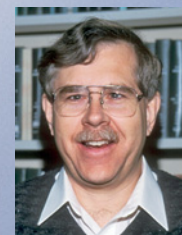
Jeffrey E. Post
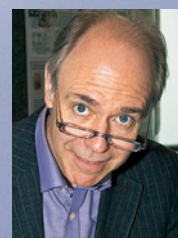
John M. King

James E. Butler

Alan T. Collins

Thomas M. Moses

Most Valuable Article

TAKE THE 2011 GEMS & GEMOLOGY
CHALLENGE

The following 25 questions are from the Spring, Summer, Fall, and Winter 2010 issues of *Gems & Gemology*. Refer to the feature articles, Notes and New Techniques, and Rapid Communications in those issues to find the **single best answer** for each question.

Mark your choice on the response card provided in this issue or visit gia.edu/gandg to take the Challenge online. Entries must be **received no later than Monday, August 1, 2011**. All entries will be acknowledged with an email, so please remember to include your name and email address (and write clearly).

Score 75% or better, and you will receive a GIA CONTINUING EDUCATION CERTIFICATE (PDF file). If you are a member of the GIA Alumni Association, you will earn 10 Carat Points. (Be sure to include your GIA Alumni membership number on your answer card and submit your Carat card for credit.) Earn a perfect score, and your name also will be listed in the Fall 2011 issue of *Gems & Gemology*. Good luck!

1. The _____ contents in the Hope and Wittelsbach-Graff diamonds are characteristic of other type IIb blue diamonds, suggesting that their intense blue color results primarily from their large size rather than from an unusually high amount of this impurity.
   A. boron
   B. carbon
   C. hydrogen
   D. nitrogen

2. Because some natural opals from _____ show absorption features similar to Mexifire synthetic fire opals, infrared spectroscopy does not provide a conclusive means of separation.
   A. Australia
   B. Ethiopia
   C. Mexico
   D. Oregon

3. The strong pink coloration of the latest CVD synthetic diamonds from Apollo is caused by _____, which efficiently absorb most yellow, green, and orange wavelengths.
   A. GR1 emissions
   B. H3 defects
   C. NV centers
   D. Si-related features

4. During the decade of the 2000s, which country emerged as a major new source of high-quality gem diamonds?
   A. Angola
   B. Brazil
   C. Canada
   D. China

5. Based on crystallographic modeling, the technology existing at the time, and historical considerations, it is most likely that the French Blue and Hope diamonds were recut from the Tavernier Blue and French Blue diamonds, respectively, by:
   A. a combination of cleaving, sawing, and grinding.
   B. cleaving and grinding.
   C. sawing and grinding.
   D. grinding alone.

6. During the past decade, the _____ movement saw diamond-producing countries assert more control over their own resources.
   A. beneficiation
   B. globalization
   C. responsible jewelry
   D. Supplier of Choice

7. The _____ of scapolite from Ihosy, Madagascar, appears to be distinctive from that of most gem scapolite found elsewhere.
   A. photoluminescence
   B. refractive index
   C. specific gravity
   D. UV fluorescence

8. The fire opal from a new source at Bemia, Madagascar, has an unusually high
   A. luster.
   B. play of color.
   C. specific gravity.
   D. transparency.

9. Since 2004, the gem industry has seen non-gem corundum transformed into transparent, facetable rubies through
   A. beryllium diffusion.
   B. dyeing.
   C. filling with lead-bearing glass.
   D. traditional heat treatment.

10. Many opals from Wegel Tena, Ethiopia, exhibit _____, a feature seldom seen in material from other countries.
    A. chatoyancy
    B. "digit patterns"
    C. hydrophane behavior
    D. play of color

11. In contrast to traditional radiography, which provides a condensed two-dimensional image, X-ray computed microtomography
    A. adds further dimensions to pearl grading.
    B. has a high-resolution modeling capability for observing fine internal structures in three dimensions.
    C. produces a three-dimensional hologram of a pearl and its inner structures.
    D. allows more precise mapping of inclusions.

12. Although they are also observed in some natural diamonds, _____ are considered an indicator of CVD-grown synthetic diamond.
    A. mineral inclusions
    B. cross-shaped luminescence patterns
    C. high-order interference colors
    D. metallic inclusions

13. _____ spectroscopy is the most powerful tool in the nondestructive identification of polymer-treated turquoise and other stones.
    A. Fourier-transform infrared
    B. Laser-induced breakdown
    C. Raman
    D. UV-visible

14. Bastnäsite-(Ce) and parisite-(Ce) from Malawi have a similar brownish orange color but can be separated on the basis of
    A. chemical composition.
    B. Raman analysis.
    C. standard gemological properties.
    D. all of the above

15. Between 2000 and 2010, which of these countries was not a source of copper-bearing tourmaline?
    A. Brazil
    B. Myanmar
    C. Mozambique
    D. Nigeria

16. The intense green, highly translucent synthetic jadeite produced by General Electric during the 2000s had properties that overlapped those of natural jadeite, except for obvious differences in
    A. birefringence.
    B. infrared spectrum.
    C. Raman spectrum.
    D. UV fluorescence.

17. The _____ infrared absorption feature, which may be used to help identify CVD synthetic diamonds, weakens significantly after heating to 525°C but is recovered upon UV exposure.
    A. 1344 cm^{-1}
    B. 3107 cm^{-1}
    C. 3123 cm^{-1}
    D. 1454 cm^{-1}

18. In 2008, the violent eviction of miners from the government-controlled Marange diamond fields in _____ led to sharp criticism of the Kimberley Process's effectiveness in combating conflict diamonds.
    A. Angola
    B. Ivory Coast
    C. Sierra Leone
    D. Zimbabwe

19. X-ray computed microtomography is best suited for examining
    A. a single strand of pearls at a time.
    B. multiple strands of pearls.
    C. single pearls.
    D. mounted pearls.

20. During the past decade, the value of trace-element analysis in determining a gem's country of origin has spurred the use of _____ spectroscopy.

A. electron paramagnetic resonance
B. laser ablation–inductively coupled plasma–mass
C. nuclear magnetic resonance
D. photoluminescence

21. Chemical analysis of a gem hibonite crystal indicated significant traces of _____, which is usually regarded as an uncommon impurity in this mineral.
    A. aluminum
    B. chromium
    C. cerium
    D. zinc

22. Parallel fibers of _____ are responsible for the spectacular chatoyancy observed in fine-quality pietersite specimens.
    A. actinolite
    B. crocidolite
    C. hematite
    D. rutile

23. Unlike many other historical gem-adorned objects, the 16th-century ciborium from Einsiedeln Abbey in Switzerland contained no
    A. doublets.
    B. glasses.
    C. imitations.
    D. any of the above

24. An important concern for the diamond community throughout the 2000s was _____ treatment to remove or induce color.
    A. dyeing
    B. high-pressure, high-temperature
    C. irradiation
    D. surface coating

25. When examined with confocal micro-Raman spectroscopy, _____ emeralds did not show Raman bands for type I or II water.
    A. flux-grown synthetic
    B. hydrothermally grown synthetic
    C. natural (high alkali content)
    D. natural (low alkali content)

G&G Online
Book Reviews

Pearls

By Hubert Bari and David Lam, 336 pp., illus., publ. by Skira Editore [www.skira.net], Milan, Italy, 2010. US$85.00

Hubert Bari and David Lam have created a delightful work, teaming with photographer Christian Creutz to produce this valuable resource. For a study of natural pearls, readers have long turned to Kunz and Stephenson's 1907 masterpiece, *The Book of the Pearl*. Since the late 20th century, writers such as Farn, Dickinson, Shirai, Ward, and Newman have contributed smaller but very helpful books on cultured and natural pearls. In recent years, enthusiasts have been treated to two important reference works, Elisabeth Stack's *Pearls* (2006) and Paul Southgate and John Lucas's *The Pearl Oyster* (2008). This new volume will be a welcome addition to the pair.

The book was published to accompany the *Pearls* exhibition held at the Museum of Islamic Art in Doha, Qatar, which ran from January to June 2010. In the preface, exhibit chair Sheikha Al-Mayassa bint Hamad bin Khalifa Al-Thani expresses her hope that the reader will discover the many aspects of the pearl and better understand the scientific and cultural layers "that play a part in the creation of this small but miraculous orb."

Six chapters deal with the nature and formation of the pearl, the various mollusks, the history of pearls, the age of great fisheries (1850–1940), cultivation, gentlemen-farmers, and, in a final section titled "Hommage to Mademoiselle," fashion designer Coco Chanel and her love of the gem. The 350 photographs are stunning.

The reader begins to appreciate the depth of the Qatar museum collection, starting with the 21 rare and unusual natural pearls featured on the cover. In addition, Bari and Lam have traveled the world to collect photos of the finest specimens from other important collections, including those of Hussein Alfardan, the British Museum, major pearl producers, numerous national archives, the Mikimoto Museum, and noted gem photographers such as Christian Creutz, Tino Hammid, John Koivula, and Jeff Scovil.

The illustrations aren't limited to photos of pearls, shells, and pearl jewelry. There is a rich tapestry of maps, early book illustrations, and photos of pearling vessels and farms through the ages that detail our fascination with the queen of gems. For many this will be an opportunity to grasp the richness of the pearl's history in the Arabian Gulf. One begins to appreciate how pearls have influenced the lives of the people who have sought them through the millennia and across the continents.

The richly told text offers a remarkable compilation of interesting items. This reviewer takes exception, though, to the authors' belief (from the beginning of chapter 3, "The Pearl: A History of Indifference and Passion") that the absence of pearl jewelry artifacts from early cultures shows that they valued shell more than pearls. Rather, the pearl was likely so rare and so prized that these treasures were kept hidden, much the way diamonds were hidden in ancient India. Only further translation of early texts will serve to reinforce one point of view or the other.

One wishes the authors had included an index, always a time-consuming task and often done just as the book is scheduled to be published. Even so, this is more than a coffee table book—one wishes to locate the photos, facts, and stories throughout it. Regardless, *Pearls* will be a remarkably affordable and treasured addition to any pearl library.

DONA M. DIRLAM
Richard T. Liddicoat Gemological Library and Information Center
GIA, Carlsbad

Terra Spinel Terra Firma

By Vladyslav Y. Yavorsky with Richard W. Hughes, 204 pp., illus., privately published [http://spinelbook.com], 2010. US$95.00

This masterful work showcases the beauty and amazing color variations found in spinel. Vladyslav Yavorsky's sincere passion is captured through each photograph and thoughtful description. He covers all the major sources with images of some of the finest examples of spinel. Every page is a new delight, as the photos seem to come to life. Yavorsky's eye for color is revealed through his pairing of the endless palette of spinel hues with images of landscapes, textiles, and beautiful people from the faraway places where these gems are found.

For those interested in the history of spinel and a bit of lore, coauthor Richard Hughes provides just enough information to capture the reader's interest while leaving one hungry for more. Hughes touches on gemology and briefly explores the history of famous spinels mistaken for rubies.

While not a scientific book, it does capture the beauty and essence of one of the most unique and underappreciated gems available.

The tour of spinel-producing countries begins in Burma, continuing through Sri Lanka and on to Tajikistan, Tanzania, and Madagascar before ending in Vietnam. Each section features a map and a brief summary highlighting the spinel-mining areas of that country. Along the way, Yavorsky shares his photographic and cutting skills, as every page reveals yet another fabulous spinel, friendly miner, or remote landscape. The kaleidoscope of gem colors includes ruby red, jacaranda lavender, metallic gray, vivid pink, saffron orange, cobalt blue, and many more, from the softest pastels to the most intense neon colors imaginable.

Yavorsky best sums up his relentless passion for discovery when he writes, "Thus I continue to travel with loupe and camera, ever seeking to expose a hitherto unrevealed face of a crystal, person or landscape, attempting to highlight that which is worthy. This is my quest, to be faithful and relentless in my search for beauty."

At the end of the book, there is a delightful surprise in the final pages showing spinel's plethora of colors. This pictorial treasure is a must for any gem enthusiast or designer searching for inspiration from one of the most unique and beautiful gems in the world.

EDWARD BOEHM
RareSource
Chattanooga, Tennessee

Colour of Paradise: The Emerald in the Age of Gunpowder Empires

By Kris E. Lane, 280 pp., illus., publ. by Yale University Press [http://yalepress.yale.edu], New Haven, CT, and London, 2010. US$40.00

Emerald green is unlike any other color in gemology. Despite comparisons to the color of spring pastures, the green of emerald is more often approached than attained outside the gem world. Here, Kris Lane presents an exhaustively researched treatise that broadens our understanding of emeralds plucked and pillaged from Colombia as they crossed the seas to Asia and Europe, centuries before their modern appearance in jewelry showcases and museums. This scholarly book tackles aspects of the emerald trade that are not widely published but are as extraordinary as the gem's elusive color.

To the Muzos, Muiscas, and other pre-Columbian tribes who valiantly but unsuccessfully attempted to protect their magical caches from European marauders, emeralds were considered essential to aspects of tribal life beyond soothsaying, jungle healing, and the preservation of female chastity. Lane presents the anguish of emerald's forced entry into global trade in painstaking detail. The subtext of his in-depth review of trade records, sailing manifests, diaries, and even shocking shipwreck discoveries underscores how incomplete our assessment remains of the wild global ride taken by *esmeralda*.

The book's subtitle references the shortcuts to empire-building unleashed by the harnessing of gunpowder, which elevated conflict from an era of crossbowmen, archers, and rams to better war through chemistry. The gunpowder empires held sway from the 16th century, when Moguls ruled Muslim Asia and European explorers colonized the Americas in search of gold and riches. Though pestilence proved nearly as effective as pugnacity in European hegemony over the New World, the net effect was the eventual wresting of emerald riches from native Indo-Americans into the hands of European explorer-warriors and multiethnic merchants, with ragtag adventurers and would-be fortune hunters bringing up the rear.

Lane, a history professor at the College of William and Mary, cites primary sources obtained from multinational archives, libraries, anthropologists, diaries, translations, and other documents that date to some of the earliest 16th century Spanish explorers. Deeper into the text, Lane delivers on the promise of his title by connecting the rare color of this exotic stone to the green Paradise of Islam. Here, the trained Latin Americanist argues that the Ottomans, Persia's Safavid dynasty, and particularly the Moguls caught "emerald fever" over a gem they interpreted as a means of divine protection. These rare treasures from another side of the world offered a link to the heavens, the ultimate fulfillment that awaited those fortunate or victorious enough to possess them. In this way, emeralds signified another manifestation of the powers bestowed on their regal owners. Lane also details the importance of emeralds in elaborate gift-giving rituals afforded to the highest ranks of these ruling civilizations, which he interprets as dramatic assertions of dominance and power rather than as acts of generosity, recognition, or reward.

Though European courts were also enamored of emeralds, their passion was more accessory-driven and hardly elevated to the fever pitch of South Asia and the Indian subcontinent. Lane shows how the initial arrival and subsequent notoriety of emeralds in South Asia conferred an "Oriental" provenance to the gem that supplanted its New World origin. Europeans, whether influenced by the blinding glitter of gold or a New World association considered déclassé at the time, came to see emeralds as Eastern objects of desire, showcased by rulers such as the despotic Nadir Shah. Lane traces this paradoxical exaltation of emerald as the gem passed from Asia and back through trade routes to Europe, where it would eventually be coveted and collected by the imperial courts, though never to the same degree as the Near East, the Indian subcontinent, and Asia.

An epilogue reviews the post-colonial turmoil of the Muzo mines, the rediscovery of the Chivor region's Somondoco mines in 1890, and 20th century emerald mining in the era of capitalists, attempted government

takeovers, and later the emerald bosses known as *esmeralderos*. Most of it isn't very pretty.

The book includes 16 well-chosen full-page color plates, as well as a variety of diagrams, maps, illustrations, tables, and appendices that detail emerald production over these earlier centuries. These should well serve future emerald scholars and historians.

Although it is a dense and difficult read, Lane's labors will be appreciated by emerald and gem scholars who seek deeper understanding of the often barbaric and tortuous history associated with one of nature's most resplendent wonders. The documentation and annotated footnotes alone may send generations of scholars back to the archives to uncover other layers behind emerald's many mysteries, from the depths of shipwreck-littered ocean floors to the impenetrable collections still sequestered in banks and subterranean vaults of countries where Americans are no longer welcome.

MATILDE PARENTE
Libertine
Indian Wells, California

Twentieth-Century Jewellery: From Art Nouveau to Contemporary Design in Europe and the United States

By Alba Cappellieri, 248 pp., illus., publ. by Skira Editore [www.skira.net], Milan, 2010. US$85.00

Broad in scope and beautiful in presentation, this book is nevertheless a bit intimidating. It truly covers the *entire* history of 20th century jewelry. And a fascinating century it was for jewelry—from Art Nouveau to Art Deco, from Tiffany to Trifari, from high art to pop art, from 1900 to 2008, the author covers it all.

The discussion is divided into six eras: 1900–1918 ("Art Nouveau and Mode Blanche"); 1919–29 ("Art Deco: White, Black and Tutti Frutti"); 1929–46 ("Somewhere Between the International Style and Organicism");

1947–67 ("From the New Look to Pop"); 1968–78 ("From Radical to Global"); and 1979–2008 ("From Materialism to Minimalism"). Each section attempts to portray what was happening in society, art, architecture, and fashion, and how those and other factors influenced jewelry materials and styles, and how it was worn.

This book is an ambitious undertaking, and it largely succeeds. The historical information is fascinating, meticulously researched, and annotated. (I particularly liked the easy-to-read glossary.) It is lavishly illustrated with many beautiful and unique pieces of jewelry.

I do feel the content would have been more interesting (or perhaps easier to absorb) if the illustrations had appeared with the corresponding text, but virtually every one of them appears in a separate section titled "Works." One must wade through some rather daunting text to reach this aesthetically satisfying section of images. And some of the captions were far removed from their related images, requiring careful examination to match descriptions with photos. I did appreciate the fact that so-called costume jewelry and art jewelry were not ignored; their inclusion gave the book a very well-rounded feel. I would recommend this work to anyone wishing to view the amazing evolution of jewelry and wearable art during the last century.

JANA MIYAHARA-SMITH
GIA, Carlsbad

Jewellery from the Orient: Treasures from the Bir Collection

By Wolf-Dieter Siewert, 320 pp., illus., publ. by Arnoldsche Art Publishers [www.arnoldsche.com], Stuggart, Germany, 2009. US$85.00

Dr. Ümit Bir was a Turkish native living in Germany who began collecting silver cultural objects in the late 1950s during his travels across Europe, North Africa, and Asia. His collection, now comprising more

than 3,000 objects, has resided at the Museum fur Volkerkunde in Leipzig since 2004. Siewert's book is a review of 775 artifacts from this collection.

Yet this book is far more than an exhibit catalog. It is better described as a historical and ethnographic review of the cultures and peoples who produced these objects. Siewert provides comprehensive details on antique silver jewelry that many in our industry have encountered, yet struggle to research and appraise. Until now there have been few, if any, books on silver's cultural influence written with such depth. This historical read reminds us that silver ornamental jewelry and objects have spanned the globe throughout the centuries. High-quality color photographs and details appear on every page.

Sections of the book cover silver's impact across the European Orient, the Mediterranean to the Atlantic, the Arabian Sea, the Indian Ocean, Indonesia, and trade routes traveled by nomadic people. The stories describe how both men and women of different cultures used this jewelry to convey meaning in every aspect of their lives: religion, love, death, marriage, fertility, medicine, travel, education, status, and the rise and fall of empires. We better understand how the jewelry we handle today has deep-rooted meaning, and how these family treasures become collector's items over time. We are reminded that jewelry did not start out as a fashion statement the way we know it today. Many of the items shown in this volume do not even appear as modern jewelry: swords, amulets, head dresses, belts, heavy bracelets, cigarette holders, and chest dresses worn by men.

Although not a light read, this book is valuable to appraisers, collectors, museums, auction houses, and anyone interested in the meaning of the exotic and difficult to identify silver jewelry and objects that might pass through their hands.

MELINDA ADDUCCI
Joseph DuMouchelle Auctioneers
Grosse Pointe Farms, Michigan

G&G Online
Gemological Abstracts

COLORED STONES AND ORGANIC MATERIALS

A contribution to the study of FTIR spectra of opals. I. Adamo [ilaria.adamo@unimi.it], C. Ghisoli, and F. Caucia, *Neues Jahrbuch für Mineralogie, Abhandlundgen*, Vol. 187, No. 1, 2010, pp. 63–68.

Opals are water-bearing micro- and non-crystalline silica minerals with the chemical formula $SiO_2 \cdot nH_2O$. On the basis of X-ray diffraction, they can be subdivided into three general groups: opal-C (relatively well-ordered α-cristobalite, with minor evidence of tridymite); opal-CT (disordered α-cristobalite with α-tridymite-type stacking); and opal-A (amorphous). Thirty-four gem-quality opal samples of known origin, comprising the most important types of natural and synthetic opal on the market (with and without play-of-color), were examined by Fourier-transform infrared (FTIR) spectroscopy. The FTIR spectra were typical of water-bearing silicates with tetrahedral coordinated silicon. Opal-C was easily identified by sharp peaks at about 620 cm^{-1}, typical of well-ordered α-cristobalite. The distinction between opal-CT and opal-A required careful comparison of the three Si-O bands at 1100, 790, and 470 cm^{-1}, particularly the second one, which is always at higher frequencies in opal-A than in opal-CT (800–796 and 792–788 cm^{-1}, respectively). Infrared spectroscopy can also easily detect the presence of clay minerals, providing useful information about the opal's genesis and the locality.   *GL*

Green andradite stones: Gemmological and mineralogical characterisation. I. Adamo, G. D. Gatta [diego.gatta@unimi.it], N. Rotiroti, V. Diella, and A. Pavese,

European Journal of Mineralogy, Vol. 23, No. 1, 2011, pp. 91–100.

Andradite is a rock-forming mineral typically found in metamorphic rocks, such as skarns and serpentinites. Green andradite (demantoid) is one of the most valued gems among the garnet-group minerals, due to its color, brilliance, and rarity. Sources include Russia (central Ural Mountains), Italy (Val Malenco, Sondrio), Iran (Kerman Province), northern Pakistan (Kaghan Valley), Namibia (Erongo Province), and northern Madagascar (Antetezambato). Samples from these sources were examined by standard gemological testing, electron microprobe analysis, UV-Vis-NIR and mid-infrared spectroscopy, and single-crystal X-ray diffraction to determine their gemological and crystallographic characteristics.

The garnets were almost pure andradite, with small amounts of other elements. The Cr content did not affect the unit-cell constant, and cell refinement suggested that Cr^{3+} can share the octahedral site with Fe^{3+} in the garnet structure. The UV-Vis-NIR spectra were characterized by Fe^{3+} absorption features, which represent the main cause of color, while the mid-IR spectra revealed the presence of hydroxyl groups. *DAZ*

The profile of trace elements, including the REE, in gem-quality green andradite from classic localities. R. Bocchio [roseangela.bocchio@unimi.it], I. Adamo, and V. Diella, *Canadian Mineralogist*, Vol. 48, No. 5, 2010, pp. 1205–1216.

Fifteen gem-quality samples of demantoid from Italy (Aosta and Val Malenco), Russia, Iran, Pakistan, Namibia, and Madagascar, and two samples of grossular and uvarovite, were analyzed by electron microprobe and LA-ICP-MS. All the andradite samples were found in serpentinite host rocks except for two samples from Namibia and Madagascar, which formed in skarns. Nine samples from Val Malenco possessed almost pure andradite end-member compositions, though a minor uvarovite component resulted from the internal diffusion of chromium from magnetite inclusions. The sample from Madagascar was also close to the pure end-member and homogeneous, while samples from Aosta, Russia, Iran, and Pakistan ranged from 91 to 96 mol.% andradite. Other garnet components detected were grossular in samples from Aosta and Russia, and uvarovite in those from Iran and Pakistan. Major and trace elements in the Namibian sample were heterogeneous, ranging from pure andradite to $And_{11}Gro_{89}$ within a single crystal, reflecting the geochemical processes involved in the skarn host rocks.

The metasomatic reactions caused higher concentrations of rare-earth elements (REE) in skarn-hosted Madagascar and Namibian demantoid than in other samples (hosted by serpentinite). The pattern of trace elements such as Sc, Ti, V, Cr, Co, Ni, Zn, Sr, Y, and Zr was similar for all the samples, showing a "U" shape. The Russian sample had no Ni and very low amounts of Y and Zr. The concentrations of Cr, Ti, and V were also very low in the samples from Madagascar and Namibia. All the Fe-rich samples ($\geq And_{98}$) contained Cr ranging from ~2 to 4189 ppm, which was correlated to color variations. They also showed a strong positive Eu anomaly and were enriched in light rare-earth elements (LREE) but poor in heavy rare-earth elements (HREE). In contrast, none of the grossular-bearing samples showed the Eu anomaly and possessed high concentrations of medium-REE and HREE. The Russian sample was very low in both LREE and HREE. The three Cr-bearing samples from Italy (Val Malenco), Iran, and Pakistan showed a relatively flat REE distribution. The positive Eu anomaly in most of the Fe- and Cr-bearing samples suggested that divalent Eu was dominant in the mineralizing fluids. The Eu^{2+} anomaly in these fluids may be caused by the hydrothermal alteration process between Eu^{3+} and Fe^{2+}, resulting in Eu^{2+} and Fe^{3+} cations. *KSM*

Inside sapphires. C. P. Smith, *Rapaport Diamond Report*, Vol. 33, No. 7, 2010, pp. 123–132.

The provenance of fine sapphires can greatly increase their value in the eyes of connoisseurs. Most sapphires can be associated with two geologic events: (1) the orogeny that created the Himalayas (55 million years ago [Ma]) and produced sapphire deposits from Afghanistan through Kashmir and east into Vietnam, and (2) the Pan-African orogeny (800–450 Ma) that produced the deposits in Sri Lanka, Madagascar, Kenya, Tanzania, and Mozambique.

Having created a source classification scheme for rubies (see *Rapaport Diamond Report*, Vol. 37, No. 47, 2008, pp. 140–148), the author presents a similar one for sapphires. This scheme has two tiers, the first separating sapphires into three groups based on broad geologic formation scenarios: Met (metamorphic), Mag (magmatic), and Met-Mag (having characteristics outside of classical Met and Mag). The second tier further divides sapphires into types I through IV based on their dominant inclusions and other features, as well as advanced analytical data. Photomicrographs illustrate the internal characteristics that differentiate sapphires produced by important localities. The current range of sapphire treatments is also reviewed. *AB*

DIAMONDS

Ages of cratonic diamond and lithosphere evolution: Constraints on Precambrian tectonics and diamond exploration. H. Helmstaedt [helmstaedt@geol.queensu.ca], J. J. Gurney, and S. H. Richardson, *Canadian Mineralogist*, Vol. 48, No. 6, 2010, pp. 1385–1408.

Age dating of syngenetic inclusions within peridotitic and eclogitic minerals shows that diamond formation occurred in episodes in the subcontinental lithospheric mantle.

From studies of the geologic record, these episodes could be correlated with important craton-forming events in the Archean and Proterozoic.

Diamonds containing *peridotitic* inclusions formed between ~3.5 and 3.2 billion years ago (Ga), in the Paleoarchean. Formation of these diamonds occurred in harzburgite, containing subcalcic garnet and/or chromite, within the lithospheric roots of the nuclei of the oldest cratons. The process appears to have been associated with a metasomatic event triggered by the infusion of CO_2-rich subduction(?)-related fluids. Post-Archean peridotitic diamonds formed later (~2.3–1.9 Ga) in lherzolite source rocks.

Diamonds with *eclogitic* inclusions formed over a longer period, some 2.9 to 0.58 billion years ago. An earlier period (~2.9–2.5 Ga) is associated with the accretion of Paleoarchean continental nuclei into composite Archean cratons. This involved subduction of the intervening seafloor, partial melting of the hydrated oceanic crust, and granitic magmatism. Later eclogitic diamonds, along with peridotitic diamonds found in lherzolite, formed during geologic events in the Proterozoic that are associated with modifications of earlier cratonic roots.

Kimberlite magmas, the most important source of gem diamonds, mainly sampled harzburgite source rocks during their rise through the subcontinental lithosphere. As a guide to diamond exploration, the authors recommend that geologists concentrate on identifying microcontinental nuclei older than 3 Ga within Archean or Proterozoic cratons. The tectonic history of these nuclei must then be analyzed to establish whether a diamond-bearing root was preserved beneath them that could have been sampled by kimberlitic magmas.

JES

Are diamond-bearing Cretaceous kimberlites related to low-angle subduction beneath western North America? C. A. Currie [claire.currie@ualberta.ca] and C. Beaumont, *Earth and Planetary Science Letters*, Vol. 303, No. 1–2, 2011, pp. 59–70.

Kimberlites, and to a lesser extent lamproites, are the main host materials for economic diamond deposits. They generally occur in continental interiors far from plate margins, making their relationship to plate tectonic processes enigmatic. One mechanism, potentially applicable to a limited subset of kimberlite events, invokes a relationship between kimberlite magmatism and lithospheric subduction.

This study investigates a subduction hypothesis for kimberlites in North America's western interior by: (1) presenting evidence that the Farallon Plate was suitably positioned beneath the continent as early as 100 Ma, (2) developing a numerical model of low-angle subduction, and (3) using the model to assess the potential for subduction-related volatiles in forming kimberlite magmas.

The numerical model places the source region of the western North America interior magmas above the low-angle Farallon Plate and directly implicates devolatilization of this plate in magma genesis. It is proposed that an influx of fluids triggered a small amount of partial melting of the deep craton lithosphere, forming a source of kimberlite and lamproite magmas.

Rapid, low-angle subduction reaching beneath cratonic continental interiors appears to be relatively rare. Therefore, subduction-related magmatism may be limited to a small number of kimberlite events. Where there is no evidence for contemporaneous low-angle subduction, other mechanisms must have been responsible for producing the kimberlites. *DAZ*

Composition of cloudy microinclusions in octahedral diamonds from the Internatsional'naya kimberlite pipe (Yakutia). S. Yu. Skuzovatov [justsquall@gmail.com], D. A. Zedgenizov, V. S. Shatsky, A. L. Ragozin, and K. E. Kuper, *Russian Geology and Geophysics*, Vol. 52, No. 1, pp. 85–96.

Octahedral diamond crystals (~1 mm) from the Internatsional'naya pipe in the Yakutian diamondiferous province contain cloudy microinclusions in their core. Diamond is an ideal container for transporting a mineral-forming medium—preserved as microinclusions—and processes such as mantle metasomatism, diamond formation, and partial melting of upper-mantle rocks can be understood by studying them. Diamond crystals from Yakutia were polished into 24 plates (0.3–0.8 mm thick), parallel to a {110} face, and studied using optical and scanning electron microscopy, cathodoluminescence, X-ray topography, and EDXRF and IR spectroscopy.

A shift from cuboid to octahedral morphology was observed, caused by different growth rates between {111}, {100}, and {110} faces. The internal structure consisted of a cubic or cuboid core, containing microinclusions and dislocations, followed by an octahedral rim. This change in growth structure was controlled by a layer-by-layer growth mechanism and a decrease in carbon supersaturation of the fluid/melt. The cubic cores contained mainly nitrogen B-centers, while cuboid cores were dominant in A-centers. The average nitrogen content was ~700 ppma. Some samples showed a higher nitrogen content and aggregation state (B-centers) in their core; hydrogen defects were also higher in the core. The $\delta_{13}C$ values of cuboid and cubic cores were similar to isotope values of carbon from the mantle—a light isotopic composition that ranged from –5.9 to –6.7‰. IR absorption bands at 3420 and 1650 cm^{-1} for water, 1430 and 880 cm^{-1} for carbonates, and 1200–900 cm^{-1} for silicates were detected in the microinclusion-bearing core region. Carbonates correlated negatively with water content, formed predominantly by OH groups rather than molecular water. The cubic cores were also rich in bivalent cations (Ca^{2+}, Mg^{2+}, and Fe^{2+}) and poor in Si and Al. The ratio of Mg/(Mg+Fe) in the cloudy microinclusions varied considerably between crystals but very slightly within each sample, suggesting a

heterogeneous diamond crystallization medium. The bulk composition was in the continuous transition between carbonate and chloride end-members, meaning the microinclusions would have been miscible fluids under diamond-forming conditions.　　　　　　　*KSM*

Sparkle returns. B. Janse, *Mining Journal*, Sept. 10, 2010, pp. 12–17.

After the economic crisis of 2008, a number of major diamond mining houses curtailed activities in the early part of 2009. Rough diamond prices declined sharply during this period. As the year progressed, however, mining activity and prices recovered strongly. This article details diamond mining in Canada, Africa, Russia, and Australia. Production from Canada, Russia, and southern Africa has rebounded, and some promising new prospects are being explored. Production from Central Africa is still uncertain, as major players who withdrew in 2008 have yet to return. The effects on Australia were minor, as Rio Tinto was in the midst of converting Argyle into an underground mine. The paper also describes exploration activities and some social issues surrounding diamond production.

　　　　　　　RS

GEM LOCALITIES

Charoite: Russia's royal gem. B. Jones, *Rock & Gem*, Vol. 40, No. 12, 2010, pp. 34–36, 62.

A rock known since 1978, charoite is composed mainly of the purple mineral charoite; the remainder may consist of more than 30 mineral species. The rock must contain 30–95% charoite mineral to be suitable for lapidary use. The varying mineral content is what creates the variations in color and pattern. Charoite's properties make it a good lapidary and ornamental stone, with most specimens showing some chatoyancy. The most sought-after color is a rich violet, and it may be tinged by blue, red, pink, or brown. Charoite is hosted by the Sirenevy Kamen deposit in Siberia. Extraction requires hard-rock mining, and the area's remoteness makes this quite difficult. Glacial action has helped expose mineralized areas, and numerous sites have been mined. Supplies should be available for many years.　　　　　　　*MK*

The conditions of formation of sapphire and zircon in the areas of alkali-basaltoid volcanism in central Vietnam. A. E. Izokh [izokh@uiggm.nsc.ru], S. Z. Smirnov, V. V. Egorova, T. T. Anh, S. V. Kovyazin, N. T. Phuong, and V. V. Kalinina, *Russian Geology and Geophysics*, Vol. 51, No. 7, 2010, pp. 719–733.

In central Vietnam, sapphire placers exist in the provinces of Gia Lai (Pleiku village), Dak Lac (Dak Nong), Bin Phuoc, Bin Tuan (Hong Liem), Lam Dong, and others. Zircon and garnet placers exist in Dong Nai (Gia Kiem). The chemical composition of associated clinopyroxene and garnet

megacrysts from the Dak Nong sapphire deposit showed that the gems are related to alkali basaltic magma that interacted with a deep-seated magma chamber. The chamber was a source of heat and CO_2-rich fluids for generating lower-crustal syenitic melts, producing zircon. Sapphires crystallized from a more fractionated iron-rich syenitic melt with the participation of CO_2 and CO_2-H_2O fluids in shallower crustal horizons.

The major and trace elements of the four minerals were analyzed to further define the formation conditions of the sapphire and the zircon. Based on their geologic relationships, the presence of zircon, clinopyroxene, and garnet can be used as a criterion for sapphire prospecting.

　　　　　　　DAZ

The genesis of the amethyst geodes at Artigas (Uruguay) and the paleohydrology of the Guaraní aquifer: Structural, geochemical, oxygen, carbon, strontium isotope and fluid inclusion study. G. Morteani, [gmorteani@gmx.de], Y. Kostitsyn, and C. Preinfalk, *International Journal of Earth Sciences*, Vol. 99, 2010, pp. 927–947.

Uruguay and Brazil are the world's leading producers of amethyst and agate from geodes. A detailed chemical analysis of the amethyst deposits of Artigas, Uruguay, as well as a review of the hydrology (current and ancient) of the Guarani aquifer in the Artigas area, was conducted to determine the formation conditions of the amethyst. The geodes were not filled by magmatic fluids but were shaped by them. The crystallization temperature of amethyst in the geodes was less than 120ºC, and the geothermal fluid from which the amethyst crystallized came from the artesian-stratified Guarani aquifer. Therefore, low-temperature fluids from the aquifer, rather than magmatic fluids, played a key role in the amethyst's genesis.

　　　　　　　DAZ

Genesis of Guatemala jadeitite and related fluid characteristics: Insight from zircon. T.-F. Yui [tfyui@earth.sinica.edu.tw], K. Maki, T. Usuki, C.-Y. Lan, U. Martens, C.-M. Wu, T.-W. Wu, and J. G. Liou, *Chemical Geology*, Vol. 270, No. 1–4, 2010, pp. 45–55.

Jadeitite is a rare rock variety (typically >90% jadeite by volume) found near subduction zones in high-pressure metamorphic rocks. Geochemical study of this gem material helps earth scientists understand the complex workings of plate boundaries. U-Pb dating of zircon within a jadeitite boulder found north of the Motagua Fault Zone in central Guatemala showed it was much older than other jadeitites from the same region (95.1 ± 3.6 Ma vs. 77–65 Ma). This older age was interpreted as the time of jadeitite formation, whereas the more recent age range corresponds with cooling after superimposed metamorphism at ~70 Ma. Rare-earth element concentrations in both jadeitite and zircon were very low and showed a variety of patterns.

For example, zircon exhibited both positive and negative Eu anomalies, suggesting a possible influence by the decomposition of associated plagioclase. Vein precipitation and metasomatic replacement (contrasting mechanisms for jadeitite genesis) are also evaluated in detail.

If the common assumption that jadeitite was formed by the serpentinization of ultramafic rocks is correct, the ultramafics must contain olivine as a major phase, the protolith must contain mica/feldspar, and a reducing fluid (of high pH) must be able to "pulse" in/out of the rock over time. This combination would provide the Al, Na, Zr, and Hf required to form and preserve jadeitite and zircon in the concentrations observed. These unique circumstances explain why jadeitite (and, by extension, jadeite) is rare in subduction zones. *KAM*

Geochemical and scintillometric characterization and correlation of amethyst geode-bearing Paraná lavas from the Quaraí and Los Catalanes Districts, Brazil and Uruguay. L. A. Hartmann [leo.hartmann@ufrgs.br], W. Wildner, L. C. Duarte, S. K. Duarte, J. Pertille, K. R. Arena, L. C. Martins, and N. L. Dias, *Geological Magazine*, Vol. 147, No. 6, 2010, pp. 954–970.

World-class lava-hosted amethyst geode deposits are located in northern Uruguay near Artigas and across the border in Rio Grande do Sul state of southern Brazil. A regional geochemical and gamma spectrometric (scintillometric) field survey differentiated six basalt, basaltic andesite, and andesite lava flows (with a total thickness of up to 300 m) of Cretaceous age, two of which host amethyst (and agate). The magmas likely formed by melting in the lithospheric mantle. After being injected into the crust and assimilating some crustal rocks, they were erupted onto the surface. The lavas flowed over Aeolian sandstones to form a stratigraphic sequence that can now be more easily distinguished in the field throughout this region. Recognition of the distinctive lava sequence provides exploration criteria for amethyst and agate. *JES*

La mine de spinelle de Lang Chap, au Nord du Vietnam [The spinel mine of Lang Chap in northern Vietnam]. D. Blauwet, *Revue de Gemmologie a.f.g.*, No. 173, September 2010, pp. 11–15 [in French].

A new red spinel mine at Lang Chap in northern Vietnam opened in April 2010. The site is a difficult two-hour drive from Luc Yen in Yen Bai Province. Mining takes place by artisanal methods, and as many as 2,000 miners have been active, though only 400 were present on the day of the author's visit. In most of the pits, rock outcrops were absent. Basic washing systems are used to clean the eluvium in bamboo baskets. The spinel crystals were water-worn and ranged up to 3 cm. The author reported purchasing a fine 6 g red spinel that yielded a 7.5 ct faceted stone. Many gem dealers have made their way to Yen Bai Province to purchase this new spinel, causing dramatic price increases in the local market. *GL*

Die Präparation spektakulärer Smaragdstufen aus der Kagem Mine, Kafubu, Sambia [The preparation of spectacular emerald specimens from the Kagem mine, Kafubu, Zambia]. S. Behling, *Lapis*, Vol. 36, No. 1, 2011, pp. 15–23.

The Kagem mine is an important producer of fine emeralds. The rough is normally trimmed and sorted from the host schist by hand. However, some emerald crystals up to 6 inches long occur in massive quartz boulders and cannot easily be processed without damaging the emeralds. In 2009, mine owner Gemfields PLC asked Collector's Edge Minerals Inc. to process these boulders. This article describes how the *Medusa*—a spectacular specimen with seven free-standing emerald "pencils"—was meticulously prepared over a period of 17 months. The article includes photos of the mine and its products, as well as a series of eight images illustrating the different stages of the *Medusa*'s preparation. *RT*

Rubin in Zoisit—ein Klassiker aus Longido in Tansania [Ruby in zoisite—A classic from Longido, Tanzania]. J. Hintze, *Lapis*, Vol. 35, No. 12, 2010, pp. 15–19.

The Mandarara mine near Longido, Tanzania, has produced cabochon-quality ruby and ornamental ruby in green zoisite since 1949. The material is sorted into three categories: ruby crystals with good hexagonal form ("specimens"); larger pieces composed of ~70% ruby, with indistinct or no crystal faces ("ruby blocks"); and zoisite pieces speckled with smaller ruby inclusions ("ruby spots").

Mining is well organized and takes place underground, with a shaft following the steeply dipping zoisite rock. The operation has reached the point where a large investment will be necessary to continue. Prospecting for similar occurrences in the surrounding area is ongoing.

RT

INSTRUMENTS AND TECHNIQUES

L'évolution des techniques de photographie des inclusions dans les gemmes: la micro-photographie numérique [Evolution of photography techniques used on inclusions in gemstones: Digital photomicrography]. M. F. Hügi, *Revue de Gemmologie a.f.g.*, No. 173, 2010, pp. 6–10.

The earliest illustrations of inclusions in minerals can be found in a 17th century book, Anathase Kircher's *Mundus Subtarreanus*, which contains many beautiful drawings of insects in amber and fluid inclusions in quartz and halite. Austrian scientist Herman Michel introduced photomicrography to gemology in the early 20th century. One of his pupils, Dr. Edward J. Gübelin, became a pioneer of this technique during the 1940s. The three-volume *Photoatlas of Inclusions in Gemstones*, which he co-wrote with John Koivula, is the culmination of these efforts.

Photomicrography does have its limitations, as the human eye perceives details in dark and light areas better than electronic sensors. Recent developments in digital photomicrography allow the extension of the dynamic range (high dynamic range imaging) as well as the depth of field. Both significantly enhance the capabilities of photomicrography, though fraudulent manipulation of the images is also possible.   *GL*

The hidden beauty of Brazilian gemstones. M. F. Hügi, *InColor*, No. 15, Fall/Winter 2010, pp. 46–51.

The author explores modern photomicrography techniques using Brazilian gems as examples. While conventional photography must deal with limitations in luminance range and depth of focus, digital photomicrography and illumination techniques developed in the last few years produce results that are closer to the actual visual impression of microscopic observation. High dynamic range imaging extends the luminance range beyond one-shot photography. A series of photographs of different exposure times (exposure bracketing) is combined using software (such as Photomatix Pro, Photosphere, and Photoshop) and finished by "tone-mapping" to produce a well-balanced photo that more accurately reproduces what the human eye sees.

A second important development in digitally photographing the inner world of gemstones is the extension of focal depth. Digital imaging software (e.g., Syncroscopy AutoMontage) can render relatively large internal features entirely in focus. This may also serve as a first step in 3-D modeling or spatial analysis of inclusions.

In addition, improved lens speed and stronger light sources such as halogen bulbs and LED illumination allow the use of polarized light as a standard technique in gemological microscopy. A microscope-mounted polarizing filter suppresses the blurring caused by birefringence, while crossed polarizers enable the examination of anisotropic mineral inclusions, twinning planes, and ADR-related characteristics. A first-order-red compensator replaces the total extinction of crossed polarizers with a purplish red first-order interference color, which is useful for reducing very strong contrast and making details within zones of extinction more visible. These new techniques can advance our knowledge and general appreciation of the hidden beauty of gemstones.

ERB

JEWELRY HISTORY

Hippologie arabe et archéogemmologie sur un harnachement mameluk 1ère partie. [Arab hippology and archaeological gemology on a Mamluk harness—Part 1]. E. Gonthier [gonthier@mnhn.fr], T. De-Noblet, and J.-P. Sage-Fresnay, *Revue de Gemmologie a.f.g.*, No. 173, 2010, pp. 23–24.

An 18th century Mamluk harness now housed in the Invalides Musée de l'Armée collection in Paris was recovered by French soldiers during Napoleon's Egyptian campaigns. It evokes the passion of the Egyptians and the Mamluk warriors for their horses and the symbolic value given to gemstones and metals, which went beyond their technical or aesthetic significance. The object is of a remarkable decorative richness, upholstered in red velvet and decorated across the entire surface with gold embroidery. The red cotton seat of the saddle is dotted with flowers interspersed with crescents, bordered with studs, and covered with cabochon-cut gemstones. These cabochons were identified as lapis lazuli, dumortierite quartz, and red coral by portable Raman spectroscopy.   *GL*

Secrecy, splendour and statecraft: The jewel accounts of King Henry III of England, 1216-72. B. L. Wild, *Historical Research*, Vol. 83, No. 221, 2010, pp. 409–410.

The 13th century jewel accounts of King Henry III are the oldest and most detailed records of their kind. They were appended to the royal wardrobe accounts and contain descriptions of gifts given to and received by the monarch during his reign. These include jewels, metal objects, regalia, and other items of importance to the royal court.

Information from the wardrobe account was based on two sets of rolls compiled annually for the exchequer, the office that collected revenue. The exchequer kept them as a record after the annual audit, which is how they have survived to this day. These rolls showed how the keeper of the wardrobe spent his funds. With each change of keeper, the organization of information in the rolls changed considerably. Each department under the keeper of the wardrobe had its own keeper, so there would be many minor rolls (sometimes a hundred) and one master roll.

The richness of the rolls is revealed in the very first jewel account, with its description of more than 2,000 objects recorded during the first years of Henry III's rule (1234–1236). The scale of these treasures is evident from the 173 rings, 103 gold brooches, and cloths of gold. In comparison, the jewel account from the final years of Henry's reign (1268–1272), describes more than 2,500 objects. The only item mentioned in the jewel rolls that still exists is one of a group of gold bullae made for Henry's second son Edmund, titular King of Sicily.

JES

SYNTHETICS AND SIMULANTS

Gas bubbles in shaped sapphire. O. M. Bunoiu [bunoiu_madalin@yahoo.com], T. Duffar, and I. Nicoara, *Progress in Crystal Growth and Characterization of Materials*, Vol. 56, No. 3–4, 2010, pp. 123–145.

This study was conducted to better understand the causes and distribution of the small bubble or "micro-void" defect commonly found in synthetic sapphire grown using the Stepanov or EFG (edge-defined film-fed growth) technique. The presence of micro-voids in synthetic sapphire is undesirable in that they undermine its optical and mechanical properties. The factors considered in this study included gas origin, thermal decomposition of molten alumina, reaction between melt and crucible, quality of raw material, growth atmosphere, crucible composition, presence of graphite in the furnace, bubble nucleation, bubble transport in the melt, the growth interface, and bubble location in the crystal. Synthetic sapphire crystals were grown with different raw materials under various growth atmospheres, pulling rates, growth shapes (rod versus ribbon), equipment setups, and heat-source conditions.

The authors propose a mechanism for micro-void formation in shaped synthetic sapphire based on their findings, coupled with their literature survey and finite element calculations. They determined that the main gas present in the voids was CO, a finding confirmed by mass spectroscopy. They were surprised to learn that the gas concentration in the crystals was independent of growth conditions or equipment setup. They did find a correlation between the crucible material and the presence of graphite in the growth chamber with the formation of micro-voids in synthetic sapphire. Specifically, molybdenum crucibles appear to enhance micro-void formation compared to tungsten or iridium crucibles. Graphite furnace parts also appear to contribute to micro-void formation.   *JS-S*

Mechanisms of the formation and morphogenetic types of fluid inclusions in crystals of synthetic minerals. O. V. Balitskaya and V. S. Balitsky [ovbalitskaya@mail.ru], *Doklady Earth Sciences*, Vol. 435, No. 1, 2010, pp. 76–80.

The authors report on methods for generating artificial fluid inclusions in hydrothermally grown synthetic gem materials. Studying these inclusions and their formation conditions offers valuable insight into the mechanisms by which natural minerals form. Among the synthetic materials studied were quartz, calcite, fluorite, and topaz. The various inclusions that formed (from both stimulated and spontaneous origin) and their characteristics are described. Inclusions of stimulated origin formed by drilling, sawing, fracturing, or etching the seed crystals under specific conditions to create vacuoles, then healing those vacuoles by various hydrothermal growth methods. Inclusions of spontaneous origin were formed from cavities on the seed crystals that were preexisting, not intentionally induced. The study was able to mimic inclusions that naturally occur in quartz, calcite, fluorite, and topaz at high temperatures and pressures in aqueous-hydrocarbon fluids.   *JS-S*

TREATMENTS

High pressure high temperature treatment of diamonds— A review of the patent literature from five decades (1960–2009). K. Schmetzer, *Journal of Gemmology*, Vol. 32, No. 1–4, 2010, pp. 52–65, plus 14 supplementary pages of appendices.

Although color treatment of diamonds by HPHT annealing was first recognized by scientists in the 1960s, its late-1990s introduction to the gem trade, and the gemological challenges of detecting this method, have caused great concern in the jewelry industry. Claims in patent documents from the U.S. and elsewhere describe several changes in color-causing optical defects in the diamond lattice that can be achieved by annealing under high temperature and pressure conditions (with a separate irradiation procedure in some cases):

1. Diffusion of boron to create a thin blue, electrically conductive layer on the diamond surface; similar experiments using aluminum seemed to "whiten" the diamond.
2. Removal of brown coloration from type IIa diamonds to render them colorless.
3. Alteration of the brown color in type II diamonds to induce either a reddish pink or a blue color.
4. Alteration of the brown color in type Ia diamonds to create green, yellow-green, or yellow colors.
5. Alteration of the brown color in type Ib diamonds to create a yellow color.

Specific patents and applications (available online) are cited for each of these changes, along with the annealing parameters and the resulting changes in diamond color and other physical properties. Some discrepancies and inconsistencies exist among the claims made in these patent documents, which involve separate research groups using different HPHT equipment and treatment conditions. Some explanation is given for the alterations in optical defects that change a diamond's color.   *JES*

MISCELLANEOUS

Beyond the "crisis of youth"? Mining, farming, and civil society in post-war Sierra Leone. R. Fanthorpe [rf21@sussex.ac.uk] and R. Maconachie, *African Affairs*, Vol. 109, No. 435, 2010, pp. 251–272.

Many youths in postwar Sierra Leone have formed cooperatives to engage in economic activities such as selling music cassette tapes. Yet efforts to organize diamond mining cooperatives have come into conflict with large corporations, most of them allied with local chiefs who have jurisdiction in the areas. These companies have increasingly turned to mechanization, which aggravates the youth unemployment problem. Nevertheless, some young peo-

ple are finding opportunities farming arable land adjacent to the diamond mines.   *RS*

Environmental stewardship in gemstone mining: Quo vadis? L. Cartier [laurent.cartier@unibas.ch], *InColor*, No. 15, Fall/Winter 2010, pp. 12–19.
This article explores some of the complex relationships between gems and the ecologies from which they are extracted. Although a number of large- and medium-scale companies are involved in colored stone mining, artisanal miners represent 80% of the extraction efforts. Protecting vulnerable ecologies is difficult when artisanal miners do not share the same sense of environmental responsibility as local people who depend on the viability of the land. Just as often, regulation and other government support for sustainability is limited or nonexistent.

The author argues that all gem industry stakeholders, including government agencies and consumers, must examine and assume responsibility for the social, economic, regulatory, and environmental interrelationships that constitute a sustainable approach to gem mining. The core sustainability question is this: Has the extraction left a viable physical and social environment that can support livelihoods in the long term once mining has ceased?

The author provides an excellent table summarizing major environmental challenges associated with gem mining. He specifies six domains (water, soil, air, flora/fauna, human, and landscape), with 18 potential long-term consequences of mining and, most importantly, mitigation strategies. The article also discusses some of the cultural, economic, and institutional variables that undergird the continued lack of progress.

Twelve general recommendations to support responsible environmental stewardship and sustainability are offered. These include cost-effective regulatory mechanisms adapted to local realities, training, incentives, and practical assistance in cleaner production methods and the reclamation of mining sites.

ERB

The geoheritage significance of crystals. M. Brocx [geoheritage@iinet.net.au] and V. Semeniuk, *Geology Today*, Vol. 26, No. 6, Nov.-Dec. 2010, pp. 216–225.
Earth can be considered a crystalline planet, with thousands of ubiquitous mineral varieties occurring in diverse environments. Like larger geologic formations, these crystals are significant in deciphering the earth's history. This article discusses how specific crystals are of geoheritage significance.

The principles of geoconservation and geoheritage as applied to geologic sites are reviewed in detail. The article also suggests that some crystals, because of their distinctive attributes (size, rarity, inclusions, etc.) or location on Earth should be afforded geoheritage status, worthy of protection through geoconservation. Eight of the 15 sig-

nificant geologic phenomena used to identify geoheritage and geoconservation significance apply to crystals and minerals.

The author illustrates a range of 18 internal features and nine crystal settings and features (e.g., veins, geodes, euhedrality, large cavities, and caves). An extensive table of notable crystal and mineral sites worldwide and their significance is provided. It includes amethyst-bearing geodes, well-formed dravite and elbaite tourmaline crystals, gypsum crystals in Mexico and Spain, zircon crystals of Jack Hills in Australia (the oldest crystals on Earth), well-formed pyrite in Spain, and Iceland spar.

ERB

Has clarity been brought to the diamond sector? A survey into AML and TF risk mitigation by diamond traders and their financiers. M. van Dijck [marten.van.dijck@nl.abnamro.com], *Crime, Law and Social Change*, Vol. 52, No. 5, 2009, pp. 74–93.
This article examines the complex legal, social, and political forces affecting the world diamond industry and the various measures taken during the past decade, such as the Kimberley Process and financial regulatory legislation, in anti-money laundering and countering the financing of terrorism. The author notes that while the diamond industry is largely clean of such illegal activities, its lack of transparency does make it a potential vehicle for money laundering and terror finance. Because the industry is so dependent on bank credit, financial institutions have assumed the role of forcing it into compliance with international laws.   *RS*

A "Kimberley protest": Diamond mining, export sanctions, and poverty in Akwatia, Ghana. G. Hilson [g.m.hilson@reading.ac.uk] and M. J. Clifford, *African Affairs*, Vol. 109, No. 436, 2010, pp. 431–450.
While the Kimberley Process has been reasonably effective in controlling illicit mining and trading of rough diamonds, it does not always take into account local dynamics, which can lead to counterproductive sanctions. The Kimberley Process enacted sanctions against Ghana in 2006 because its government could not account for an increase in rough diamond exports since 2000. Some analysts had attributed the increase to smuggling from neighboring Ivory Coast, which was (and remains) in the midst of a civil conflict. However, the vast majority of the increase in rough diamond exports came from informal diggings in Akwatia, the country's main diamondiferous area, but outside the traditional mining concession set up years earlier by Ghana Consolidated Diamonds. The government kept poor records of such stones, even though the buyers had purchased and exported the stones legally. The ensuing temporary embargo on Ghana's diamonds in 2006–2007 created a great deal of hardship in the country's diamond industry.   *RS*

Sierra Leone's illicit diamonds: The challenges and the way forward. S. A. Wilson [wilsonsi@msu.edu], *GeoJournal*, DOI 10.1007/s10708-009-9321-6, 2009, 22 pp.

Dating back to its colonial era, Sierra Leone's widely scattered alluvial diamond deposits have created huge challenges for authorities to bring about full legitimacy. The deposits are in remote locations, far removed from any government center, attracting local and international buyers who smuggle rough out of the country or bribe officials to avoid paying mining license fees, rents on concessions, and customs duties. These issues became particularly acute during the country's civil war of the 1990s and remain troublesome today. Cooperative efforts to bring international buyers into producing areas to buy directly from miners increase the likelihood of legal compliance, providing a higher return to the government from taxes and allowing miners to realize better prices for their diamonds.

RS

Tanzanite as a conflict gem: Certifying a secure commodity chain in Tanzania. R. A. Schroeder [rschroed@rci.rutgers.edu], *Geoforum*, Vol. 41, No. 1, 2010, pp. 56–65.

The author recounts the efforts by tanzanite miners to counteract negativity publicity following a 2001 *Wall Street Journal* article that alleged the gem was being sold to finance terror. While the allegations were soon disproved, conflicts between artisanal miners and the large South African mining company Afgem (now TanzaniteOne), as well as conditions in the artisanal workings, created ongoing public relations problems. In response, Afgem branded itself as an ethical miner. Doing so, however, brought unexpected scrutiny upon the firm. The supply-chain accountability requirements of the U.S. PATRIOT Act forced all suppliers to comply with minimum standards, requiring Afgem to rebrand itself once again.

RS

Because Public Education Happens At The Counter.

GIA's Retailer Support Kit and website

A $97.00 value, shipping and handling extra.
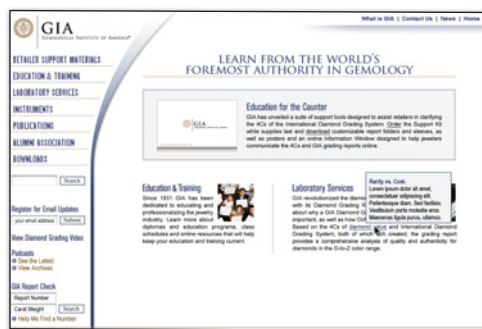
GIA's Retailer Support Kit has been developed to help sales associates educate the public about diamonds, the 4Cs, and thoroughly explain a GIA grading report. Take full advantage of all that GIA has to offer by visiting www.retailer.gia.edu

To order your FREE kit, log on to www.retailer.gia.edu

GIA®